THE ROLE OF HEPATOCYTE D-β-HYDROXYBUTYRATE DEHYDROGENASE IN KETONE BODY METABOLISM AND LIVER HEALTH

A THESIS

SUBMITTED TO THE FACULTY OF THE

UNIVERSITY OF MINNESOTA

BY:

David Blake Stagg

IN PARTIAL FULFILLMENT OF THE REQUIREMENTS

FOR THE DEGREE OF

DOCTOR OF PHILOSOPHY

Advisor:

Peter A. Crawford, MD, PhD

Professor

Medicine, Division of Molecular Medicine

Biochemistry, Molecular biology, and Biophysics

September 2021

© David Blake Stagg 2021

Acknowledgments

My first time picking a pipette off a lab bench happened nearly eleven years ago. It was my senior year of undergrad at Duke University, and I had just started my independent study project in Dr. Laura Rusche's lab working on yeast sirtuins. I spent the whole year trying to CHIP a protein that ended up not being there. With that experience, some might have quit their research careers, but I kept going. Thank you, Dr. Rusche, for giving me my start.

After graduating, I was fortunate to start a research technician position in Dr. Nancy Andrews' lab at Duke. Thank you, Dr. Andrews, for giving me a job and showing me the leadership possibilities a career as a physician scientist could provide. Most importantly, thank you for letting me work with Dr. Karin Finberg. Beyond lab techniques and mouse genetics, my two years working with Dr. Finberg taught me how to be a rigorous, detail-oriented scientist. Thank you, Karin.

I next had the opportunity to learn an entirely different skill set by joining Dr. Donald McDonnell's lab, also at Duke. Dr. McDonnell was excellent at managing people and delegating, making running a 20+ member lab look like a breeze. Thanks for your example, Dr. McDonnell. There I worked extensively with Dr. John Norris, who is the reason why none of my experiments are ever small. Thank you John for helping me learn how much I was capable of. I would also like to thank Drs. Ching-Yi Chang, Suzanne Wardell, and Stephanie Ellison, in addition to all the other members of the McDonnell lab.

Six years ago, I began my time at the University of Minnesota, where I have been lucky enough to be a student in the Medical Scientist Training Program. Thank you Dr. Yoji Shimizu for being a great program director and for your wisdom and mentorship. Thanks Dr. Bryce Binstadt, Dr. Lisa Schimmenti, Susan Shurson, and Nick Berg for all of your help and guidance. Additionally, thanks to my 2015 cohort members who have made my time in the Twin Cities so enjoyable.

Which brings me to my thesis work in Dr. Peter Crawford's lab. Peter, thank you for letting me join your lab and for being my research mentor. You helped me grow as a scientist with the perfect balance of independence and supervision. I hope to one day match your skillful scientific communication and your ability to compose a multi-paragraph email in under five minutes. Thanks for everything Peter, I am forever grateful. Dr. Patrycja (Pati) Puchalska, thank you for teaching me the fundamentals of mass spectrometry and for answering my many questions. Dr. Justin Lengfeld, thanks for always being willing to help me out with my experiments and for being a sounding board to bounce off ideas. Dr. Andre d'Avignon, thanks for teaching me the ways of oxidative flux assessments and being a great lab neighbor. Alisa Nelson, thanks for sharing the grad student journey with me and always being willing to offer a hand with experiments. Drs. Curtis Hughey and Sarah Wernimont, thanks for all the great advice on science and on life. Thank you Diana Cook, Jacob Gillingham, and Alisha Seay for all of your technical support. Lastly, thanks Drs. Doug Mashek, Tim Griffin, and Christine Wendt for serving on my thesis committee and for your always appreciated research guidance.

Dedication

This work is dedicated to my family, who have been with me since the start and have helped me to the end. Love you Mom, Dad, Suzanne, Faith, Aunt Dee, Marisol, and especially Josh. I promise that I am almost done with school.

Abstract

Throughout the last decade, interest has intensified in intermittent fasting, ketogenic diets, and exogenous ketone therapies as prospective health-promoting, therapeutic, and performance-enhancing agents. However, the regulatory roles of ketogenesis and ketone metabolism on liver homeostasis remain unclear. This thesis seeks to develop a better understanding of the metabolic consequences of hepatic ketone body metabolism by focusing on the redox-dependent interconversion of acetoacetate (AcAc) and D-β-hydroxybutyrate (D-βOHB).

Using targeted and isotope tracing high-resolution liquid chromatography-mass spectrometry, dual stable isotope tracer nuclear magnetic resonance spectroscopy-based metabolic flux modeling, dietary-induced mouse models of nonalcoholic fatty liver disease (NAFLD), and complementary physiological approaches in novel cell type-specific knockout mice, the roles of hepatocyte D-β-hydroxybutyrate dehydrogenase (BDH1), a mitochondrial enzyme required for NAD^+/NADH-dependent oxidation/reduction of ketone bodies, are quantified. Exogenously administered AcAc is reduced to D-βOHB, and increases hepatic NAD^+/NADH ratio, reflecting hepatic BDH1 activity. Livers of hepatocyte-specific BDH1 deficient mice produced no D-βOHB, but due to extrahepatic BDH1, these mice nonetheless remained capable of AcAc/D-βOHB interconversion. Compared to littermate controls, hepatocyte specific BDH1 deficient mice, maintained on either a chow or NAFLD-inducing western-style diet, showed diminished liver tricarboxylic acid (TCA) cycle flux and impaired gluconeogenesis but normal

overall hepatic energy charge. Furthermore, the livers of knockout mice maintained on a 60% high fat diet were less fibrotic, with reduced markers of oxidative stress, than littermate controls.

Collectively, this thesis illustrates how ketone bodies and BDH1 activity influence liver homeostasis and health. While liver BDH1 is not required for whole body equilibration of AcAc and D-βOHB, loss of the ability to interconvert these ketone bodies in hepatocytes results in impaired TCA cycle flux and glucose production, with a beneficial effect on liver fibrosis. Therefore, BDH1 is a significant contributor to hepatic mitochondrial redox, liver physiology, and organism-wide ketone body homeostasis, and augmentation of hepatic BDH1 activity could prove beneficial in the treatment of NAFLD.

Table of Contents

Acknowledgments i

Dedication iii

Abstract iv

List of tables vii

List of figures viii

Abbreviations x

Chapter 1. Introduction to nonalcoholic fatty liver disease and ketone body metabolism 1

Chapter 2. Ketone interconversion and the effects of hepatocyte-specific D-β-hydroxybutyrate dehydrogenase loss 11

Chapter 3. Reduced hepatic TCA cycle flux, glucose production, and liver fibrosis in D-β-hydroxybutyrate dehydrogenase hepatocyte-deficient mice maintained on NAFLD-inducing diets 71

Chapter 4. Conclusions and future directions 108

References 115

List of Tables

Supplemental Table 2.1. Genotyping primer sequences 68

Supplemental Table 2.2. MS parameters for energy metabolite quantification. 68

Supplemental Table 2.3. Gene expression primer sequences 69

Supplemental Table 2.4. MS parameters for glutamate dehydrogenase system metabolite quantification 69

Supplemental Table 2.5. Distribution of genotypes in offspring of Albumin-$Cre^{+/-}$, *Bdh1*$^{flox/flox}$ X $Cre^{-/-}$, *Bdh1*$^{flox/flox}$ crosses 70

Supplemental Table 3.1. Genotyping primer sequences 107

List of Figures

Figure 1.1. Progression of nonalcoholic fatty liver disease 9

Figure 1.2. Overview of ketone body metabolism 10

Figure 2.1. Effects of boluses of exogenous AcAc and D-βOHB on circulating ketones and liver redox 48

Figure 2.2. Confirmation of hepatocyte-specific BDH1-KO mice 49

Figure 2.3. Hepatocyte-BDH1-KO mice exhibit impaired ketogenesis and ketone interconversion 50

Figure 2.4. Hepatocyte-BDH1-KO mice maintain liver redox state 52

Figure 2.5. Loss of hepatic BDH1 diminishes hepatic oxidative fluxes 53

Figure 2.6. Altered glucose homeostasis in Hepatocyte-BDH1-KO mice 55

Figure 2.7. Hepatocyte-BDH1-KO mice remain insulin sensitive, with an intact ketone response to insulin 56

Figure 2.8. Summary of hepatocyte-specific BDH1-KO induced changes on ketone equilibration 57

Supplemental Figure 2.1. Increased hepatic BDH1 expression in wild-type mice maintained on a 60% HFD 58

Supplemental Figure 2.2. Loss of hepatic BDH1 expression by 8 weeks of age in hepatocyte-specific BDH1-KO mice 59

Supplemental Figure 2.3. Fasting body weights and circulating lipids do not differ with hepatic BDH1 loss 60

Supplemental Figure 2.4. Effects of hepatocyte BDH1 loss on equilibration of circulating ketones 61

Supplemental Figure 2.5. Abundance of ketogenic mediators in mouse kidney 62

Supplemental Figure 2.6. Loss of hepatic BDH1 diminishes hepatic oxidative fluxes while maintaining total liver energy charge 63

Supplemental Figure 2.7. Glucose homeostasis in Hepatocyte-BDH1-KO mice 64

Supplemental Figure 2.8. Intact ketone response to insulin in Hepatocyte-BDH1-KO mice 65

Supplemental Figure 2.9. Response to exogenous glucose in Hepatocyte-BDH1-KO mice 66

Supplemental Figure 2.10. Renal markers of glucose homeostasis..... 67

Figure 3.1. Diminished circulating ketones and impaired hepatic ketogenesis in hepatocyte-specific BDH1 KO mice maintained on a NAFLD-provoking western-style diet 96

Figure 3.2. In mice maintained on a western-style diet, fasting body weights and circulating lipids do not differ with hepatic BDH1 loss..... 97

Figure 3.3. Loss of hepatic BDH1 diminishes hepatic oxidative fluxes in mice maintained on a western-style diet 98

Figure 3.4. Preserved liver energy charge in Hepatocyte-BDH1-KO mice maintained on a western-style diet 99

Figure 3.5. Altered glucose homeostasis in Hepatocyte-BDH1-KO mice maintained on a western-style diet 100

Figure 3.6. Insulin signaling in Hepatocyte-BDH1-KO mice maintained on a western-style diet remains comparable to controls..... 101

Figure 3.7. Loss of hepatic BDH1 reduces markers of fibrosis in mice maintained on a 60% high fat diet..... 102

Supplemental Figure 3.1. Body weight and circulating lipid assessment in Hepatocyte-BDH1-KO mice maintained on a 60% high fat diet..... 103

Supplemental Figure 3.2. Body weight and circulating lipid assessment in Hepatocyte-BDH1-KO mice maintained on a choline-deficient, methionine-limited high fat diet..... 104

Supplemental Figure 3.3. Markers of fibrosis and oxidative stress in Hepatocyte-BDH1-KO mice maintained on a western-style diet..... 105

Supplemental Figure 3.4. Assessment of fibrosis in Hepatocyte-BDH1-KO mice maintained on a choline-deficient, methionine-limited high fat diet..... 106

Abbreviations

AcAc	Acetoacetate
Acaca	Acetyl-CoA carboxylase alpha
Acacb	Acetyl-CoA carboxylase beta
Acadl	Acyl-CoA dehydrogenase long chain
Acadm	Acyl-CoA dehydrogenase medium chain
Acsl1	Acyl-CoA synthetase long chain family member 1
Acsl3	Acyl-CoA synthetase long chain family member 3
Acta2	Actin alpha 2, smooth muscle
ADP	Adenosine diphosphate
AKT	Protein kinase B
AMP	Adenosine monophosphate
AMPKα	AMP-activated protein kinase alpha
AOC	Area of curve
ATP	Adenosine trisphosphate
AUC	Area under curve
BCA	Bicinchoninic acid
BDH1	D-β-hydroxybutyrate dehydrogenase
BDH2	3-hydroxybutyrate dehydrogenase 2
BEH	Ethylene bridged hybrid
βox	β-oxidation
BSA	Bovine serum albumin
cAMP	Cyclic adenosine monophosphate
Cd36	CD36 molecule, fatty acid translocase
CDAHFD	Choline-deficient, methionine-limited high fat diet
CIL	Cambridge Isotope Laboratories
CoA	Coenzyme A
CoA-SH	CoA sodium salt hydrate

Col1a1	Collagen type I alpha 1 chain
Col3a1	Collagen type III alpha 1 chain
Col4a1	Collagen type IV alpha 1 chain
CPT	Carnitine palmitoyltransferase
Cpt1a	Carnitine palmitoyltransferase 1A
Cpt2	Carnitine palmitoyltransferase 2
Cs	Citrate synthase
DAPI	4′,6-diamidino-2-phenylindole
DBAA	Dibutylammonium acetate
D-βOHB	D-β-hydroxybutyrate
e^-	Electron
EDTA	Ethylenediaminetetraacetic acid
EGTA	Ethylene glycol bis (2-aminoethyl ether)-N,N,N′,N′-tetraacetic acid
ELISA	Enzyme-linked immunosorbent assay
ETC	Electron transport chain
Ethyl-AcAc	Ethyl-acetoacetate
FGF21	Fibroblast growth factor 21
FOXA2	Forkhead box A2
H3K27	27^{th} amino acid in histone H3
H&E	Hematoxylin and eosin
HDTE	4-hydroxy-dodecatrienal
HEPES	4-(2-hydroxyethyl)-1-piperazineethanesulfonic acid
HESI	Heated electrospray ionization
HFD	High fat diet
HGP	Hepatic glucose production
HHE	4-hydroxy-2E-hexenal
HMGCL	3-hydroxymethylglutaryl-CoA lyase
HMGCS2	Hydroxymethylglutaryl-CoA synthase 2
HNDE	4-hydroxy-nondienal
HNE	4-hydroxy-2E-nonenal

HOMA-IR	Homeostatic model assessment for insulin resistance
HRP	Horseradish peroxidase
IgG	Immunoglobulin G
i.p.	Intraperitoneal
IPGTT	Intraperitoneal glucose tolerance test
IPITT	Intraperitoneal insulin tolerance test
IRβ	Insulin receptor beta
K_{eq}	Equilibrium constant
KO	Hepatocyte-specific BDH1 knockout mice
LC	Liquid chromatography
Lipc	Lipase C, hepatic type
MCT1	Monocarboxylate transporter 1
MCT2	Monocarboxylate transporter 2
MIM	Mitochondrial isolation medium
MS	Mass spectrometry
MS/MS	Tandem mass spectrometry
mThiolase	Mitochondrial thiolase
mTORC1	Mammalian target of rapamycin complex 1
m/z	Mass to charge ratio
$NaBD_4$	Sodium borodeuteride
NAD^+	Oxidized nicotinamide adenine dinucleotide
NADH	Reduced nicotinamide adenine dinucleotide
NAFL	Nonalcoholic fatty liver
NAFLD	Nonalcoholic fatty liver disease
NASH	Nonalcoholic steatohepatitis
N(CE)	Normalized collision energy
NEFA	Non-esterified fatty acids
NMR	Nuclear magnetic resonance
Nox2	NADPH oxidase 2
OCT	Optimal cutting temperature

Oxct1	3-oxoacid CoA-transferase 1
pAKT	Phosphorylated AKT
pAMPKα	Phosphorylated AMPKα
PBS	Phosphate buffered saline
Pc	Pyruvate carboxylase
Pck1	Phosphoenolpyruvate carboxykinase 1
PCR	Polymerase chain reaction
PEP	Phospho*eno*lpyruvate
pIRβ	Phosphorylated insulin receptor beta
PLB	Protein lysis buffer
PPARα	Peroxisome proliferator activated receptor alpha
Pparg	Peroxisome proliferator activated receptor gamma
Ppargc1a	Pparg coactivator 1 alpha
PRM	Parallel reaction monitoring
PTM	Post translational modification
RE	Reducing equivalent
Rna18s5	RNA 18S ribosomal 5
Rpl32	Ribosomal protein L32
RT-PCR	Reverse-transcription polymerase chain reaction
SCOT	Succinyl-CoA:3-oxoacid-CoA transferase
SIRT3	Sirtuin 3
Slc2a1	Glucose transporter protein type1
Slc2a2	Glucose transporter protein type2
Slc5a1	Sodium/glucose cotransporter 1
Slc5a2	Sodium/glucose cotransporter 2
TAG	Triacylglycerols
TCA	Tricarboxylic acid
TKB	Total ketone bodies
UPLC	Ultra performance liquid chromatography
WD	Western-style diet

Chapter 1: Introduction to nonalcoholic fatty liver disease and ketone body metabolism

1.1 Nonalcoholic fatty liver disease

Twenty-five percent of the United States' population has nonalcoholic fatty liver disease (NAFLD, **Figure 1.1**) [1; 2], a multi-organ condition that includes hepatic fat infiltration alone (simple steatosis) or steatosis plus inflammation, liver cell injury (ballooning) and death (nonalcoholic steatohepatitis [NASH]). Hepatic steatosis alone (storage of excess triacylglycerols in hepatocytes, >5% of liver weight) [3] can be a stable clinical condition existing as the hepatic manifestation of obesity-related insulin resistance. Cirrhosis due to NASH develops in 2% of all Americans, driven through failed attempts to regenerate healthy liver, promoting activated hepatic stellate cells' execution of fibrogenesis. While the risk of hepatocellular carcinoma in NASH patients is 2% per year [4], one of the leading causes of death in patients with NASH is cardiovascular disease. Patients with NAFLD have increased cardiovascular morbidity and mortality due to increases in atherosclerosis [5-7], arrhythmia [8; 9], and cardiomyopathy [10-12]. Several mechanisms, including endothelial dysfunction, altered lipid metabolism, systemic insulin resistance, oxidative stress, plaque formation/instability, and systemic inflammation have been proposed as ways NAFLD increases cardiovascular disease [13]. With no durable pharmaceutical interventions and lifestyle modification remaining the standard of care, a profound need exists for the identification of novel therapeutic targets in the treatment of NAFLD [14].

As mitochondrial dysfunction contributes to NAFLD pathogenesis, a better understanding of mitochondrial metabolism in NAFLD may reveal potential therapeutic targets. While not all studies have been concordant [15], five independent methodologies have observed increased hepatic oxidative energy fluxes [i.e., tricarboxylic acid (TCA) cycle flux and gluconeogenesis] in obesity and/or NAFLD [16-20]. Oxidative flux provides a fate for a portion of excess delivered fat, but does not fully compensate for the hepatocyte load, contributing to ectopic fat accumulation. Acting as an overflow for the hepatocyte TCA cycle, particularly active when carbohydrates are in short supply, hepatic ketogenesis can provide an additional fate for excess fat.

1.2 Ketone body metabolism

At a basic level, ketone body metabolism (**Figure 1.2**), consists of ketone body production (ketogenesis) and ketone body consumption (ketolysis) [21]. Ketogenesis predominantly occurs in the mitochondria of hepatocytes where fatty acid β-oxidation-derived acetyl coenzyme A (acetyl-CoA) undergoes a sequence of reactions, requiring the fate-determining mitochondrial matrix enzyme 3-hydroxymethylglutaryl-CoA synthase 2 (HMGCS2), to generate the ketone body acetoacetate (AcAc). AcAc is then reduced to D-β-hydroxybutyrate (D-βOHB) by the mitochondrial phosphatidylcholine-dependent, inner membrane-associated enzyme D-βOHB dehydrogenase (BDH1), which catalyzes a near-equilibrium reaction requiring oxidized (NAD^+) and reduced (NADH) forms of nicotinamide adenine dinucleotide. Through BDH1, hepatocyte ketogenesis oxidizes

mitochondrial NADH back to NAD^+, and the AcAc/D-βOHB ratio is proportional to the mitochondrial NAD^+/NADH equilibrium [22-24].

Although the transporters required for mitochondrial to cytoplasmic transfer of ketone bodies have yet to be identified, ketones are exported across the hepatocyte plasma membrane into the circulation and imported into extrahepatic tissues via monocarboxylate transporters 1 and 2 (MCT1and MCT2) [25; 26]. After AcAc and D-βOHB are released into the circulation, extrahepatic mitochondria terminally oxidize ketone bodies. Through mass action, mitochondrial BDH1 oxidizes D-βOHB back to AcAc, and mitochondrial succinyl-CoA:3-oxoacid-CoA transferase (SCOT, encoded by nuclear *Oxct1*) catalyzes the obligate fate-committing reaction ultimately converting AcAc to acetyl-CoA [25].

In healthy adults, concentrations of ketone bodies fluctuate between 50 and 250 μM and contribute as little as ~5% of total energy expenditure in the fed state, increasing to ~20% in the fasted and starved states [21; 27; 28]. Larger oscillations in circulating ketone body levels occur upon fasting, acutely after exercise, during adherence to low-carbohydrate, high-fat diets, in the neonatal period, and during late pregnancy [29]. Prolonged exercise or a 24-hour fast can increase circulating ketone body levels to nearly 1 mM, but this is nowhere near the ketone body concentrations upwards of 20mM seen in pathological states such as diabetic ketoacidosis [27; 29]. Despite a more rapid induction in response to fasting than humans, mice remain an excellent model of human ketone turnover, with similar excursions in circulating concentrations during the fed-fast cycle, as well as comparable rates of ketone body appearance and disposal [20; 21].

1.3 Regulation of ketone body turnover

As acetyl-CoA is the substrate for ketogenesis, any process affecting acetyl-CoA levels, such as hepatic carbohydrate fluxes, mitochondrial redox potential, β-oxidation rates, concentration of TCA cycle intermediates, and insulin/glucagon signaling, will alter the rate of ketogenesis [30-33]. Additionally, ketogenesis is regulated at the transcriptional and posttranslational levels, although these mechanism remain poorly understood.

The highest expression of HMGCS2 in most mammals occurs in hepatocytes and colonic epithelium. Loss-of-function *HMGCS2* mutations in humans can cause hypoketotic hypoglycemia and coma, along with fatty liver [34]. Additionally, hepatic knockdown of *Hmgcs2* in adult mice causes hepatic injury and remodeled lipidome under high-fat-diet conditions [35; 36]. *Hmgcs2* transcription is silenced by methylation in nonketogenic tissues and the fetal liver, which is reversed at birth, allowing *Hmgcs2* to become responsive to hormonal regulators [30]. Both insulin and glucagon regulate hepatic ketogenesis postnatally. By inhibition of adipose tissue lipolysis, insulin removes the primary ketogenic substrate from the circulation, and suppresses the transcription of the *Hmgcs2* gene by phosphatidylinoxitol-3-kinase/AKT-dependent inhibition of the transcriptional factor FOXA2 [30; 37]. In contrast, glucagon stimulates transcription of the *Hmgcs2* gene via the cAMP-p300-FOXA2 signaling pathway [38]. Free fatty acids or glucocorticoid induction of peroxisome proliferator activated receptor alpha (PPARα), and its target fibroblast growth factor 21 (FGF21), can also alter *Hmgcs2* gene expression [39]. Fasting-induced ketogenesis may also be

controlled by mammalian target of rapamycin complex 1 (mTORC1), diminishing PPARα signaling.

Contrasting from HMGCS2, SCOT, encoded by the *Oxct1* gene, is expressed in all mammalian mitochondria except those of hepatocytes. Inborn errors in SCOT function present early in life, resulting in severe ketoacidosis requiring therapeutic interventions [40]. SCOT knockout mice are unable to oxidize ketones, resulting in hyperketonemic hypoglycemia and neonatal death [25]. Selective SCOT knockout models do not cause lethality, but do generate irregular phenotypes [41-45]. In hepatocytes, *Oxct1* gene expression is suppressed during the fetal to natal transition by microRNA 122 and H3K27 histone methylation [46; 47]. In prolonged ketotic states, *Oxct* mRNA, SCOT protein, and activity in heart a muscle diminish significantly, possibly in a PPAR-dependent manner, decreasing ketone body disposal.

Compared with HMGCS2 and SCOT, relatively less is known about BDH1. Contrasting with the near ubiquitous expression of SCOT, BDH1 expression varies among cell types [44]. BDH1 activity is greatest in the liver, with activity in the kidney, heart, brain, and skeletal muscle [23; 48]. This variability in activity potentially relates to the unique role of BDH1 in catalyzing both the last step of ketogenesis (primarily hepatocytes), and the first step of ketone oxidation (extrahepatic tissues). Additionally, without BDH1 expression and activity, a range of cell types, such as macrophages [44], exist which cannot utilize D-βOHB, and therefore can only oxidize AcAc. Loss of BDH1 function in humans has not been reported, suggesting either mild physiological or, less likely, severe developmental

consequences. Germline BDH1 deficiency in mice in compatible with life, only leading to subtle impairments of fasting liver lipid content [34]. Selective loss of BDH1 in cardiac myocytes exacerbates heart failure, suggesting an adaptive and protective function of D-βOHB oxidation in these cells [49]. As with *Hmgcs2*, *Bdh1* in the liver is responsive to a ketogenic diet in a PPARα-FGF21-dependent manner [39], and in heart and skeletal muscle under ketotic states, *Bdh1* gene expression becomes diminished, mirroring *Oxct1* expression [50].

HMGCS2, SCOT, and BDH1 are marked by various post translational modifications (PTMs). In response to ketogenesis, catalytic activity of HMGCS2 is enhanced by serine phosphorylation [51]. Sirtuin 3 (SIRT3) deacetylates lysine residues and may activate HMGCS2, while lysine residues of HMGCS2 and BDH1 are targets for succinylation in hepatic mitochondria [52-54]. Succinyl-CoA, 3-methylglutaryl-CoA, glutaryl-CoA, and HMG-CoA acylation nonenzymatically modify HMGCS2 and BDH1 [55]. However, the physiological roles of these PTMs all remain incompletely defined.

1.4 Ketones and nonalcoholic fatty liver disease

Unfortunately, the specific roles of mitochondrial dysfunction remain unclear in NAFLD pathogenesis. While several studies report increased hepatic oxidative fluxes in obesity and/or NAFLD [16-20], an opposing view contends that mitochondrial fat oxidation is normal, or diminished in NAFLD, and that increasing liver fat oxidation could provide therapeutic benefit. As such, agents that augment liver fat oxidation, including ketogenic diets, intermittent fasting, and ketogenic

pharmacotherapies (i.e. acetyl-CoA carboxylase inhibitors, FGF21, sodium/glucose cotransporter 2 inhibitors) are emerging as potential treatments for obesity, insulin resistance, and NAFLD [56-59]. However, numerous examples exist in skeletal muscle and in liver whereby decreasing mitochondrial fuel supply optimizes energy supply/demand balance in a manner that may not decrease steatosis, but could diminish tissue injury and insulin resistance [60; 61].

Ketogenesis provides an index of hepatic fat oxidation, however independent quantifications of both ketogenesis and TCA cycle flux are needed for a complete index of hepatic fat oxidation. For instance a recent study showed that fasting hepatic ketogenesis rates are inversely correlated with the severity of hepatic steatosis in human NAFLD, while fasting TCA cycle flux was directly correlated with hepatic steatosis [62]. Decreasing fasting ketogenesis as NAFLD progresses in consistent with prior reports comparing human liver biopsies, which show that hepatic HMGCS2 and BDH1 protein decrease in progressive human NASH, with corresponding decreases in fasting circulating ketone bodies [63]. Additionally, loss of hepatic ketone metabolism has been linked to increased liver injury and fibrosis [35].

Moreover, ketogenesis rates vary in NAFLD. In livers with simple steatosis, ketogenesis is preserved or increased [16-20; 36; 64], while NASH progression in humans and animal models correlates with decreased ketogenesis and decreased expression of enzymatic mediators of ketone metabolism, before TCA cycle flux becomes impaired [17; 20; 64-69]. As there is rapidly-emerging interest in exploiting oscillatory feeding behavior, ketogenic diets, and exogenous ketone

therapies as prospective health-promoting, therapeutic, and performance-enhancing agents, the time is particularly ripe for a mechanistic determination of the role ketone metabolism and signaling in liver [22; 28; 70-75].

Our group previously observed that treatment with exogenous AcAc attenuates hepatic fibrosis in wild-type mice fed a fibrogenic diet for 4 weeks, while D-βOHB administration modestly exacerbates fibrosis [44]. As the interconversion of AcAc and D-βOHB involves an oxidation-reduction (redox) reaction catalyzed by BDH1, this result suggests that mitochondrial redox potential, which is predominantly set by the NAD^+/NADH ratio, may contribute to the fibrotic response. Considering the single histological feature of NAFLD associated with long-term mortality is fibrosis [3; 76], these results warranted further investigation.

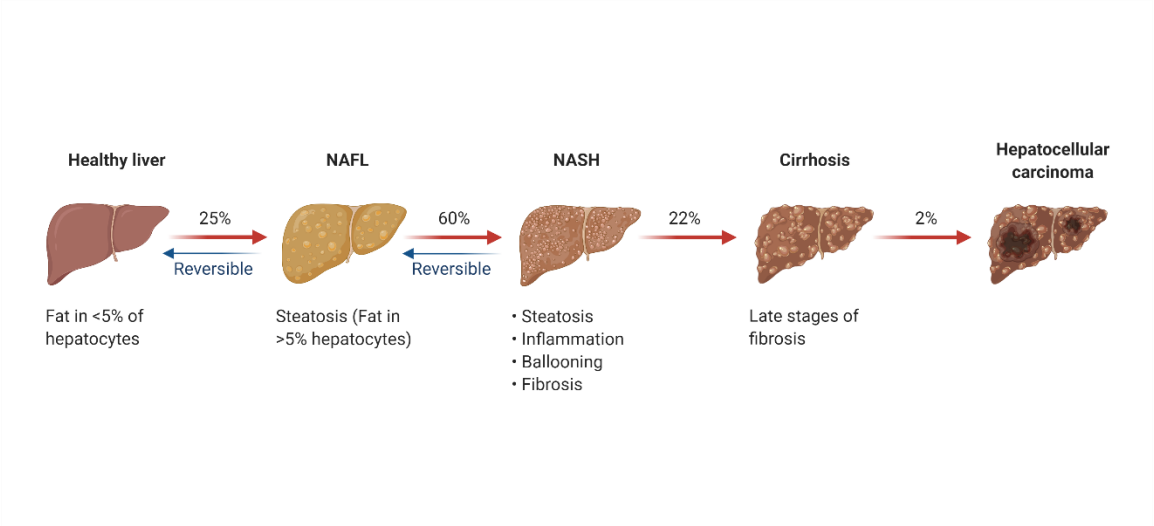

Figure 1.1. Progression of Nonalcoholic fatty liver disease. Schematic detailing the progression of NAFLD from simple steatosis (NAFL), to NASH, cirrhosis and hepatocellular carcinoma. Abbreviations: NAFL, nonalcoholic fatty liver; NASH, nonalcoholic steatohepatitis. Figure created with BioRender.com

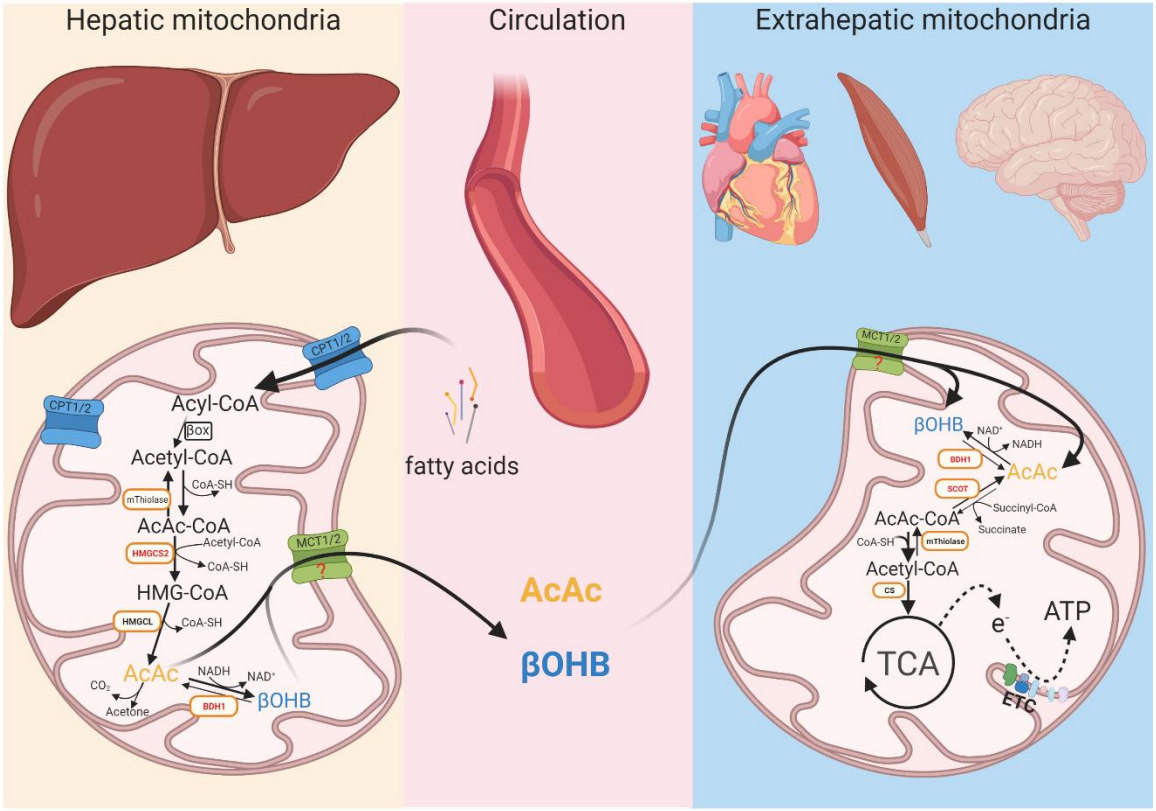

Figure 1.2. Overview of Ketone body metabolism. Ketone bodies are primarily generated in hepatic mitochondria from fatty acid-derived acetyl-CoA by the sequence of reactions requiring the fate-committing enzyme HMGCS2. AcAc and βOHB are transported through the circulation to extrahepatic tissues for terminal oxidation through reactions requiring the enzyme SCOT. Abbreviations: AcAc, acetoacetate; ATP, adenosine triphosphate; BDH1, D-β-hydroxybutyrate dehydrogenase 1; βOHB, β-hydroxybutyrate; βox, β-oxidation; CoA, coenzyme A; CoA-SH, CoA sodium salt hydrate; CPT, carnitine palmitoyltransferase; Cs, citrate synthase; e^- electron; ETC, electron transport chain; HMGCL, 3-hydroxymethylglutaryl-CoA lyase; HMGCS2, 3-hydroxymethylglutaryl-CoA synthase 2; mThiolase, mitochondrial thiolase; SCOT, succinyl-CoA:3-oxoacid-CoA transferase; TCA, tricarboxylic acid. Question marks represent uncertain molecular identity of mitochondrial ketone transporters. Figure created with Biorender.com.

Chapter 2: Ketone interconversion and the effects of hepatocyte-specific D-β-hydroxybutyrate dehydrogenase loss

This chapter was adapted with permissions from the following article:

Stagg DB, Gillingham JR, Nelson AB, Lengfeld JE, d'Avignon DA, Puchalska P, Crawford PA. Diminished ketone interconversion, hepatic TCA cycle flux, and glucose production in D-β-hydroxybutyrate dehydrogenase hepatocyte-deficient mice. Mol Metab. 2021 Jun 8;53:101269. doi: 10.1016/j.molmet.2021.101269. Epub ahead of print. PMID: 34116232; PMCID: PMC8259407.

Abstract

Objective: Throughout the last decade, interest has intensified in intermittent fasting, ketogenic diets, and exogenous ketone therapies as prospective health-promoting, therapeutic, and performance-enhancing agents. However, the regulatory roles of ketogenesis and ketone metabolism on liver homeostasis remain unclear. Therefore, we sought to develop a better understanding of the metabolic consequences of hepatic ketone body metabolism by focusing on the redox-dependent interconversion of acetoacetate (AcAc) and D-β-hydroxybutyrate (D-βOHB).

Methods: Using targeted and isotope tracing high-resolution liquid chromatography-mass spectrometry, dual stable isotope tracer nuclear magnetic resonance spectroscopy-based metabolic flux modeling, and complementary physiological approaches in novel cell type-specific knockout mice, we quantified the roles of hepatocyte D-β-hydroxybutyrate dehydrogenase (BDH1), a

mitochondrial enzyme required for NAD^+/NADH-dependent oxidation/reduction of ketone bodies.

Results: Exogenously administered AcAc is reduced to D-βOHB, and increases hepatic NAD^+/NADH ratio, reflecting hepatic BDH1 activity. Livers of hepatocyte-specific BDH1 deficient mice produced no D-βOHB, but due to extrahepatic BDH1, these mice nonetheless remained capable of AcAc/D-βOHB interconversion. Compared to littermate controls, hepatocyte specific BDH1 deficient mice showed diminished liver tricarboxylic acid (TCA) cycle flux and impaired gluconeogenesis, but normal overall hepatic energy charge. Glycemic recovery after acute insulin challenge was impaired in knockout mice, but they were not more susceptible to starvation-induced hypoglycemia.

Conclusions: Ketone bodies influence liver homeostasis. While liver BDH1 is not required for whole body equilibration of AcAc and D-βOHB, loss of the ability to interconvert these ketone bodies in hepatocytes results in impaired TCA cycle flux and glucose production. Therefore, through oxidation/reduction of ketone bodies, BDH1 is a significant contributor to hepatic mitochondrial redox, liver physiology, and organism-wide ketone body homeostasis.

2.1 Introduction

With rapidly emerging interest in exploiting intermittent fasting, ketogenic diets, and exogenous ketone therapies as prospective health-promoting, therapeutic, and performance-enhancing agents, the role of ketone metabolism and signaling in

liver remains relatively underexplored [28; 70; 71; 77; 78]. Hepatic ketogenesis, acting as an overflow for the hepatocyte tricarboxylic acid (TCA) cycle, is a source of energy particularly engaged when carbohydrates are in short supply. Robust ketogenesis occurs through a fate-committing reaction catalyzed by the mitochondrial matrix enzyme 3-hydroxymethylglutaryl-CoA synthase (HMGCS2), which generates HMG-CoA from β-oxidation-derived acetoacetyl-CoA and acetyl-CoA [22]. After a lyase-dependent release of acetyl-CoA from HMG-CoA, the ketone body acetoacetate (AcAc) is formed, which is then reduced to D-β-hydroxybutyrate (βOHB) by the mitochondrial matrix enzyme D-βOHB dehydrogenase (BDH1), which catalyzes a near-equilibrium reaction requiring reduced (NADH) and generating oxidized (NAD^+) forms of nicotinamide adenine dinucleotide [23; 24; 79]. AcAc and D-βOHB are released into the circulation for extrahepatic terminal oxidation. Through mass action, mitochondrial BDH1 oxidizes D-βOHB back to AcAc, and mitochondrial succinyl-CoA-oxoacid transferase (SCOT, encoded by nuclear gene *Oxct1*) catalyzes the obligate fate-committing reaction ultimately converting AcAc to acetyl-CoA [25]. SCOT is a mitochondrial enzyme that transfers a CoA moiety to AcAc, supporting its ultimate conversion to acetyl-CoA, and is abundant in all mammalian mitochondria except those of hepatocytes [22]. HMGCS2 is relatively restricted to hepatocytes, and thus the liver is likely the only organ capable of contributing to circulating ketone bodies [30]. In contrast to the near ubiquitous expression of SCOT, BDH1 expression varies among cell types [44]. BDH1 activity is greatest in the liver, with activity in the kidney, heart, brain, and skeletal muscle [23; 48]. This variability in

activity potentially relates to the unique role of BDH1 in catalyzing both the last step of ketogenesis (primarily hepatocytes), and the first step of ketone oxidation (extrahepatic tissues).

The liver plays a central role in equilibrating circulating AcAc and D-βOHB [80]. As the ratio of circulating AcAc/D-βOHB is directly proportional to the liver mitochondrial NAD^+/NADH ratio, BDH1 activity modulates mitochondrial redox potential [24; 81]. With this in mind, any perturbations to the circulating ketone equilibrium, *i.e.,* exogenous ketones, could influence liver mitochondrial redox potential. To test this hypothesis, we generated a hepatocyte-specific BDH1-deficient mouse model. Using intersectional approaches in physiology and analytical biochemistry of static and dynamic metabolic signatures, we quantified the role of this hepatic ketone equilibration reaction on both liver and whole-body metabolism in the chow-fed and fasted states.

2.2 Materials and methods

2.2.1 Animals and diet

All animal experiments were approved by the Institutional Animal Care and Use Committee at the University of Minnesota. Hepatocyte-specific BDH1 knockout mice (KO) were generated by crossing *Bdh1*^{flox} mice [49] to mice expressing Cre recombinase under control of the albumin promoter [82] and maintained for at least 10 generations on a C57BL/6NJ sub-strain hybrid background (Albumin-Cre X *Bdh1*$^{flox/flox}$). Littermate Cre-negative (*Bdh1*$^{flox/flox}$) mice were used as controls.

Primer sequences used for genotyping are listed in **Supplemental Table 2.1.** Adult male and female mice (as identified in **Results** and **Figure Legends**) over the age of 12 weeks were used for all experiments. Mice were maintained on a standard low-fat chow diet (2016 Teklad global 16% protein rodent diet) and received autoclaved water ad libitum. A cohort of wild-type control mice was maintained on a 60% high fat diet (D12492; Research Diets; 60% kcal fat, 20% protein, 20% carbohydrate). Mice were housed on corncob bedding in groups of 4 to 5 with lights off between 2000 and 0600 in a room maintained at 22°C. For fasting experiments, mice were housed on paper bedding with water provided ad libitum. Overnight, 18h fasts commenced at 1600 with experiments conducted at 1000 the next day. If mice were used for multiple studies, at least 1 week lapsed between experiments.

2.2.2 Exogenous delivery of ketones

Ethyl-acetoacetate (ethyl-AcAc) was obtained from Millipore Sigma (W241512). (R)-(-)-3-Hydroxybutyric acid sodium salt was obtained from Santa Cruz Biotechnology (sc-229050). Ethyl-[U-$^{13}C_4$]AcAc and sodium D-[U-$^{13}C_4$]βOHB salt were purchased from Cambridge Isotope Laboratories (CIL, CLM-3297 and CLM-3853 respectively). AcAc and [U-$^{13}C_4$]AcAc were synthetized by the base-catalyzed hydrolysis of ethyl-AcAc or ethyl-[U-$^{13}C_4$]AcAc, respectively, as previously described [44]. To control for the equimolar quantity of ethanol produced in the synthesis of AcAc, equimolar quantities of ethanol were added to D-βOHB, D-[U-$^{13}C_4$]βOHB, and saline vehicle control preparations. Random-fed male mice received an intraperitoneal (i.p.) injection of unlabeled ketones at 10 μmol/g body

weight or ^{13}C-labeled ketones at 1 μmol/g body weight. For circulating ketone assessments, serum was obtained prior to and at multiple time points post injection for ketone body quantification. For liver energy metabolite assessments, 15 minutes post ketone or vehicle injection, mice were sacrificed by cervical dislocation, and livers were harvested and freeze-clamped within 15 seconds.

2.2.3 Serum ketone body quantification

Serum ketones were quantified using a method previously described by our group [83]. For serum or perfusion effluent (see **Section 2.2.9**) samples containing unlabeled ketones, 10 μL of diluted serum/perfusion effluent were extracted with 40 μL of cold 1:1 acetonitrile:methanol containing the internal standards [3,4,4,4-D_4]βOHB and [U-$^{13}C_4$]AcAc both at 50 μM. Samples were vortexed, and centrifuged at 4°C, 15,000 x g for 10 min before analyzing the supernatant by UPLC-MS/MS. As this method utilizes [U-$^{13}C_4$]AcAc as an internal standard, it cannot be used to quantify serum levels of [U-$^{13}C_4$]AcAc. For samples containing ^{13}C-labeled ketones, first 4 μL of the internal standard [3,4,4,4-D_4]βOHB (50 μM) was added to 20 μL of diluted serum. 24 μL of freshly prepared 1.8 M $NaBD_4$ in 0.1 M NaOH was next added, resulting in the reduction of [U-$^{13}C_4$]AcAc present in serum to [3-D_1,U-$^{13}C_4$]βOHB. After incubating for 5 min at room temperature, 44 μL of acetonitrile was added and samples were vortexed. Following centrifugation at 4°C, 15,000 x g for 10 min, samples were loaded into a cation exchange column, necessary to desalt the sample of excess Na^+, eluted in 3 mL of LC-MS grade water, and dried via SpeedVac. Dried samples were resuspended in 48 μL of 98%

H_2O/2% methanol/0.0125% acetic acid, vortexed, and centrifuged at 4°C, 15,000 x g for 10 min before analyzing the supernatant by UPLC-MS/MS.

2.2.4 Energy metabolite quantification

Frozen liver sections (weighed frozen) or mitochondrial pellets (quantified by protein content) were homogenized in an 0.4 M perchloric acid, 0.5 mM EGTA extraction solution containing [$^{13}C_{10}$,$^{15}N_5$]ATP sodium salt (100 µM), [$^{13}C_{10}$,$^{15}N_5$]AMP sodium salt (100 µM), [1,2-$^{13}C_2$]acetyl-CoA lithium salt (5 µM), and [1,2,3-$^{13}C_3$]malonyl-CoA lithium salt (5 µM) purchased from Sigma. After incubation on ice for 10 min, samples were centrifuged at 15,000 x g for 15 min at 4°C. The resulting supernatants were neutralized with freshly prepared 0.5 M K_2CO_3, vortexed, and centrifuged at 15,000 x g for 30 min at 4°C. Final extracts were then analyzed by LC-MS/MS as previously described with modifications [84]. Briefly, analysis of energy metabolites was performed using a Vanquish LC system. Separation was achieved on a reverse-phase C_{18} column (Waters Xbridge , 150 x 2.1 mm, 3 µm) using the following mobile phases: A) 95% water/5% methanol with 4 mM dibutylammonium acetate (DBAA, Millipore Sigma, 73345) and B) 25% water/75% acetonitrile with 4mM DBAA. The Ion-pairing mobile phase additive DBAA provided for adequate chromatographic separation. Samples were separated using the following binary gradient: 0-80% B for 8 min, 80-100% B for 5 min, 100% B for 3 min, and 100-0% B for 5 min. The flow rate was 100 µL/min, with a diverter valve used for the first 2 min to minimize matrix components entering the MS. The column was maintained at 30°C and the injection volume was 2 µL. The LC system was hyphenated to a Thermo Q Exactive Plus MS equipped with

heated electrospray ionization. The MS was operated in positive ionization mode with PRM mode used for quantitative targeted analysis. The isolation window was set to *m/z* 1.0, resolution was 17,500, and collision energy 35 (arbitrary units). Retention times and *m/z* transitions for each metabolite are detailed in **Supplemental Table 2.2**.

2.2.5 Immunoblot

Protein extracts were prepared in a protein lysis buffer (PLB) containing 20 mM Tris, 150 mM NaCl, 1 mM EDTA, 1% Triton-X 100, protease inhibitors (Roche) and phosphatase inhibitors (Sigma) as previously described [45]. Whole tissue protein lysates were prepared from frozen tissues and homogenized in ten times volume (microliters) to mass PLB. Protein targets of interest were probed with the following primary antibodies: HMGCS2 (Santa Cruz, Sc-33828), BDH1 (Atlas Antibodies, HPA030947), pAMPKα (Thr172), total AMPKα, pAKT (Ser473), and total AKT (Cell Signaling, 2535, 2532, 9271, and 9272 respectively). Horseradish peroxidase (HRP)-conjugated secondary antibodies included goat anti-rabbit IgG and goat anti-mouse IgG (Southern Biotech 4030-05 and 1015-05 respectively). Protein loading was assessed by BlotFastStain (G-Biosciences, 786-34), or by immunoblot against actin (Sigma A2066) and HRP-conjugated goat anti-rabbit IgG. Blots were developed using Immobilon Cresendo Western HRP substrate (Millipore Sigma, WBLUR0500) and imaged using film or Bio-Rad ChemiDoc MP imaging system. Band intensities were densitometrically quantified using ImageJ software.

2.2.6 Histology and immunohistochemical staining

Following euthanasia by cervical dislocation, mouse liver sections were either fixed in 10% neutral buffered formalin or cryo-preserved in OCT compound. Formalin tissue embedding, sectioning, and staining with hematoxylin and eosin was performed by the University of Minnesota Clinical and Translational Science Institute histology core. Frozen liver sections preserved in OCT were cut in 10 µm slices using a Leica CM1860 Cryostat at -20°C. Tissue sections were fixed on slides using 2% paraformaldehyde for 1h, permeabilized for 20 min in 0.25% Triton-X 100, and blocked in 5% BSA/PBS/0.1% Triton-X 100 for 1h. Rabbit anti-BDH1 (Atlas Antibodies, HPA030947) was incubated for 1h at room temperature, followed by Alexa Flour 488 conjugated goat anti-rabbit IgG (Invitrogen, A11008) for 30 min and mounted with Vectashield mounting medium with DAPI (Vector Laboratories, H1200). Primary and secondary antibodies were prepared in 5% BSA/1x PBS/0.1% Triton-X 100. Images were obtained using a Leica DM5500 B microscope.

2.2.7 Gene expression analysis.

RNA was purified from liver or kidney lysates homogenized in RLT buffer (Qiagen) with 1% 2-Mercaptoethanol using the RNeasy Mini Kit (Qiagen, 74016) following the manufacturer's instructions. Reverse transcripts were generated using Iscript (Bio-Rad, 1708891) and real-time reverse-transcription polymerase chain reaction (RT-PCR) was performed using SsoAdvanced Universal SYBR Green Supermix (Bio-Rad, 172-5274) on a CFX384 Real-Time System (Bio-Rad). Transcripts were quantified using the $2^{-\Delta\Delta Ct}$ method. Liver and kidney transcripts were normalized to

Rpl32 and *Rna18s5* respectively. Primer sequences used for gene expression are listed in **Supplemental Table 2.3**.

2.2.8 Serum measurements

Blood was acquired via submandibular bleed for fasting serum measurements. Blood glucose measurements were performed in duplicate using two CVS Health Advanced glucometers per collection, and the mean was taken. If the variance exceeded 10%, a third reading was taken and the outlier removed. Non-esterified fatty acids (NEFA; Fujifilm, HR Series NEFA-HR2), triacylglycerols (TAG; Thermo Scientific, TR22421), and cholesterol (Fujifilm, 999-02601 and 993-02501) serum measurements were made using colorimetric assays following the manufacturer's instructions. ELISAs were used to measure serum insulin (Millipore Sigma, EZRMI-13K) and glucagon (Mercodia, 10-1271-01). All colorimetric assays were quantified using a Biotek Synergy HTX plate reader. HOMA-IR values were calculated as (Blood glucose (mg/dL) X Insulin (μU/mL)] / 405) [85].

2.2.9 Metabolic flux studies

Portal vein perfusions were performed as previously described [36]. Briefly, mice were anesthetized with 50 μL of sodium pentobarbital (65 mg/mL, Vortech) administered i.p., and once fully unconscious and unresponsive to toe pinch (approximately 5 minutes following delivery), the portal vein was exposed and cannulated with a 24-gauge catheter needle, the abdominal aorta and inferior vena cava cut, and the catheter was firmly tied into the portal vein. The beating heart was then exposed, and right atrium cut to prevent recirculation of buffer to the liver

and to terminate perfusion to the brain. Livers were perfused with an oxygenated, glucose-free Krebs-Henseleit buffer, containing 3% $^{2}H_2O$, 0.1 mM sodium [U-$^{13}C_3$]propionate, 1.5 mM sodium lactate, 0.15 mM sodium pyruvate, 0.25% glycerol, and unlabeled 0.2 mM sodium octanoate as an exogenous fat source. The buffer was prewarmed to 45°C (determined empirically to counter heat loss in tubing such that tissue delivery is maintained at physiological temperature) in a thermostat-controlled water bath. The buffer delivery was maintained at a rate of 8 mL/min using a peristaltic pump for a period of 1 hour. The perfusate effluent from the final 30 minutes of the procedure was collected and frozen for further processing. Hepatic oxidative fluxes were quantified using a ^{2}H-NMR and ^{13}C-NMR based approach as previously detailed [35; 36] by profiling monoacetone [$^{13}C/^{2}H$] glucose derivatized from hepatic venous effluent $^{13}C/^{2}H$-labeled glucose. ^{1}H-NMR, as previously described, was used to quantify total hepatic glucose and acetate production, octanoate consumption, and the uniformity of the perfusion procedure from separate perfusate effluent aliquots collected every 10 minutes. Perfusion effluent ketone bodies were quantified by LC-MS/MS as described in **Section 2.2.3** to determine their rates of production. Acetyl-CoA accounting was performed by assuming that 4 moles of acetyl-CoA are produced from each mole of octanoate consumed. Each mole of βOHB, AcAc, and acetate produced consumed 2, 2, and 1 moles of acetyl-CoA respectively while each turn of the TCA cycle disposes 1 mole of acetyl-CoA. Reducing equivalents (RE) were estimated from fluxes as RE = (5.75 x TCA) + (3.5 x AcAc) + (2.5 x βOHB) + (1.75 x acetate) + (glycerol flux to glucose) – (0.1 x phospho*enol*pyruvate flux to glucose) [19].

2.2.10 Mitochondria isolation

Liver mitochondria were isolated as previously described [45]. Briefly, mice were sacrificed by cervical dislocation, livers harvested, and immediately homogenized in ice-cold mitochondrial isolation medium (MIM; 300 mM sucrose, 0.2 mM EDTA, 10 mM Na HEPES, BSA 1 mg/mL, pH 7.4). Homogenates were centrifuged at 600 x g for 10 min at 4°C, and the resulting mitochondria-containing supernatant, was further centrifuged at 8000 x g for 15 min at 4°C. Mitochondrial pellets were resuspended in ice-cold MIM, aliquoted, and centrifuged again at 8000 x g for 15 min at 4°C. Pellets were briefly washed in ice-cold MIM without BSA, then snap frozen for down-stream assays. Mitochondrial protein content was quantified by BCA protein assay kit per the manufacturer's instructions (Thermo Fisher 23225).

2.2.11 NAD^+/NADH mass action ratio

For quantification of α-ketoglutarate and glutamate, frozen liver tissue was lyophilized and extracted as described previously [44], using cold (-20°C) 2:2:1 methanol:acetonitrile:H_2O containing an appropriate amount of the internal standard [U-$^{13}C_5$]glutamine (CIL). Extracted liver samples were spiked with 20 mM ammonium phosphate to improve peak shape [86], then analyzed by LC/MS using Waters Acuity UPLC BEH Amide (130Å, 1.7 µm, 2.1 mm X 150 mm) with the following mobile phases: A) 10 mM ammonium acetate and 10 mM ammonium hydroxide in 95% water, and B), 10 mM ammonium acetate and 10 mM ammonium hydroxide in 95% acetonitrile. Separation was performed using the following gradient: 100% B for 2 min, 100-30% B for 3 min, 30-20% B for 1.5 min, 20-30% B for 0.5 min, 30-100% B for 0.5 min, and 100% B for 2.5 min. Separation was

carried out at a flow rate of 0.4 mL/min, column temperature 45°C, and sample injection volume of 4 µL. A Thermo Q Exactive Plus MS in PRM mode was used for quantitative targeted analysis. The mass spectrometer operated in negative ion mode with optimized HESI conditions: sheath gas 35, Auxiliary gas 10, Sweep gas 1, Spray voltage 3.6, Capillary temperature 275°C, S lens RF 50, and Auxiliary gas temperature 150°C. For PRM mode, the AGC target was set to 2e5, while the resolution was set to 17,500. Retention times, *m/z* transitions, and optimal normalized collision energies [N(CE)] for each metabolite are detailed in **Supplemental Table 2.4**. The linearity between α-ketoglutarate or glutamate and internal standard were checked, and correction factor calculated based on three independently prepared calibration curves. Ammonia was quantified from frozen liver tissue by a colorimetric assay (Sigma, AA0100) per the manufacturer's instructions. The mass action NAD^+/NADH ratio was then calculated as previously described [87].

2.2.12 Insulin and glucose tolerance tests

Blood glucose measurements were performed prior to, and at regular intervals following intraperitoneal insulin/glucose injection. For intraperitoneal insulin tolerance tests (IPITT), male mice were administered i.p. human insulin (Lilly, HI-213) at 0.75 U/Kg body weight for 18h fasting tests, or 1 U/Kg body weight for 4h fasting and random fed tests. For glucose tolerance tests (IPGTT), after fasting overnight (18h), a bolus of a sterile-filtered glucose solution was delivered i.p. to female (2 mg glucose/g body weight) or male (1 mg glucose/g body weight) mice. The dosage of glucose for male mice was lowered because the 2 mg glucose/g

body weight dose resulted in blood glucose readings outside the range of our glucometer.

2.2.13 Kidney lactate tracer experiment

Sodium lactate and sodium [U-$^{13}C_3$]lactate were purchased respectively from Millipore Sigma (L7022), and CIL (CLM-1579). Overnight-fasted male mice were administered [U-$^{13}C_3$]lactate (5 µmol/g body weight) by i.p. injection. Fifteen minutes post injection, mice were sacrificed by cervical dislocation, kidneys harvested, and rapidly freeze-clamped. Kidney tissue was lyophilized prior to extracting metabolites using cold (-20°C) 2:2:1 methanol:acetonitrile:H_2O. Kidney metabolites were then analyzed using the LC/MS parameters detailed in **Section 2.2.11**. Detected TCA metabolites were validated by use of external standards. Thermo Quan Browser was used to integrate peaks manually using a mass tolerance of 5 ppm and retention time window of 30 seconds. All possible isotopologues were integrated. Metabolite enrichment was corrected for natural abundance using R package, IsoCorrectoR, as previously described [88].

2.2.14 Statistical analyses

Analyses were performed with GraphPad version 9.0.0 software (Prism, San Diego, CA) using tests described in the figure legends. P values describe comparisons between (or among) group means for measured values, accounting for the variances. Confidence intervals (CI, 95%) or percent differences within the text define the range spanning fold- or percent differences between groups.

2.3 Results

2.3.1 Distinct effects of exogenous AcAc versus D-βOHB on circulating ketones and liver redox

To determine the equilibration kinetics of exogenously delivered ketones, random fed, wild type mice were injected with an intraperitoneal (i.p.) bolus of either AcAc, D-βOHB (both at 10 μmol/g body weight), or vehicle control. Tail bleeds were performed prior to injection and at regular intervals post-injection. Serum ketones were extracted and measured by LC-MS/MS using a recently developed method [83]. No differences in serum levels of AcAc, βOHB, or total ketone bodies (TKB), were observed prior to injections (compare the three panels of **Supplemental Figure 2.1A**). At 15 min post injection, both AcAc and D-βOHB injected mice showed sharp increases in circulating TKB with minimal change in vehicle injected mice (**Figure 2.1A**). Vehicle injected mice showed a minimal increase in TKB at 60 min that dissipated by 120 min (note graph inset, left panel of **Figure 2.1A**), perhaps attributable to modest stress-induced lipolysis [89].

Injection of exogenous AcAc increased serum concentrations of both AcAc and βOHB, with βOHB concentrations surpassing those of AcAc by 30 min. In contrast, injection of exogenous D-βOHB predominantly increased serum βOHB levels, with only minimal increase in serum AcAc. BDH1 catalyzes the NAD^+/NADH-dependent redox reaction responsible for the interconversion of AcAc and D-βOHB (**Figure 2.1B**), and equilibration of circulating ketones has been posed to occur exclusively in the liver [80]. Collectively, these results suggest two

fates for circulating AcAc: (i) equilibration into the circulating D-βOHB pool and (ii) terminal disposal, largely via oxidation in extrahepatic tissues. Conversely, bolus-delivered D-βOHB does not as readily equilibrate into the circulating AcAc pool but is nonetheless rapidly and terminally disposed via oxidation in extrahepatic tissues. These findings are consistent with the K_{eq} of the reaction catalyzed by NAD^+/NADH-dependent BDH1, which favors D-βOHB production, but mass action can drive terminal oxidation of D-βOHB [24; 79].

To determine if the reduction of exogenously delivered AcAc to D-βOHB, and corresponding oxidation of NADH to NAD^+, could alter liver redox status, randomly fed, wild-type mice were injected with an i.p. bolus of AcAc, D-βOHB, or vehicle control. Fifteen minutes post injection, mice were sacrificed via cervical dislocation and livers were immediately freeze clamped for quantification of energy-related metabolites by LC-MS/MS. Livers of mice receiving exogenous AcAc showed a modest but non-statistically significant increase (17.3 ± 7.2%, p = 0.11) in hepatic NAD^+ concentration over that of vehicle-treated controls, with a modest but non-statistically significant decrease in NADH content, together leading to an increased NAD^+/NADH ratio (29.9 ± 6.2%, $p < 0.05$; **Figure 2.1C**). NAD^+ and NADH contents of livers of mice injected with exogenous D-βOHB were not significantly different from vehicle controls, suggesting that exogenous AcAc, but not D-βOHB, can transiently alter liver redox status.

Pioneering studies [24; 31; 80; 81] revealed the relationship among ketogenesis, mitochondrial redox, and liver metabolism. However, interventional testing of this relationship has been tested only preliminarily, and it has not been

fully characterized in pathological states. Previous work by our group and others has shown that rates of ketogenesis increase when mice are maintained on a high fat diet (HFD) [19; 36]. However, humans with steatotic livers exhibit decreased ketogenesis and overall decreased equilibration between AcAc and D-βOHB in the fasting state [62]. To determine whether expression of hepatic mediators of ketogenesis is dynamic in response to HFD, we quantified hepatic HMGCS2 and BDH1 protein abundances in 26-week-old wild type maintained on either a chow, or on a 60% HFD for 16 weeks. Although HMGCS2 expression was unchanged with HFD treatment, BDH1 expression was significantly increased (**Supplemental Figure 2.1B-C**). Whether dynamic expression of BDH1 is a cause, consequence, or bystander of altered ketone turnover is unclear. To determine the role of hepatocyte BDH1 in liver physiology, we therefore elected to study mice with hepatocyte specific deficiency of this enzyme, focusing in this study on male and female mice in the chow diet-fed and fasted states.

2.3.2 Generation of hepatocyte specific BDH1 knockout mouse

Hepatocyte-specific BDH1 knockout mice (KO) were generated by crossing an Albumin-Cre strain [82] to a *Bdh1*^{flox} allele [49] maintained on a C57BL/6NJ background. Knockout of hepatic BDH1 was confirmed by hepatic protein (immunoblot and immunohistochemistry) and mRNA abundance (**Figure 2.2A-C**). Hepatocyte-BDH1-KO mice reached weaning at the expected Mendelian ratios (**Supplemental Table 2.5**). Hepatic BDH1 expression in both male and female KO mice was greatly reduced at 4 weeks of age and completely absent by 8 weeks (**Supplemental Figure 2.2A-B**). Although hepatic loss of BDH1 increased liver

Hmgcs2 mRNA abundance (**Figure 2.2D**) no differences in HMGCS2 protein expression were observed (**Figure 2.2A, Supplemental Figure 2.2A-B**). Additionally, the knockout was specific to liver with cardiac BDH1 expression in KO mice remaining intact (**Figure 2.2E**). Fasting body weights in 26-week-old mice were similar between control and KO mice, with no significant differences in fasting serum levels of triacylglycerols (TAG), non-esterified fatty acids (NEFA), or cholesterol for both sexes (**Supplemental Figure 2.3A-C**). Additionally, no hepatic morphological differences were observed in hematoxylin and eosin-stained liver sections obtained from control and KO mice that were fasted for 18h prior to tissue harvest (**Supplemental Figure 2.3D**).

2.3.3 Hepatic BDH1 loss diminishes liver ketogenesis, but hepatic BDH1 is not required for systemic ketone equilibration

To determine the effect of hepatic BDH1 loss on circulating ketones, male and female mice were fasted 18h, and serum was collected. Compared to littermate controls, serum AcAc levels were elevated by 38.9 ± 12.0% ($p < 0.05$) in KO mice **(Figure 2.3A)** while serum βOHB levels were diminished by 57.7 ± 8.5% ($p < 0.0001$), yielding a net decrease of 34.3 ± 9.9% ($p < 0.001$) in circulating TKB in KO mice. Similar circulating ketone alterations were observed in female mice fasted for 18h (**Supplemental Figure 2.4A**), male mice fasted for 4h (**Supplemental Figure 2.4B**), and in random-fed mice of both sexes (**Supplemental Figure 2.4C-D**), although the TKB decrease was less apparent in the fed state.

To determine the distribution of ketones produced by the liver, we next performed ex-vivo portal vein perfusions in male KO and littermate control mice following an 18h fast. Sixty-minute perfusions were conducted using an oxygenated, glucose-free Krebs-Henseleit buffer, containing unlabeled 0.2 mM sodium octanoate as an exogenous fat source. The hepatic venous effluent was collected and used for LC-MS/MS ketone quantification. Livers of KO mice produced AcAc at a rate 2.3-fold (95% CI 1.8-3.0, $p < 0.0001$) greater than livers from littermate controls, while βOHB production was essentially zero at a rate of 0.04-fold (95% CI 0.03 – 0.05, $p < 0.0001$) that of littermate controls (**Figure 2.3B**). TKB production rate was diminished in livers of KO mice at a rate of 0.7-fold (95% CI 0.6 - 0.9, $p < 0.05$) relative to littermate controls.

The very high [AcAc]/[βOHB] ratio in hepatic venous effluent [28.6 (± 2.5)-to-1] from livers of perfused KO mice (**Figure 2.3B**) was discordant from that of the circulating ketone pool [1.0 (± 0.1)-to-1] in these mice (**Figure 2.3A**). Conversely, hepatic venous effluents from perfused livers of littermate control mice showed [AcAc]/[βOHB] ratios [0.47 (± 0.04)-to-1] that were much more concordant with circulating ratios [0.32 (± 0.01)-to-1]. To test the hypothesis that extrahepatic equilibration of circulating ketones explains recovery of [AcAc]/[βOHB] ratios in the circulation of Hepatocyte-BDH1-KO mice, we injected KO mice and their littermate controls (i.p.) with [U-$^{13}C_4$]AcAc (1 µmol/g body weight), and quantified the appearance of [U-$^{13}C_4$]βOHB in serum over time. Circulating [U-$^{13}C_4$]βOHB was detected at 10 and 20 min post injection in both control and KO [U-$^{13}C_4$]AcAc-treated mice, although [U-$^{13}C_4$]βOHB levels were 38.0 ± 12.8% ($p < 0.01$) and 41.6

± 12.0% ($p < 0.01$) lower in KO mice respectively (**Figure 2.3C** and **Supplemental Figure 2.4E**). Similarly, following an injection of uniformly labelled D-[U-$^{13}C_4$]βOHB, circulating [U-$^{13}C_4$]AcAc was detected in both control and KO mice, with 36.6 ± 10.7% ($p < 0.01$) and 31.5 ± 9.6% ($p < 0.01$) lower conversion in KO mice at 10 and 20 min post injection (**Figure 2.3D** and **Supplemental 2.4F**). The kinetic responses to (**Figure 2.3E**) and fractional enrichments of (**Supplemental Figure 2.4G-H**) exogenous ^{13}C-labelled ketones were concordant with the responses to unlabeled exogenous ketones (**Figure 2.1A**), with [U-$^{13}C_4$]AcAc readily reduced to [U-$^{13}C_4$]βOHB, but the oxidation product of exogenously delivered D-[U-$^{13}C_4$]βOHB, [U-$^{13}C_4$]AcAc, apparent in the circulation to much lower extent in both KO and control mice.

Responses to exogenous ^{13}C-labelled ketones strongly suggest that extrahepatic tissues contribute to the equilibration of circulating ketones in the absence of hepatic BDH1, with only a modest deficiency. In fact, hepatic loss of BDH1 increased kidney mRNA abundances for both *Bdh1* and *Hmgcs2* (**Supplemental Figure 2.5A-B**), though no differences in abundances for the encoded proteins were observed (**Supplemental Figure 2.5C**). The other theoretical source of AcAc/βOHB equilibration in the circulation is a non-BDH1-dependent hepatic enzyme such as BDH2 [90], but this is highly unlikely given the absence of any βOHB produced by perfused livers from Hepatocyte-BDH1-KO mice.

2.3.4 Loss of hepatic BDH1 diminishes TCA cycle flux, anaplerosis, and phospho*enol*pyruvate sourced gluconeogenesis without altering liver energy charge

Loss of hepatocyte BDH1 provokes a large increase in the mass action ratio of the reaction normally catalyzed by BDH1, [AcAc]/[βOHB], for ketones exported from the liver, from 0.47 in livers of littermate controls to 28.6 in the KO (**Figure 2.3B**). Application of the equilibrium constant for BDH1 (0.0493) would normally suggest a corresponding increase in mitochondrial NAD^+/NADH ratio, from ~10 to ~580, respectively in response to this [AcAc]/[βOHB] ratio increase [87]. However, the absence of BDH1 prevents hepatic mitochondrial equilibration of the two ketones and thus abrogates a conduit for NADH re-oxidation to NAD^+. Therefore, we quantified static concentrations of NAD^+ and NADH in livers of mice fasted for 18h, using an LC-MS/MS approach that quantifies these nucleotides against an authentic internal standard [84]. Intriguingly, no differences were observed between KO and control mice, either within isolated mitochondria, or at the whole-tissue level (**Figure 2.4A-B**). Furthermore, the summed static concentrations of NAD^+ and NADH did not vary between KO and control mice in both isolated mitochondria (152.1 ± 21.9 vs. 163.9 ± 28.3 nmol/mg protein, respectively, n = 6-9 per group, p = 0.75) and whole liver tissue (1,133.4 ± 34.7 vs. 1,125.4 ± 27.7 nmol/g liver, respectively, n = 10-12 per group, p = 0.86). To further assess the effect of hepatocyte BDH1 loss on liver redox, we determined the mitochondrial NAD^+/NADH mass action ratio [87] from the products and reactants of the glutamate dehydrogenase system. No differences in whole liver tissue levels of α-

ketoglutarate, glutamate, and ammonia were observed between KO and control mice (**Figure 2.4C-D**, **Supplemental Figure 2.6A**), resulting in similar mass action NAD^+/NADH ratios of 1.3 ± 0.3 and 1.1 ± 0.2 respectively, comparable to those determined by isolated mitochondria direct measurements of 1.1 ± 0.2 for KO mice and 1.4 ± 0.3 for control mice (**Figure 2.4E**).

While perhaps surprising, the absence of a difference in static NAD^+ and NADH nucleotide concentrations in hepatic mitochondria and in whole liver tissue harvested from fasting mice lacking hepatocyte BDH1, and no differences in NAD^+/NADH ratios, could be explained by several mechanisms that are not mutually exclusive. First, overall NAD^+/NADH equilibrium may be preserved by other matrix (mitochondria) and cellular (whole tissue) dehydrogenases, because BDH1 is one of several mitochondrial matrix enzymes capable of re-oxidizing NADH [24]. Second, the total nucleotide pool, much of which is protein-bound, may not reflect the free pool that is immediately accessible to matrix dehydrogenase enzymes, although measurement of the mass action ratio for the glutamate dehydrogenase system mitigates this concern [91]. A third possibility is that static NAD^+ and NADH concentrations do not reflect rates of exchange of electrons among redox reactions that determine turnover rates in oxidative metabolism, and thus absence of a difference in snapshot concentrations may not reflect an absence on NADH-dependent redox homeostasis. Therefore, because exclusively NAD^+ (and not $NADP^+$) is required to accept electrons from the intermediates α-ketoglutarate and malate as hepatic fat is terminally oxidized through in the TCA cycle, we hypothesized that loss of BDH1-dependent re-oxidation of NADH could

yield diminished TCA cycle flux due to impaired bioavailability of matrix NAD^+. To test this hypothesis, ex-vivo 60-minute portal vein perfusions were performed on littermate control and Hepatocyte-BDH1-KO mice following an overnight fast. Perfusions were performed using oxygenated Krebs-Henseleit buffer lacking glucose, but containing unlabeled 0.2 mM sodium octanoate (exogenous fat source), and flux tracers 3% ^2H_2O and 0.1 mM sodium [U-$^{13}C_3$]propionate, then collecting the hepatic venous effluent. After quantification of total glucose production and octanoate consumption using ^{1}H-NMR, the hepatic ^{13}C/^{2}H–labeled glucose pool was extracted and converted to monoacetone glucose, from which ^{2}H- and ^{13}C-NMR spectra were collected, allowing hepatic oxidative fluxes and glucose sourcing to be determined (schematized in **Figure 2.5A**) [36; 92]. Indeed, TCA cycle flux in livers of KO mice was diminished to 0.3-fold (95% CI 0.2 - 0.6, $p < 0.01$) that of littermate controls (**Figure 2.5B**) with corresponding decreases in the rates of anaplerosis, 0.5-fold (95% CI 0.3 - 0.8, $p < 0.01$, **Figure 2.5C**), and pyruvate cycling, 0.5-fold (95% CI 0.2 - 0.8, $p < 0.01$, **Supplemental Figure 2.6B**). Total hepatic glucose production (HGP) was modestly, but not significantly, decreased in KO mice (**Figure 2.5D**) with non-significant decreases in both glycogenolysis and glycerol contributions to HGP (**Supplemental Figure 2.6C-D**). As expected, given the diminution in TCA cycle flux, the contribution of phospho*enol*pyruvate (PEP, *i.e.,* TCA cycle-sourced) to HGP was decreased in KO mice to 0.5-fold (95% CI 0.3 - 0.8, $p < 0.01$) that of littermate controls (**Figure 2.5E**). No differences in the rates of acetate production were observed between KO and control mice (**Figure 2.5F**). Overall octanoate consumption was modestly

diminished in livers of KO mice, but this did not reach statistical significance (**Figure 2.5G**).

To determine if there was evidence for an energy imbalance incurred by loss of BDH1 in hepatocytes, the consumption rates of exogenously supplied octanoate were reconciled against the measured fates of octanoate oxidation, with the assumption that β-oxidation of 1 mol octanoate yields 4 mol acetyl-CoA. Terminal acetyl-CoA oxidation through the TCA cycle represented a minor fate (<1%) in control mice, and an even smaller fate for KO mice (<0.5%) for carbon available from octanoate-derived acetyl-CoA (**Figure 2.5H**). Acetate production subsumed a similar proportion of the carbon pool in both KO mice and controls, 29.2 ± 4.5% and 28.5 ± 2.0% respectively. Proportionately, total ketogenesis was the major carbon product in both KO (60.6 ± 9.2%) and control (65.9 ± 2.0) mice. However, the fraction of the oxidized carbon pool delivered as AcAc was 58.4 ± 9.1% in KO, while it was 20.6 ± 0.6% in littermate controls ($p < 0.0001$). As storage of octanoate is minimal, unaccounted fates for oxidized octanoate, 10.0 ± 3.2% in KO, 5.2 ± 2.6% in littermate controls, are likely subsumed by incompletely oxidized intermediates, including short- and medium-chain acylcarnitines, or peroxisomal β-oxidation [93; 94]. While flux through acetyl-CoA is very rapid and high capacity during fat oxidation, static concentrations of acetyl-CoA are normally very low and are thus a negligible contributor as a terminal fate of fat oxidation. Nonetheless, mitochondrial (but not whole liver) acetyl-CoA concentrations were increased 39.5 ± 9.9% ($p < 0.001$) in KO mice, with a corresponding 43.6 ± 17.5% ($p < 0.01$) diminution in mitochondrial succinyl-CoA concentrations (**Figure 2.5I** and

Supplemental Figure 2.6E), together supportive of the impaired TCA cycle flux observation acquired using an orthogonal method. Overall, however, the estimated number of reducing equivalents (RE) produced did not differ between the genotypes, with 4.5 ± 0.2 RE generated in the Hepatocyte-BDH1-KO liver, against 5.1 ± 0.4 RE in livers of littermate controls (n = 6-8 per group, p = 0.22). Thus, it was not surprising that mitochondrial and liver static tissue concentrations of ATP, ADP, and AMP, measured by LC-MS/MS using authentic internal standards from unperfused livers of fasting mice also showed no differences between genotypes (**Supplemental Figure 2.6F-G**). Moreover, no difference between total or phosphorylated hepatic AMPKα levels were observed in unperfused livers (**Figure 2.5J**). Nonetheless, significant increases in the abundances of *Ppargc1a* (1.53-fold, 95% CI 1.01 - 2.53, $p < 0.05$), *Pparg* (1.82-fold, 95% CI 1.20 - 2.76, $p < 0.01$), and *Pc* (1.57-fold, 95% CI 1.15 - 2.15, $p < 0.01$) mRNAs were shown in unperfused livers of fasting KO mice (**Figure 2.5K**). This upregulation might represent a compensation for deficits in TCA flux and TCA cycle-sourced gluconeogenesis in KO mice. Given the subtle decrease in octanoate consumption in KO mice, increases in *Acadm* (1.47-fold, 95% CI 1.05 - 2.01, $p < 0.05$) and *Cpt2* (1.42-fold, 95% CI 1.06 - 1.87, $p < 0.05$) possibly represent upregulation of β-oxidation machinery. Additionally, though not relevant to transport of medium chain fatty acids used in the perfusion experiments, upregulation of *Lipc* and *Cd36* in livers of unperfused KO mice could represent compensation to increase triglyceride hydrolysis and fatty acid uptake, respectively (**Supplemental Figure 2.6H**). No differences in *Acaca*, *Acacb*, *Acsl1*, or *Acsl3* expression between KO and control

mice were observed. Changes in liver gene expression in KO mice could represent compensatory mechanisms to maintain energy homeostasis in the context of challenged redox control.

2.3.5 Hepatic loss of BDH1 alters whole body glucose homeostasis

Given the impairment of TCA cycle-sourced gluconeogenesis in KO mice (**Figure 2.5E**), we next wanted to determine whether loss of hepatocyte BDH1 also affects whole-body glucose homeostasis. 18h fasting blood glucose levels in male KO mice were modestly, but not significantly, elevated over controls (**Figure 2.6A**). Fasting serum insulin and calculated HOMA-IR (**Figure 2.6B-C**) were also mildly elevated without statistical significance, with no change in fasting serum glucagon (**Figure 2.6D**). Measures of fasting glucose homeostasis were similar in female KO mice compared to their littermate controls, with no difference in fasting blood glucose (**Supplemental Figure 2.7A-D**). Additionally, blood glucose levels in male KO mice starved for 48 hours and female KO mice starved for 24 hours were comparable to controls (**Figure 2.6E-F**). These data indicate no impairment of glycemic maintenance in the setting of starvation in mice lacking hepatic BDH1. To determine the ability of these mice to defend glycemia after an insulin challenge, we performed i.p. insulin tolerance tests (IPITT). The acute responses to insulin in both fed and 18h fasting states were similar between male KO and littermate control mice (**Figure 2.6G and Supplemental Figure 2.7E**). Additionally, liver Akt phosphorylation 15 minutes post insulin injection was comparable between KO and control mice, suggesting no effect of hepatic BDH1 loss on insulin sensitivity (**Figure 2.7A**). However, late recovery of blood glucose

was impaired in KO mice 2 hours post injection, either in those treated with i.p. insulin in the fed state, in which blood glucose levels relative to baseline were 23.0 ± 8.7% lower than those of littermate controls 2h after insulin administration ($p < 0.05$, **Figure 2.6G**), or the 18h fasted state, in which blood glucose levels relative to baseline were 28.3 ± 10.2% lower than those of littermate controls 2h after insulin administration ($p < 0.01$, **Supplemental Figure 2.7E**), together suggesting a modest defect in the ability of KO mice to return to normoglycemia after an insulin challenge. Biomarkers of insulin responsiveness, including liver Akt phosphorylation and circulating NEFA concentrations did not vary between KO and control mice 2h post-insulin injection (**Figure 2.7B**, **Supplemental Figure 2.8A**).

To determine if the relative impairment in glycemic defense after an insulin challenge in BDH1-Hepatocyte-KO mice could be explained by enhanced insulin-mediated suppression of ketogenesis, and thus greater reliance of extrahepatic tissues on glucose, due to less 'glucose sparing' [41], we quantified serum ketone concentrations in BDH1-Hepatocyte-KO mice and littermate controls following i.p. administration of either insulin or saline control following a 4h fast. In saline treated mice of both genotypes, circulating ketone concentrations modestly increased over the 2h period, consistent with the continued fast, from 4-6h (**Figure 2.7C-D, Supplemental Figure 2.8B**). However, in insulin treated KO and control mice, circulating ketone concentrations sharply decreased after 30 min, but then recovered the same trajectory as that observed in saline-treated mice. By 2 hours post injection, all ketone concentrations in insulin treated mice, regardless of genotype, were comparable to saline treated mice. Additionally, the total increase

in TKB concentration over the 2h period was similar between insulin-injected KO (176.2 ± 21.9 µM) and control (212.4 ± 38.0 µM) mice (p = 0.40). Taken together with similar NEFA concentrations 2h post-insulin administration (**Supplemental Figure 2.8A**), these results indicate comparable degrees of insulin-mediated suppression of ketogenesis in mice lacking hepatic BDH1, with normal recovery of circulating ketones. The comparable ability of the KO to recover ketogenesis following acute insulin suggests that latency to restore glycemia post insulin in these mice cannot explained by increased extrahepatic glucose clearance due to suppressed ketosis. However, impaired recovery of glycemia did correlate with impaired TCA cycle-sourced gluconeogenesis. If this gluconeogenic impairment exposes these mice to a risk for hypoglycemia, hepatic and/or extrahepatic mechanisms compensate for this deficiency during a chronic hypoglycemic stress such as starvation. To assess glycemic excursion after an exogenous glucose load, we performed performing a fasting (18h) i.p. glucose tolerance test (IPGTT). Although blood glucose levels were 20.2 ± 5.3% higher in male KO mice 15 min post glucose injection ($p < 0.05$), the overall area under the curve (AUC) showed no difference between KO mice and controls in either male or female mice (**Supplemental Figure 2.9A-B**).

Finally, as the kidney is a gluconeogenic organ [95], and since compensation through renal glucose production has been shown in another hepatocyte-specific knockout mouse models that impair hepatic glucose production [96], we determined whether there was evidence of increased renal glucose production in Heptocyte-BDH1-KO mice. Statistically significant ($p < 0.05$)

fold increases in *Ppargc1a* [1.86-fold (95% CI 1.22 - 2.62) and *Pck1* (2.25-fold, 95% CI 1.23 - 3.95)], were shown in kidneys harvested from fasting (18h) Hepatocyte-BDH1-KO mice (**Supplemental Figure 2.10A**) suggesting increased fat oxidation, required for increased TCA cycle-sourced gluconeogenesis. To determine if evidence for increased gluconeogenesis could be observed, we administered 5 µmol/g body weight [U-$^{13}C_3$]lactate i.p. to 18h fasted mice, and harvested kidneys 15 minutes later. Use of liquid chromatography high mass accuracy mass spectrometry study failed to show evidence of increased ^{13}C-labeling of TCA cycle intermediates that would have suggested increased renal gluconeogenesis in Hepatocyte-BDH1-KO mice (**Supplemental Figure 2.10B**). However, renal mRNA abundances encoding mediators of glucose reabsorption after glomerular filtration, i.e., the glucose transporters *Slc2a1* [2.30-fold (95% CI 1.09 - 4.47), *Slc2a2* (2.17-fold, 95% CI 1.13 – 3.56), *Slc5a1* (2.66-fold, 95% CI 1.40 – 4.63), and *Slc5a2* (2.47-fold, 95% CI 1.36 – 4.30)], were all significantly ($p < 0.05$) elevated in kidneys of Hepatocyte-BDH1-KO mice (**Supplemental Figure 2.10C**), suggesting a possible renal compensation to protect against hypoglycemia in Hepatocyte-BDH1-KO mice.

2.4 Discussion

Using high-resolution LC-MS/MS, dual isotope tracer NMR spectroscopy, and integrated physiological approaches in novel hepatocyte specific BDH1 knockout mice, our results reveal new insight into the role of hepatic mitochondrial

interconversion of the ketone bodies AcAc and D-βOHB. Rather than remaining in circulation until terminal ketolysis, much of the circulating AcAc pool is first reduced to D-βOHB in a BDH1-dependent manner by the liver and other BDH1-expressing tissues (schematized in **Figure 2.8A**). Although the reaction catalyzed by BDH1 is a near-equilibrium reaction, the equilibrium constant and mid-point reduction potential of the AcAc/D-βOHB half-reaction modestly favors D-βOHB and NAD^+ formation [24; 79]. However, in vivo, mitochondrial redox potential, ketone body mass action, and SCOT-dependent extrahepatic AcAc terminal oxidation together govern circulating AcAc/D-βOHB ratio [97]. The increase in static liver NAD^+/NADH ratios that were provoked by exogenously administered AcAc underscores its two primary fates: SCOT-dependent extrahepatic oxidation and BDH1-dependent reduction to D-βOHB, in liver and other BDH1 expressing tissues. Conversely, bolus-delivered D-βOHB did not as readily equilibrate in the circulation to the same extent as AcAc, and failed to reduce the hepatic NAD^+ pool, indicating that proportionately more of the D-βOHB pool was retained and terminally oxidized within the cells that oxidized it to AcAc. Thus, conversion of circulating AcAc to D-βOHB may target circulating AcAc to BDH1-expressing tissues, such as the brain, heart, and skeletal muscle. This could be physiologically significant, because while all extrahepatic cells express SCOT, BDH1 is not ubiquitously expressed [44].

In the fed state, the circulating [AcAc]/[D-βOHB] ratio is between 1:1 and 1:2, and this ratio decreases with progressively increasing physiological ketoses [24; 27; 87]. While it has been posed that preferential extrahepatic disposal of AcAc

may occur during ketosis, and thus explains this low ratio [80], our data suggest that while this may be true, equilibration of AcAc into the D-βOHB pool may also be a relatively favored process in vivo, a possibility supported by recent work by Deja et al. [98]. A limitation of our approach was that bolus delivery may confer distinct equilibrium kinetics in vivo than infusions that achieve steady state concentrations, and these equilibria and their kinetics will vary by (patho)physiological state-dependent redox and substrate balances [80; 99]. However, with respect to rapid infusions, understanding the impact of acute exogenous bolus ketone administration is highly relevant, given widespread interest in ketone ester formulations for prospective health and wellness applications, but that vary in their deliveries of D-βOHB or AcAc [77; 100; 101]. Another consideration is the circulating pool sampled, as the arterial [AcAc]/[D-βOHB] ratio more closely reflects hepatic mitochondrial NAD^+/NADH ratio than does venous [AcAc]/[D-βOHB] ratio. However, venous sampling provides a better index of whole-body equilibration between AcAc and D-βOHB. Moreover, in our experiments, portal venous perfusions provided direct insight into AcAc and D-βOHB exported from the liver.

These studies provide further insight into the tissue distribution of equilibrating circulating ketones. Fifty years ago, McGarry and Foster demonstrated that liver was the primary site of equilibration between AcAc and D-βOHB [80]. In that study, normal interconversion of exogenous AcAc or D-βOHB was nearly abolished in functionally hepatectomized rats. Our studies show that the liver is a primary site of ketone body equilibration, but extrahepatic organs

contribute to ketone equilibration (schematized in **Figure 2.8B**). Residual hepatic BDH1 or theoretical compensation from hepatic cytoplasmic BDH2 [90] are unlikely explanations for relative preservation of ketone body equilibration in Hepatocyte-BDH1-KO mice, because when livers from these animals were perfused via the portal vein, only AcAc, and not βOHB was produced. This suggests BDH2 does not have a role in ketone body-mediated redox homeostasis in the liver. Another possible explanation for the retention of ketone equilibration in the absence of hepatocyte BDH1 is an extrahepatic compensation for the chronic absence of hepatic BDH1. For example, while *Bdh1* mRNA was elevated in kidneys of BDH1-Hepatocyte-KO mice, BDH1 protein was not elevated (Supplemental Figure 5). Nonetheless, future study using a more acute deletion or inhibition of hepatocyte selective BDH1 may test whether adaptation of extrahepatic BDH1 can occur.

Hepatocyte-specific loss of BDH1 diminished total circulating ketone concentrations. Despite a modest increase in circulating AcAc, KO mice show decreases in both circulating βOHB and TKB levels in both the fasting, and to a lesser extent, fed states. These changes in circulating ketones are similar to those recently published in a total BDH1 knockout mouse model [34]. Although BDH1 is not the rate limiting step in ketogenesis, our portal vein perfusion data indicate that this decrease in circulating ketones in KO mice reflects a modest decrease in overall hepatic ketogenesis. Perfusion studies showed more AcAc exported from the livers of KO mice than from livers of littermate controls, while the majority of the AcAc produced by livers of control mice is reduced to D-βOHB before its export

from the liver. Alternatively, but not mutually exclusively, the decrease in circulating ketone concentrations in Hepatocyte-BDH1-KO mice could represent increased clearance by extrahepatic tissues. Indeed, clearance of all ^{13}C-labeled ketones (^{13}C-TKB) from mice administered [U-$^{13}C_4$]AcAc was more rapid in KO than in littermate control mice, while clearance of exogenously delivered D-[U-$^{13}C_4$]βOHB was relatively slower in the KO (**Figure 2.3C-E** and **Supplemental Figure 2.4E-F**). In this experiment, the mild impairment in equilibration of [U-$^{13}C_4$]AcAc with the circulating pool of D-[U-$^{13}C_4$]βOHB in Hepatocyte-BDH1-KO mice prospectively favors terminal disposal of [U-$^{13}C_4$]AcAc through SCOT-dependent pathways. However, absence of hepatic interconversion of AcAc to βOHB may also support increased consumption of extrahepatic NADH, via extrahepatic conversion to D-βOHB (**Figure 2.8B**). This could bear relevance to the relative latency to defend glycemia in the setting of an acute insulin challenge in mice lacking hepatic BDH1. While the kinetic responses of circulating ketones to insulin were comparable to those of littermate controls, serum AcAc concentrations were always modestly higher in the KO (**Figure 2.7C-D**, **Supplemental Figure 2.8B**). It is possible that NADH consumption through extrahepatic conversion of AcAc to βOHB increases extrahepatic glucose disposal, although augmented glucose disposal was not evident in glucose tolerance tests. It is also of interest that after 48h starvation, KO mice did not become more hypoglycemic than littermate controls. This suggests adaptation of mice lacking BDH1 in hepatocytes that overcomes a deficit in TCA cycle-sourced hepatic glucose production, possibly through extrahepatic glucose production/reclamation, and/or mechanisms that impair peripheral glucose uptake.

Augmentation of a gene signature of energy turnover and re-uptake of filtered glucose in kidney of Hepatocyte-BDH1-KO mice are consistent with the former mechanism. Future direct interrogation of extrahepatic tissue metabolism in mice lacking hepatic BDH1 will add greater insight into the role of hepatic redox in the dynamic regulation of integrated glucose homeostasis, because these relationships are of great interest in the setting of ketogenic diets and exogenous ketone ester administrations.

We previously showed that ketogenic insufficiency provoked by loss of hepatic HMGCS2 increases TCA cycle flux [36], which is the opposite outcome of the ketogenic defect incurred by BDH1 deficiency. With loss of HMGCS2, acetyl-CoA cannot undergo ketogenesis, and proportionately more is terminally oxidized in the TCA cycle. The different outcome observed in livers of Hepatocyte-BDH1-KO mice is likely based in the mitochondrial matrix redox implications of BDH1 loss, which loss of HMGCS2 does not directly provoke. Without BDH1, liver mitochondria have lost a conduit to re-generate NAD^+ from NADH. Impairment in TCA cycle flux, and the corresponding decrease in TCA cycle-sourced gluconeogenesis, both observed in livers of KO mice, most likely results primarily a consequence of this redox perturbation. It is also possible that without BDH1, liver mitochondria could retain more NADH, decreasing the demand for oxidative metabolism in the liver.

As BDH1 is one of several mitochondrial dehydrogenases [24; 87], loss of BDH1 in hepatocytes may provoke compensations that protect against more pronounced abnormalities of redox homeostasis: while hepatic TCA cycle flux was

diminished in livers lacking BDH1, overall energy balance fell within normal limits, and energy charge, as measured by static abundances of ATP, ADP, and AMP, was normal. Mitochondrial and whole liver tissue redox status appeared to be normal, but as discussed in **Results**, static quantifications of total pools of NAD^+ and NADH encompass both free and protein-bound levels, which could mask a change in turnover rates [91]. Dynamic measurements of specific mitochondrial dehydrogenase activities against incrementally controlled variations of energy charge will be required to fully understand the redox effects of BDH1 loss on hepatocyte mitochondria, because exogenously administered AcAc does increase total liver NAD^+/NADH ratio, and loss of BDH1 from hepatocytes provokes measurable changes in oxidative turnover rates.

Another consequence of ketogenic insufficiency is loss of non-canonical signaling mechanisms conferred by ketone bodies. Metabolism-independent signaling roles of ketones may explain many of their physiological properties in vivo and should be considered prospective mechanisms to explain phenotypes in loss- or gain- of ketone turnover models or human participant studies [22]. AcAc and βOHB each confer distinct signaling effects through unique G protein coupled receptor targets, components of the immune and inflammatory signaling systems, cytoplasmic signal transduction cascades, as well as post-translational histone modification. It is possible that differences between HMGCS2 and BDH1 loss of function models relate to distinct signaling outcomes attributable to loss of both AcAc and βOHB, versus the preservation of AcAc, and the relative loss of βOHB alone.

The perfused liver model employed herein confers an experimental limitation as substrate delivery in this model does not reflect the physiological fatty acid supply sampled by hepatocytes in vivo, as the delivery of the carnitine palmitoyltransferase–independent fat octanoate in the livers of animals in the fasted state provokes a convergence of β-oxidation and ketogenic demand not commonly encountered in vivo. This may overemphasize in vivo differences attributable to genetic perturbations of ketone metabolism, and result in variations among relative contributions to HGP, compared with those collected through in vivo studies. Nonetheless, the octanoate perfusion model was employed to specifically reveal the effect of deranged hepatic mitochondrial metabolism on downstream canonical glucose metabolism. Moreover, the portal vein perfusion model specifically quantifies hepatic ketone export and HGP, unlike in vivo approaches that administer tracers via a central vein to track labeled glucose, which do not exclude extrahepatic gluconeogenesis.

In conclusion, equilibration of circulating ketones occurs primarily in the liver, but in the absence of hepatic BDH1, extrahepatic tissues support ongoing interconversion between the two ketone bodies in a manner that continues to favor reduction of AcAc to D-βOHB, with re-oxidation of NADH. Additionally, hepatic loss of BDH1 diminishes TCA cycle flux rate and provokes subtle changes in whole body glucose homeostasis, but with minimal overall effect on liver energy charge. Future studies that quantify the impact of hepatocyte BDH1 in varying metabolic contexts, such as nonalcoholic fatty liver disease, or in response to exogenous ketone body supplements, which provoke the unusual state of net ketone body

import into hepatocyte mitochondria, may provide further insight into the roles of ketone body-governed mitochondrial redox homeostasis in metabolic physiology.

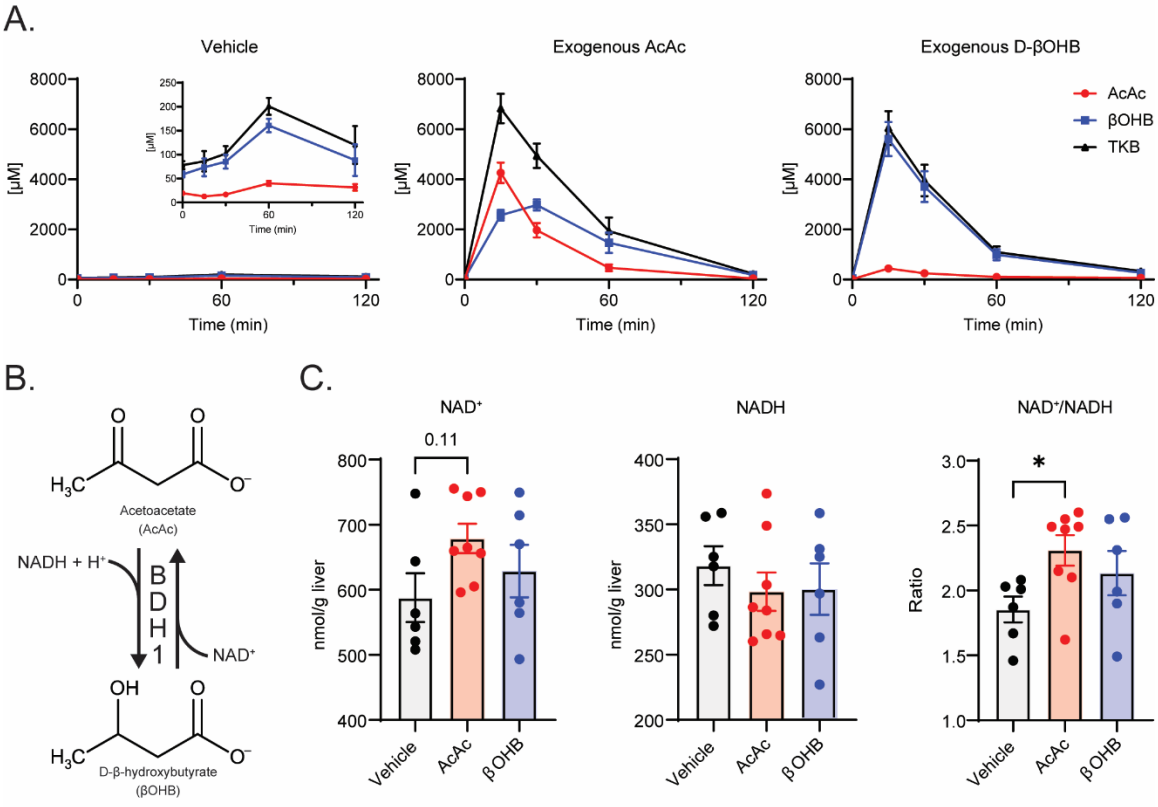

Figure 2.1. Effects of boluses of exogenous AcAc and D-βOHB on circulating ketones and liver redox. (A) Kinetic study of exogenously delivered AcAc (*middle*) and D-βOHB (*right*) turnover in random-fed C57BL/6NJ mice. Mice were injected i.p. [10 μmol/g body weight; vehicle was an equimolar concentration of ethanol vehicle] and blood was collected at the indicated time points (μM; n = 5-10/group). **(B)** Schematic of D-βOHB dehydrogenase 1 (BDH1) catalyzed interconversion of AcAc and D-βOHB. **(C)** Liver NAD^+ (nmol/g liver), NADH (nmol/g liver), and NAD^+/NADH ratio 15 min post exogenous ketone injections as described in **(A)** (n = 6-8/group). Data presented as mean ± SEM. *P <0.05 by one-way ANOVA with Tukey's multiple comparisons test.

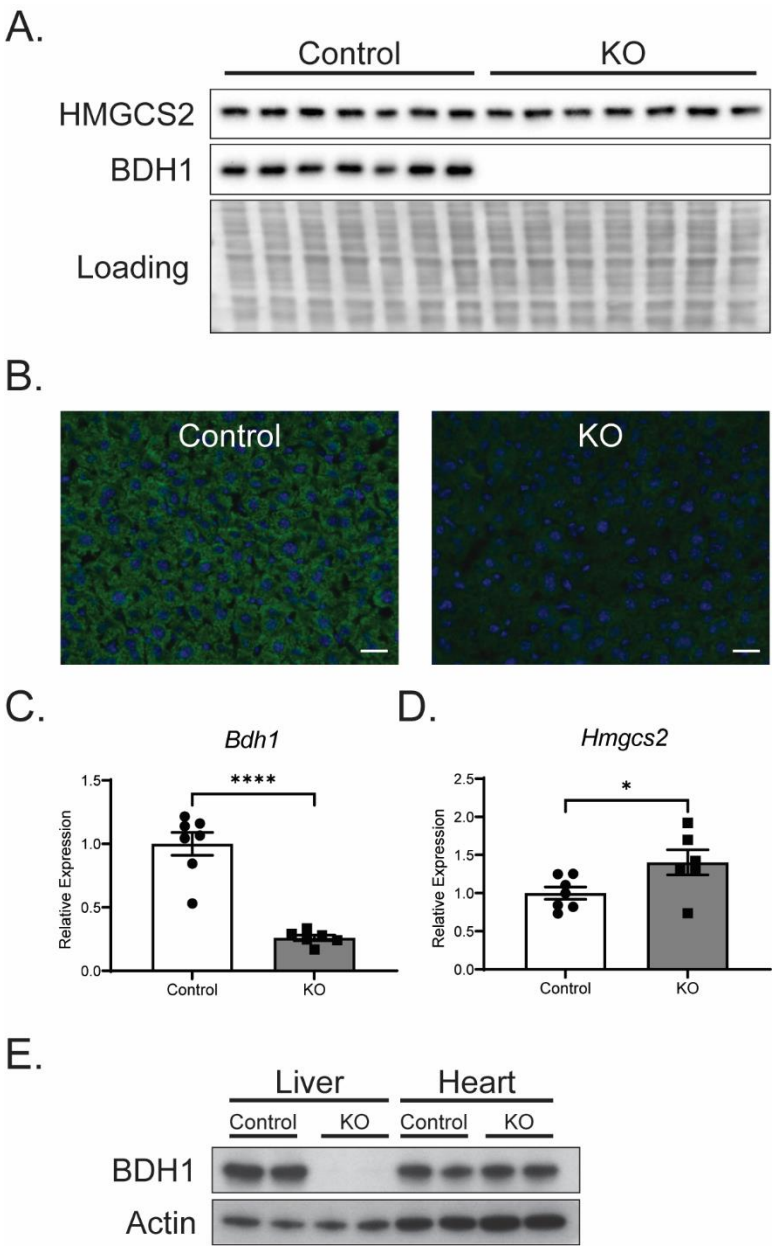

Figure 2.2. Confirmation of hepatocyte-specific BDH1-KO mice. (A) Immunoblots of HMGCS2, BDH1, and protein loading obtained from liver protein lysates of fasting littermate control (*Bdh1*$^{flox/flox}$) and Hepatocyte-BDH1-KO (Albumin-Cre X *Bdh1*$^{flox/flox}$) mice (*n* = 6/group). (**B**) Representative 20X magnification of immunohistochemical stain for BDH1 in fasting liver cryosections. Scale bar = 25 µm. **(C)** Fasting liver transcript abundances of *Bdh1* and (**D**) *Hmgcs2* in control and KO mice (*n* = 6-7/group). **(E)** Immunoblots of BDH1 and Actin obtained from liver and heart protein lysates of fasting, male control and KO mice (*n* = 2/group). Data presented as mean ± SEM. **P* <0.05; *****P* <0.0001 by Student's *t* test.

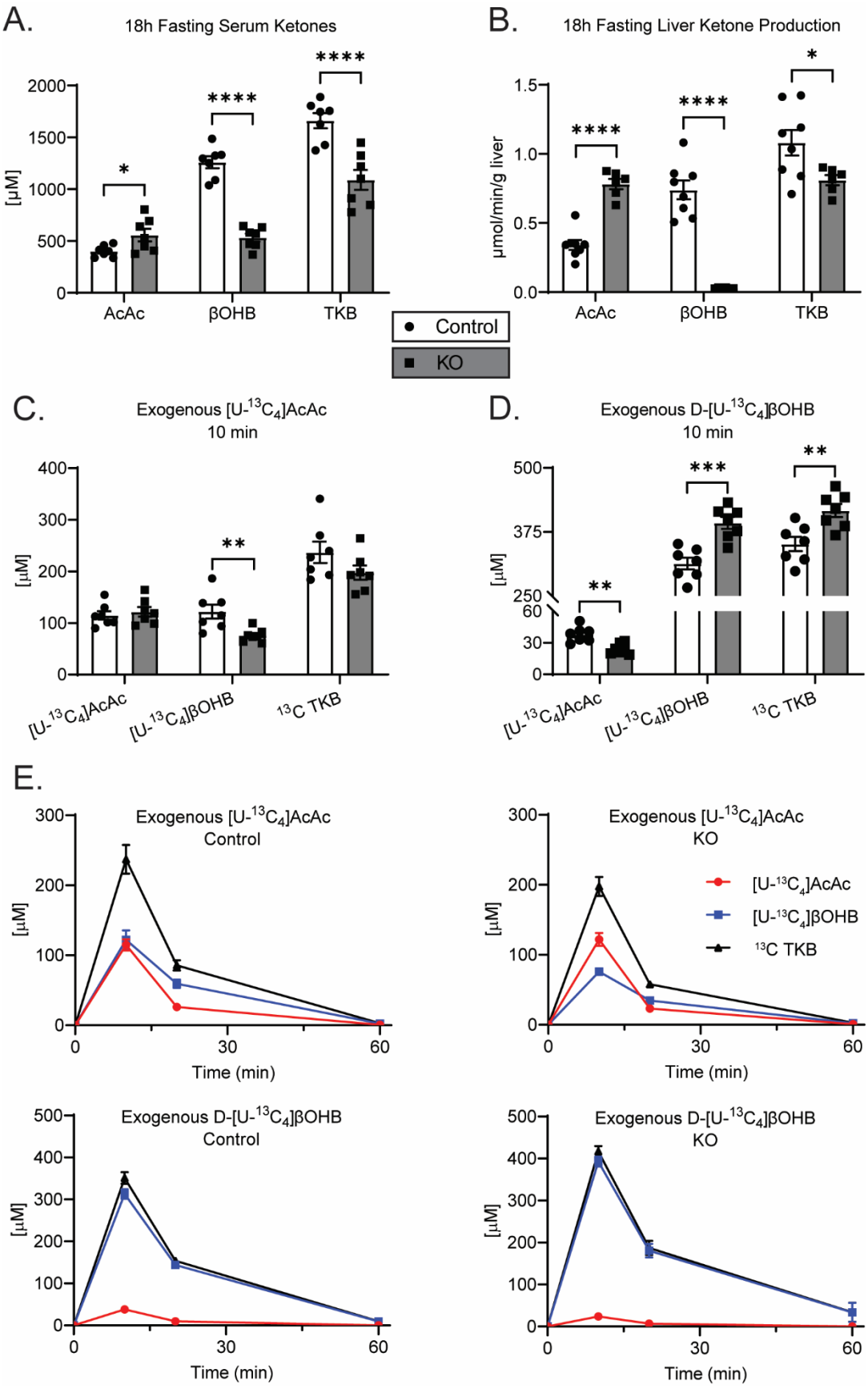
A.
18h Fasting Serum Ketones
[μM]
2000
1500
1000
500
0
*
****
****
AcAc
βOHB
TKB
B.
18h Fasting Liver Ketone Production
μmol/min/g liver
1.5
1.0
0.5
0.0
****
****
*
AcAc
βOHB
TKB
Control
KO
C.
Exogenous [U-13C4]AcAc
10 min
[μM]
400
300
200
100
0
**
[U-13C4]AcAc
[U-13C4]βOHB
13C TKB
D.
Exogenous D-[U-13C4]βOHB
10 min
[μM]
500
375
250
60
30
0
**
***
**
[U-13C4]AcAc
[U-13C4]βOHB
13C TKB
E.
Exogenous [U-13C4]AcAc
Control
[μM]
300
200
100
0
0
30
60
Time (min)
Exogenous [U-13C4]AcAc
KO
[U-13C4]AcAc
[U-13C4]βOHB
13C TKB
Exogenous D-[U-13C4]βOHB
Control
500
400
300
200
100
Exogenous D-[U-13C4]βOHB
KO

Figure 2.3. Hepatocyte-BDH1-KO mice exhibit impaired ketogenesis and ketone interconversion. (A) Fasting (18h) serum ketones (μM; *n* = 7/group). **(B)** Liver ketone production, quantified by LC-MS of hepatic venous effluent from 60-min portal vein perfusion using an oxygenated buffer containing 0.2 mM unlabeled sodium octanoate as exogenous fat from 18h fasted mice (μmol/min/g liver; *n* = 6-8/group). **(C)** Labeled circulating ketones (μM) 10 min post i.p. [U-$^{13}C_4$]AcAc or **(D)** D-[U-$^{13}C_4$]βOHB injection (1 μmol/g body weight) in random-fed control and KO mice (*n* = 7/group). **(E)** Full kinetics of [U-$^{13}C_4$]AcAc and D-[U-$^{13}C_4$]βOHB metabolism in random-fed control and KO mice. Mice were injected i.p. (1 μmol/g body weight) and blood was collected at the indicated time points (*n* = 7/group). The ten-minute time points for this experiment are also presented in panels **(C-D)**. Twenty minute time points are shown in **Supplemental Figure 2.4E-F**, and fractional contributions of all endogenous and exogenous ketones to the total pools are shown in **Supplemental Figure 2.4G-H**. Data presented as mean ± SEM. **P* <0.05; ***P* <0.01; ****P* <0.001; *****P* <0.0001 by Student's *t* test.

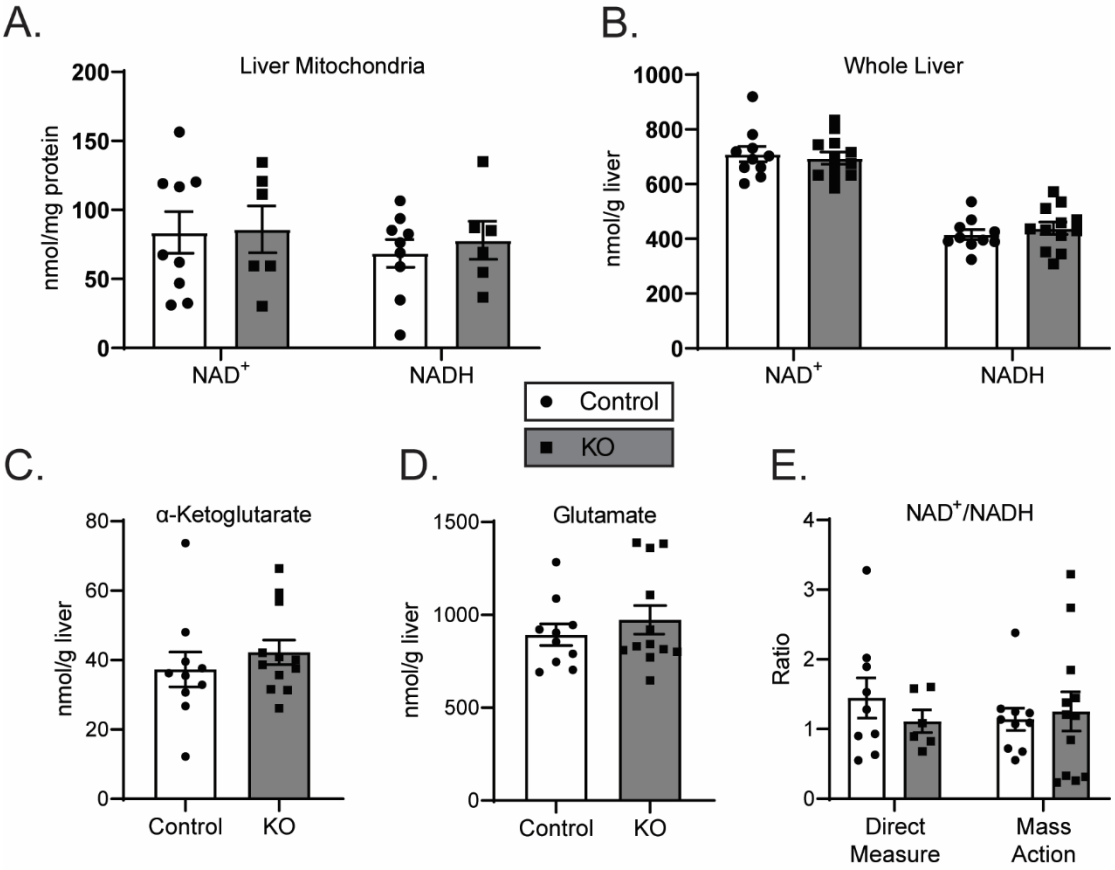

Figure 2.4. Hepatocyte-BDH1-KO mice maintain liver redox state. (A) LC-MS-determined static quantities of liver mitochondrial (nmol/mg protein) and **(B)** whole tissue (nmol/g liver) total NAD^+ and NADH in fasting (18h) control and KO mice (*n* = 6-12/group). **(C)** Measured static quantities of liver α-ketoglutarate and (**D**) glutamate in fasting (18h) control and KO mice (nmol/g liver, *n* = 10-12/group). **(E)** Liver mitochondrial NAD^+/NADH ratios determined from direct NAD^+ and NADH measurements from isolated mitochondria (*left*) and calculated from mass action ratio of glutamate dehydrogenase system from whole liver tissue (*right*) (*n* = 6-12/group). Data presented as mean ± SEM.

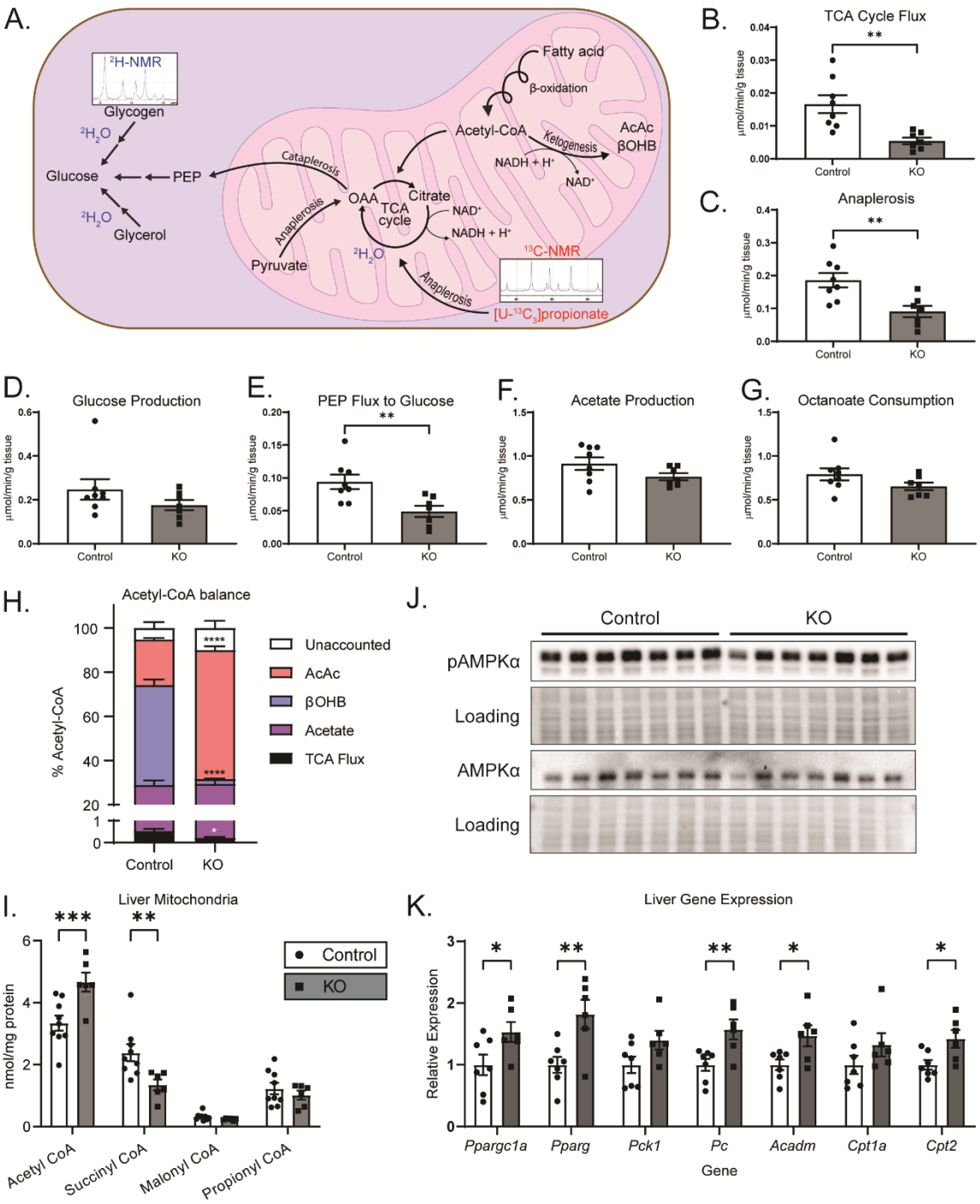

Figure 2.5. Loss of hepatic BDH1 diminishes hepatic oxidative fluxes. (A) Schematic highlighting hepatic oxidative fluxes obtained from liver perfusions using a ^{2}H-NMR and ^{13}C-NMR based approach. **(B)** TCA cycle flux, **(C)** anaplerosis flux, **(D)** hepatic glucose production, **(E)** phospho*enol*pyruvate (PEP)-supported (TCA cycle-sourced) flux to gluconeogenesis (glycogen- and glycerol-sourced fluxes to hepatic glucose production are shown in **Supplemental Figure 2.6C-D**), **(F)** acetate production, and **(G)** octanoate consumption rates, quantified

by ^{13}C-, ^{2}H-, and ^{1}H-NMR, from perfusions using an oxygenated buffer containing 0.2 mM unlabeled sodium octanoate, 3% $^{2}H_2O$, and 0.1 mM sodium [U-$^{13}C_3$]propionate in control and KO mice (μmol/min/g liver; *n* = 7-8/group). **(H)** Imputed balances of octanoate-derived acetyl-CoA fates based on measured disposal of acetyl-CoA through the TCA cycle and production of AcAc, βOHB, and acetate (*n* = 6-8/group). **(I)** Measured static quantities of liver mitochondrial (nmol/mg protein) total acetyl-CoA, succinyl-CoA, malonyl-CoA, and propionyl-CoA in fasting (18h) unperfused control and KO mice (*n* = 6-12/group). **(J)** Immunoblots of phosphorylated AMPKα (pAMPKα), total AMPKα, and protein loading obtained from fasting (18h) unperfused liver protein lysates of control and KO mice (*n* = 7/group). **(K)** Transcript abundances of *Ppargc1a*, *Pparg*, *Pck1*, *Pc*, *Acadm*, *Cpt1a*, and *Cpt2* from livers of fasting (18h) unperfused control and KO mice. (*n* = 6-7/group). Data presented as mean ± SEM. **P* <0.05; ***P* <0.01; ****P* <0.001 *****P* <0.0001 by Student's *t* test.

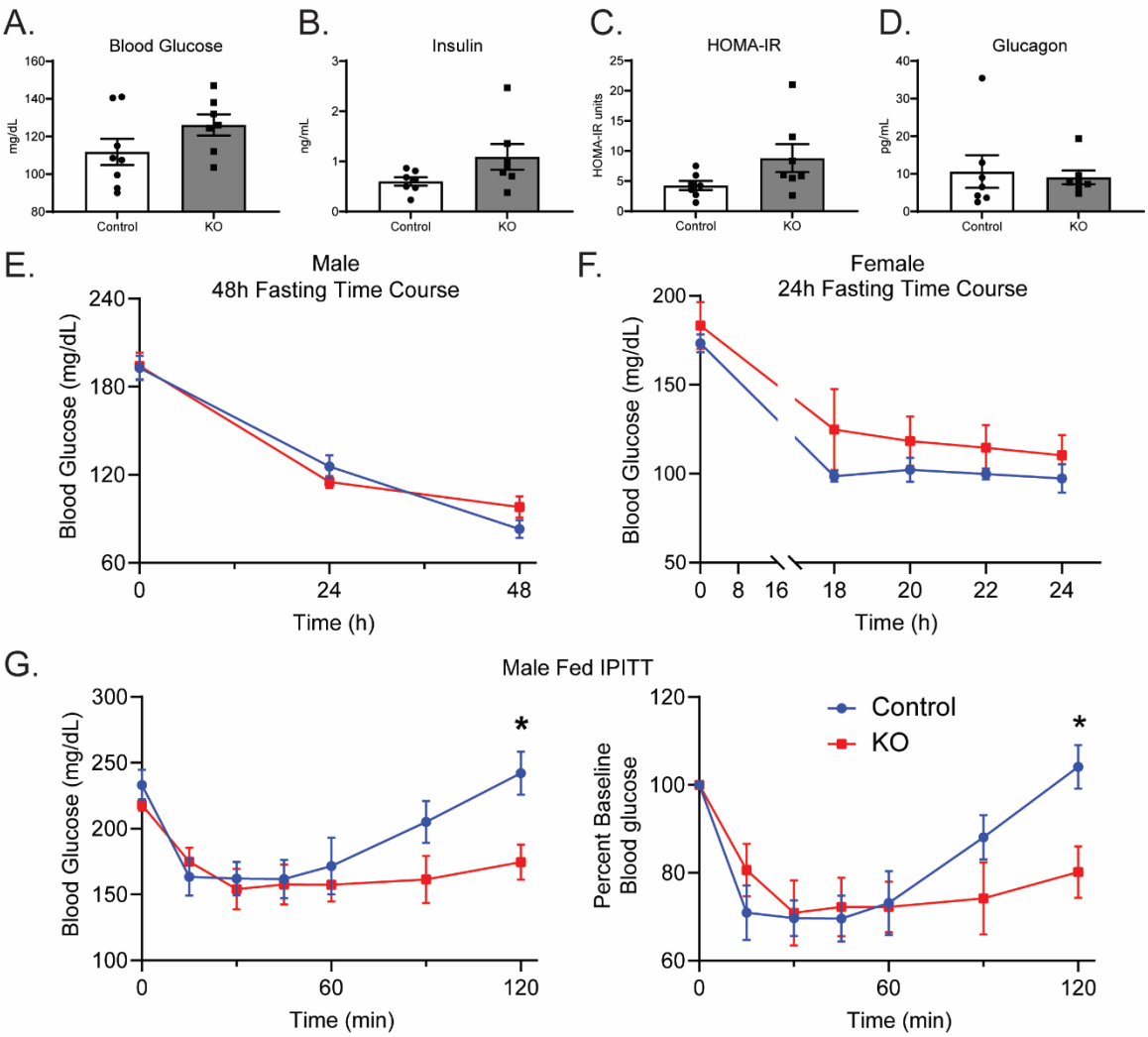

Figure 2.6. Altered glucose homeostasis in Hepatocyte-BDH1-KO mice. (A) Fasting serum measures of glucose (mg/dL), **(B)** insulin (ng/mL), **(C)** HOMA-IR, and **(D)** glucagon (pg/mL) in male control and KO mice (*n* = 7-8/group). **(E)** Blood glucose (mg/dL) time course in male control and KO mice during a 48h starvation experiment (*n* = 8/group). **(F)** Blood glucose (mg/dL) time course in female control and KO mice during a 24h starvation experiment (*n* = 4/group). **(G)** Random-fed IPITT (1 U/Kg body weight) with absolute and relative to baseline blood glucose curves (*n* = 8/group). Data presented as mean ± SEM. **P* <0.05 by repeated measures ANOVA with Sidak's multiple comparisons.

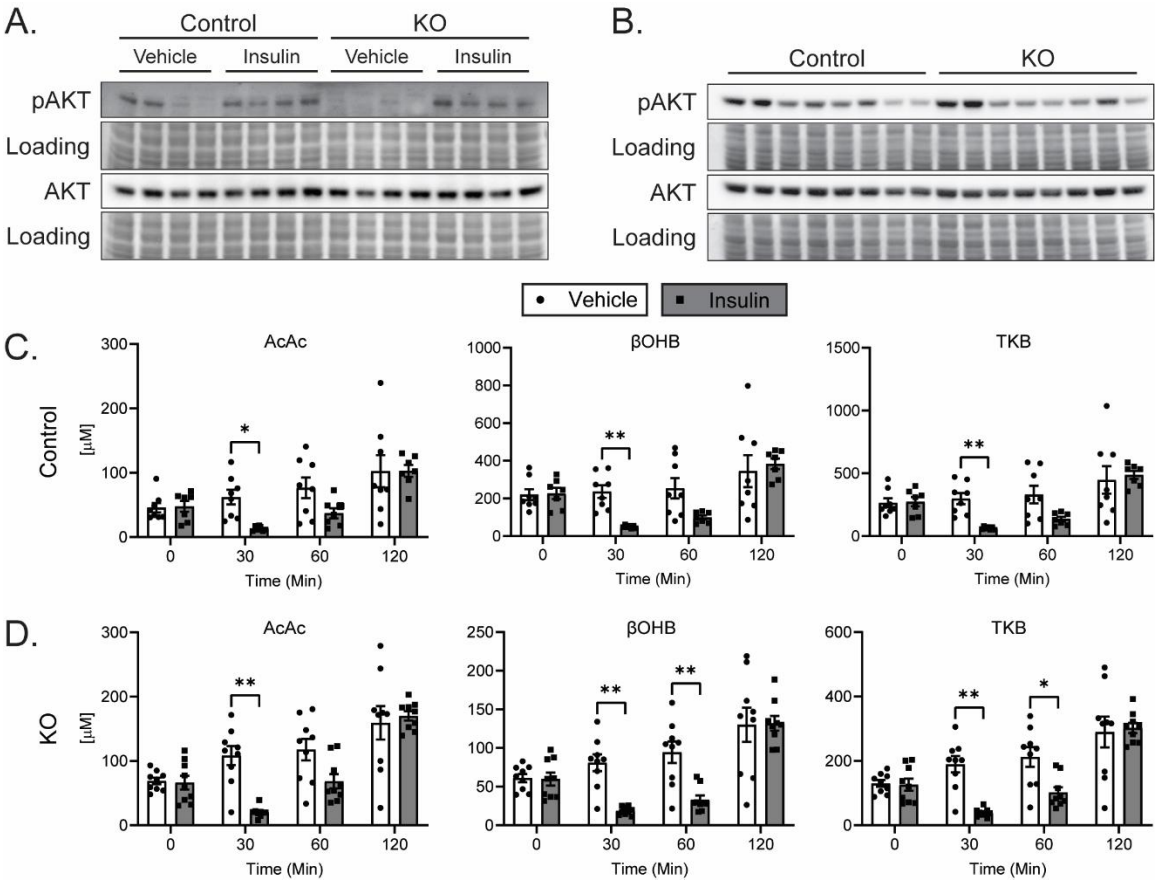

Figure 2.7. Hepatocyte-BDH1-KO mice remain insulin sensitive, with an intact ketone response to insulin. (**A**) Immunoblots of phosphorylated AKT (pAKT), total AKT, and protein loading obtained from 18h fasting liver protein lysates of control and KO mice 15 min post insulin (0.75 U/Kg body weight) or saline vehicle injection (*n* = 4/group). (**B**) Immunoblots of pAKT, total AKT, and protein loading obtained from protein lysates of control and KO mice fasted for 4h, injected with insulin (1 U/Kg body weight), then harvested 2h post injection (*n* = 8/group). **(C)** Effect of insulin (1 U/Kg body weight) on circulating ketones in control and **(D)** KO mice (*n* = 7-9/group). The full kinetic course for these data are presented in **Supplemental Figure 2.8B**. Data presented as mean ± SEM. **P* <0.05; ***P* <0.01 by repeated measures ANOVA with Sidak's multiple comparisons.

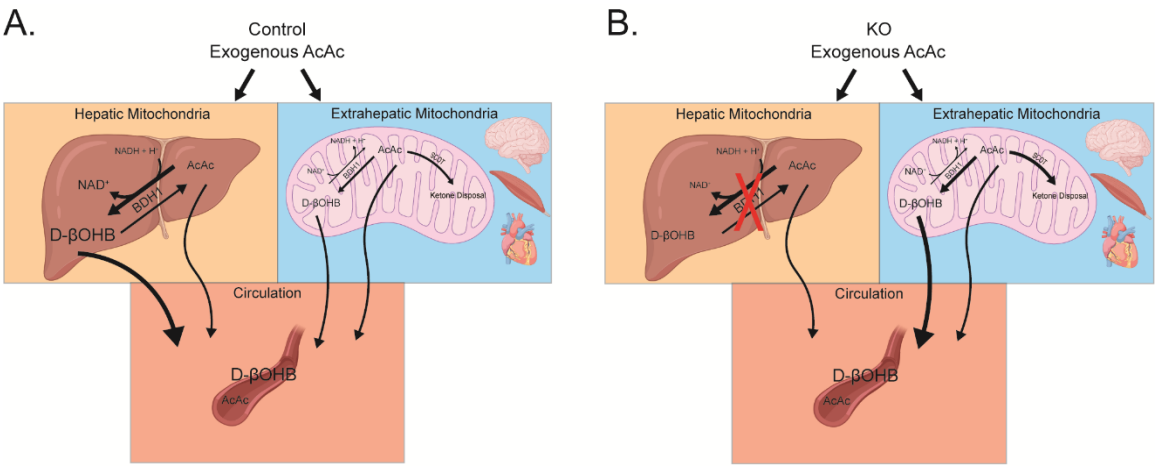

Figure 2.8. Summary of hepatocyte-specific BDH1-KO induced changes on ketone equilibration. (A) Schematic detailing the effect of an exogenous bolus of AcAc on circulating ketone equilibration in control and **(B)** KO mice. In vivo, liver mitochondrial NAD^+/NADH redox potential, ketone body mass action, and SCOT-dependent extrahepatic AcAc terminal oxidation together govern circulating AcAc/D-βOHB ratio. The results provided here suggest that governance of circulating AcAc/D-βOHB ratio is shared between hepatic and extrahepatic BDH1.

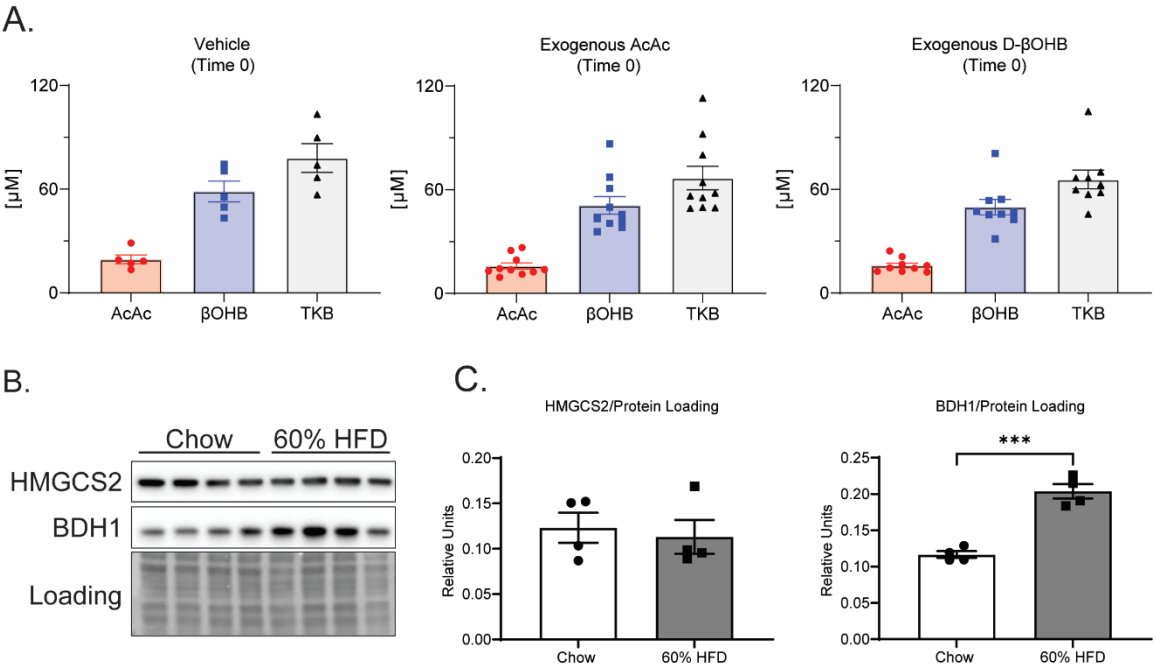

Supplemental Figure 2.1 (paired with Figure 2.1). Increased hepatic BDH1 expression in wild-type mice maintained on a 60% HFD. (A) Serum ketone levels prior to exogenous ketone injections in random fed wild-type male mice (μM; *n* = 5-10/group). **(B)** Immunoblots of HMGCS2, BDH1, and protein loading obtained from liver protein lysates of 26 week-old male mice maintained on either chow or 60% HFD for 16 weeks. **(C)** Densitometric quantifications of HMGCS2 and BDH1 normalized to protein loading (*n* = 4/group). Data presented as mean ± SEM. ****P* <0.001 by Student's *t* test.

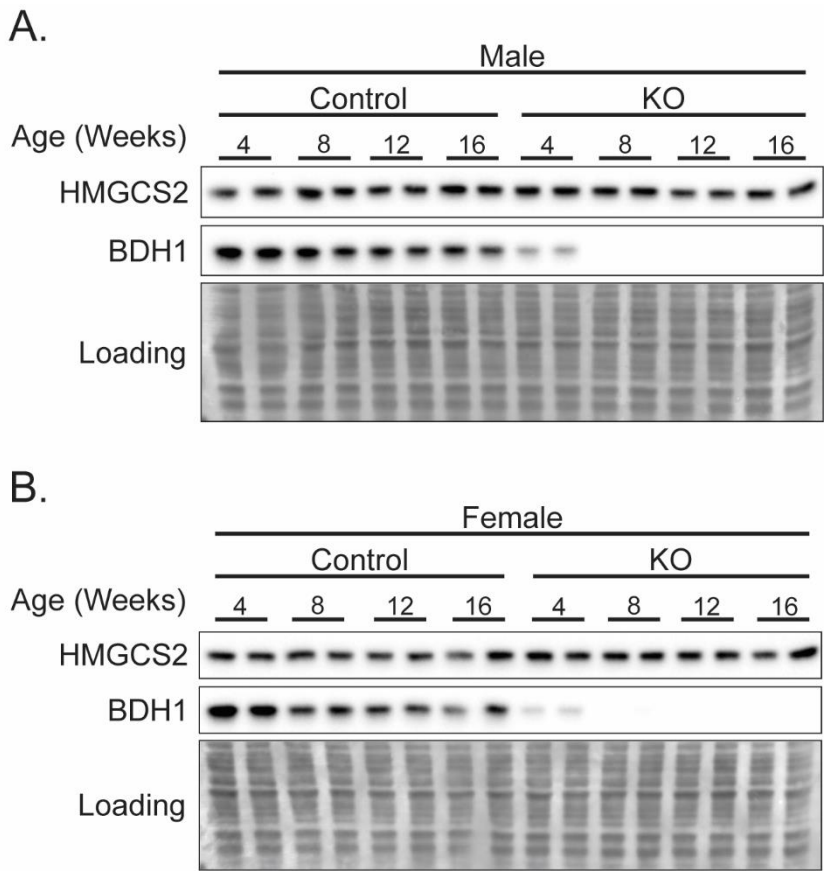

Supplemental Figure 2.2 (paired with Figure 2.2). Loss of hepatic BDH1 expression by 8 weeks of age in hepatocyte-specific BDH1-KO mice. (A) Immunoblots of HMGCS2, BDH1, and protein loading control obtained from liver protein lysates of random-fed male and **(B)** female control and KO mice at different ages (*n* = 2/group).

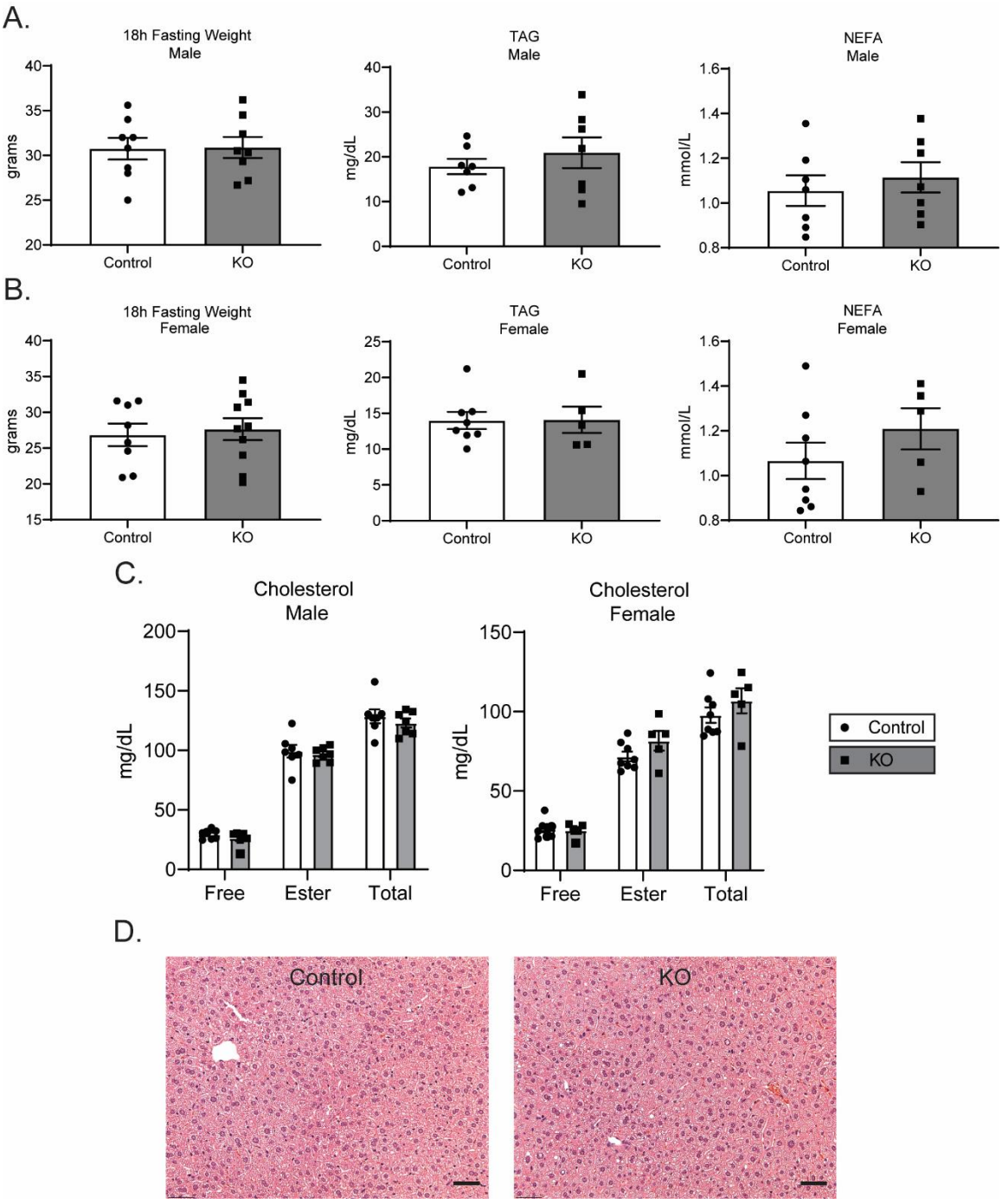

Supplemental Figure 2.3 (paired with Figure 2.2). Fasting body weights and circulating lipids do not differ with hepatic BDH1 loss. (A) Fasting (18h) body weight (g), serum triacylglycerols (TAG; mg/dL), and non-esterified fatty acids (NEFA, mmol/L) in male and **(B)** female control and KO 26-week old mice (*n* = 5-8/group). **(C)** Free, ester-bound, and total circulating cholesterol (mg/dL) in fasting male and female control and KO mice (*n* = 5-8/group). **(D)** Representative H&E staining of liver sections from fasting control and KO mice. Data presented as mean ± SEM. Scale bars = 50 μm.

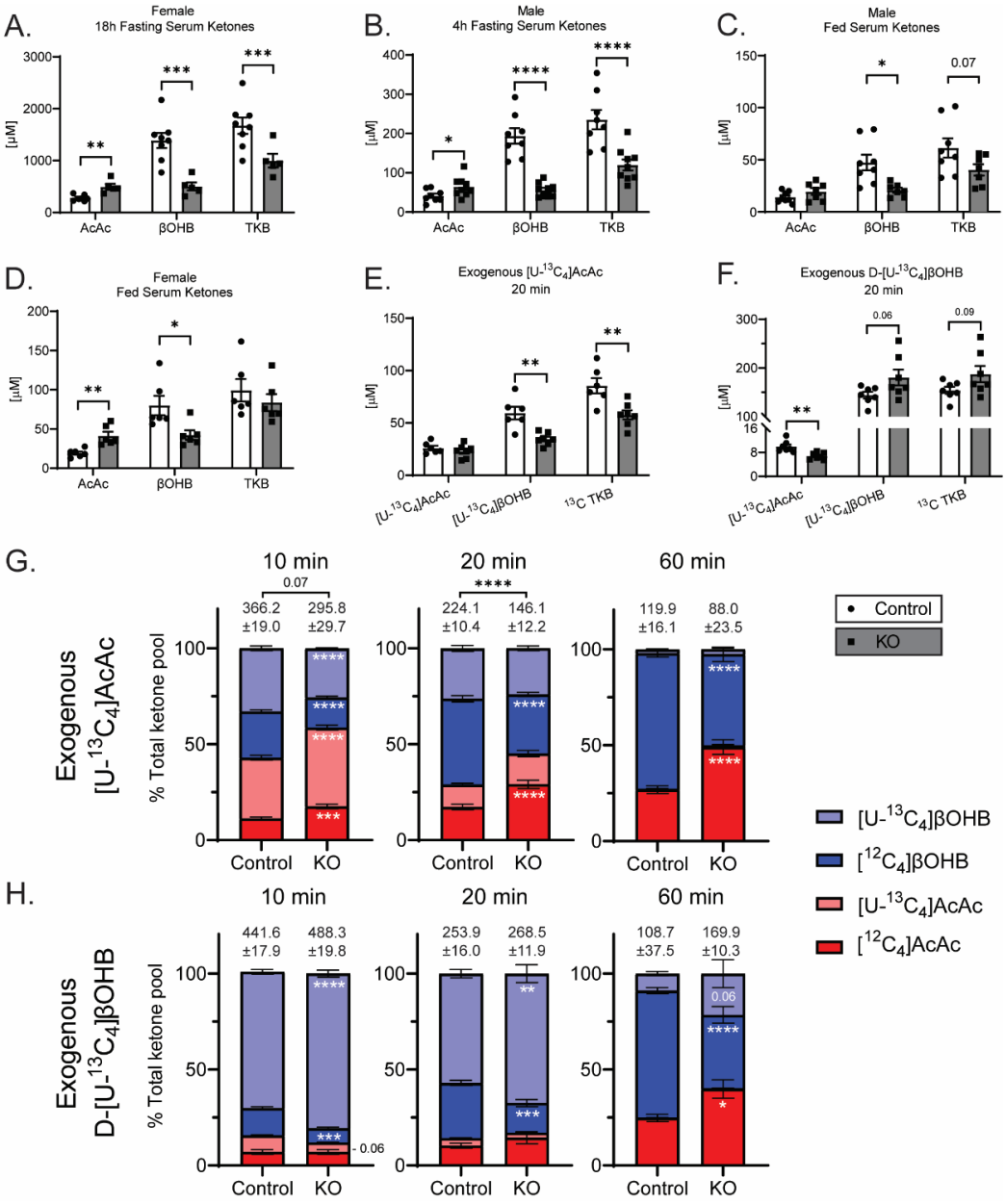

Supplemental Figure 2.4 (paired with Figure 2.3). Effects of hepatocyte BDH1 loss on equilibration of circulating ketones. (A) Fasting (18h) serum ketones in female control and KO mice (μM; *n* = 5-8/group). **(B)** Fasting (4h) serum ketones in male control and KO mice (μM; *n* = 8-9/group). **(C)** Random-fed serum ketones in male and **(D)** female control and KO mice (μM; *n* = 6-8/group). **(E)** Labeled circulating ketones (μM) 20 min post [U-$^{13}C_4$]AcAc or **(F)** D-[U-$^{13}C_4$]βOHB injection (1 μmol/g body weight) in random-fed control and KO mice (*n* = 7/group). The full time course for the data presented in panels E-F are presented in **Figure 2.3E**. **(G)** Replotted data from the experiment presented in **Figure 2.3E** showing total ketone pool enrichments for mice injected with [U-$^{13}C_4$]AcAc and **(H)** D-[U-$^{13}C_4$]βOHB. Values above bars indicate total ketone pool sizes (μM; *n* = 7/group). Data presented as mean ± SEM. **P* <0.05; ***P* <0.01; ****P* <0.001 by Student's *t* test.

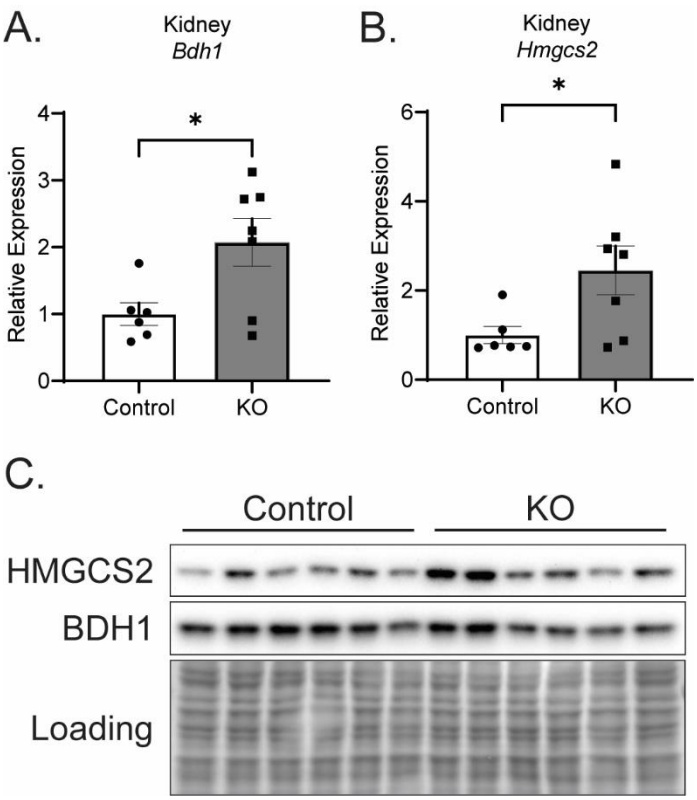

Supplemental Figure 2.5 (paired with Figure 2.3). Abundance of ketogenic mediators in mouse kidney. (A) Fasting (18h) kidney mRNA transcript abundances of *Hmgcs2* and **(B)** *Bdh1* in control and KO mice. (*n* = 6-7/group). **(C)** Immunoblots of HMGCS2, BDH1, and protein loading control obtained from kidney protein lysates of fasting (18h) control and KO mice (*n* = 6/group). Data presented as mean ± SEM. **P* <0.05 by Student's *t* test.

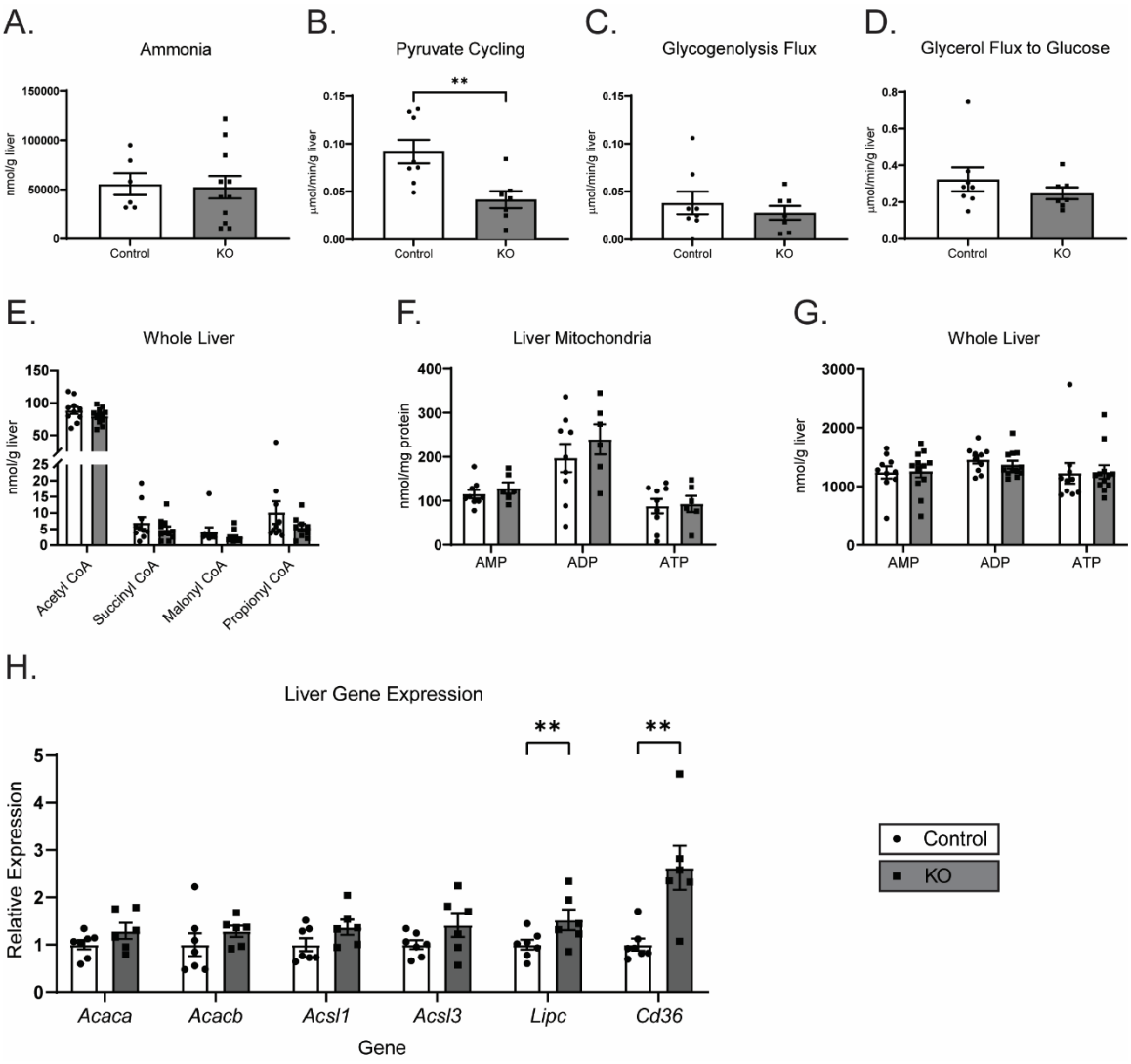

Supplemental Figure 2.6 (paired with Figures 2.4 and 2.5). Loss of hepatic BDH1 diminishes hepatic oxidative fluxes while maintaining total liver energy charge. (A) Measured static quantities of liver ammonia in fasting (18h) control and KO mice (nmol/g liver, *n* = 6-11/group). **(B)** Pyruvate cycling, **(C)** glycogenolysis flux to hepatic glucose production, and **(D)** glycerol flux to hepatic glucose production, quantified by ^{13}C-, ^{2}H-, and ^{1}H-NMR, from perfusions using an oxygenated buffer containing 0.2 mM unlabeled sodium octanoate, 3% $^{2}H_2O$, and 0.1 mM sodium [U-$^{13}C_3$]propionate in control and KO mice (μmol/min/g liver; *n* = 7-8/group). **(E)** Measured static quantities of whole liver tissue (nmol/g liver) acetyl-CoA, succinyl-CoA, malonyl-CoA, and propionyl-CoA in fasting (18h) unperfused control and KO mice (*n* = 6-12/group). **(F)** LC-MS-measured static quantities of liver mitochondrial (nmol/mg protein) and **(G)** whole tissue (nmol/g liver) total AMP, ADP, and ATP in fasting (18h) unperfused control and KO mice (*n* = 6-12/group). **(H)** Fasting (18h), unperfused liver transcript abundances of *Acaca*, *Acacb*, *Acsl1*, *Acsl3*, *Lipc*, and *Cd36* in control and KO mice. (*n* = 6-7/group). Data presented as mean ± SEM. ***P* <0.01 by Student's *t* test.

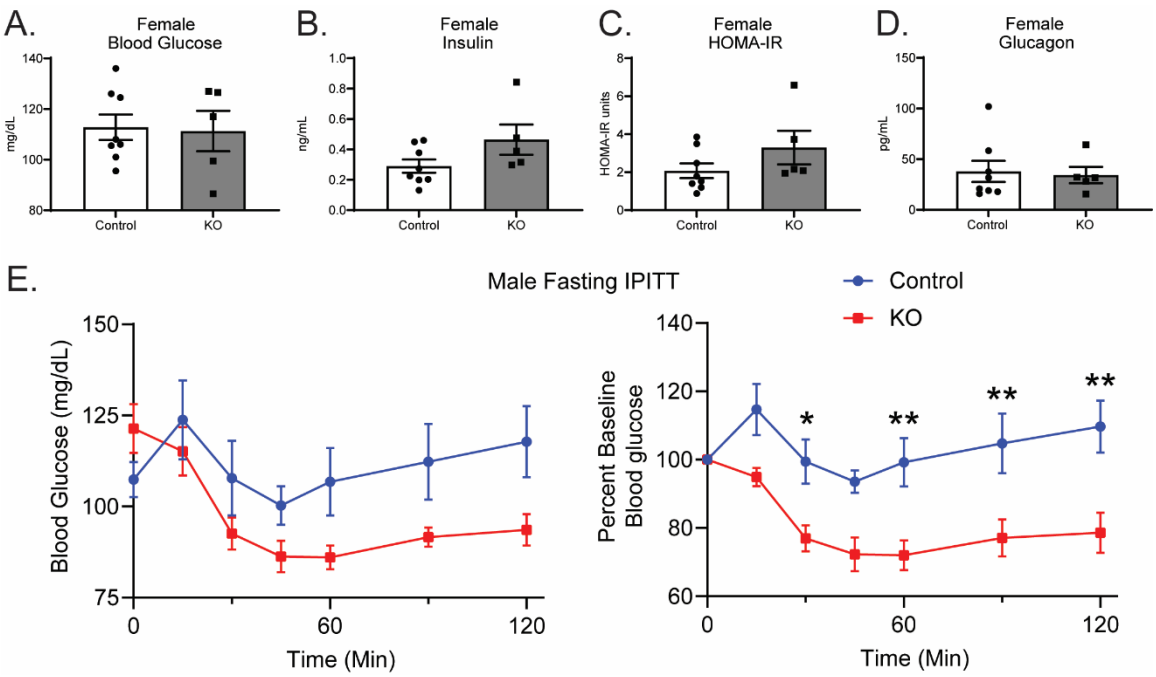

Supplemental Figure 2.7 (paired with Figure 2.6). Glucose homeostasis in Hepatocyte-BDH1-KO mice. (A) Fasting (18h) serum measures of glucose (mg/dL), **(B)** insulin (ng/mL), **(C)** HOMA-IR, and **(D)** glucagon (pg/mL) in female control and KO mice (*n* = 7-8/group). **(E)** Male fasting (18h) IPITT (0.75 U/Kg body weight) with absolute and relative to baseline blood glucose curves (*n* = 7-8/group). Data presented as mean ± SEM. **P* <0.05; ***P* <0.01 by repeated measures ANOVA with Sidak's multiple comparisons.

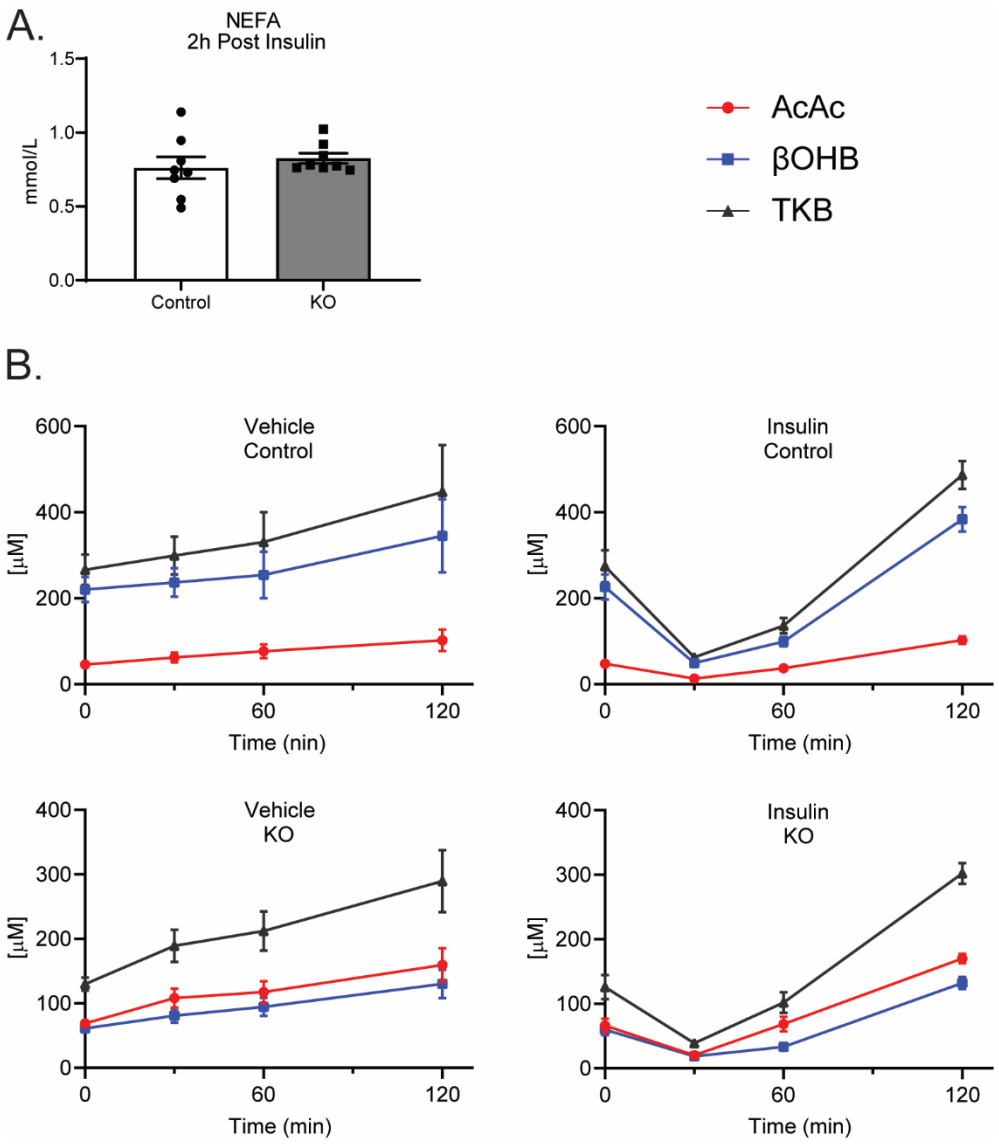

Supplemental Figure 2.8 (paired with Figure 2.7). Intact ketone response to insulin in Hepatocyte-BDH1-KO mice. (A) Circulating NEFA levels (mmol/L) in control and KO mice fasted for 4h, injected with insulin (1 U/Kg body weight), then harvested 2h post injection (*n* = 8/group). **(B)** Replotted data from the experiment shown in **Figure 2.7C-D** showing the kinetics of circulating ketones following injection with insulin (1 U/Kg body weight) or saline vehicle in 4h fasted control and KO mice (*n* = 7-9/group). Data presented as mean ± SEM.

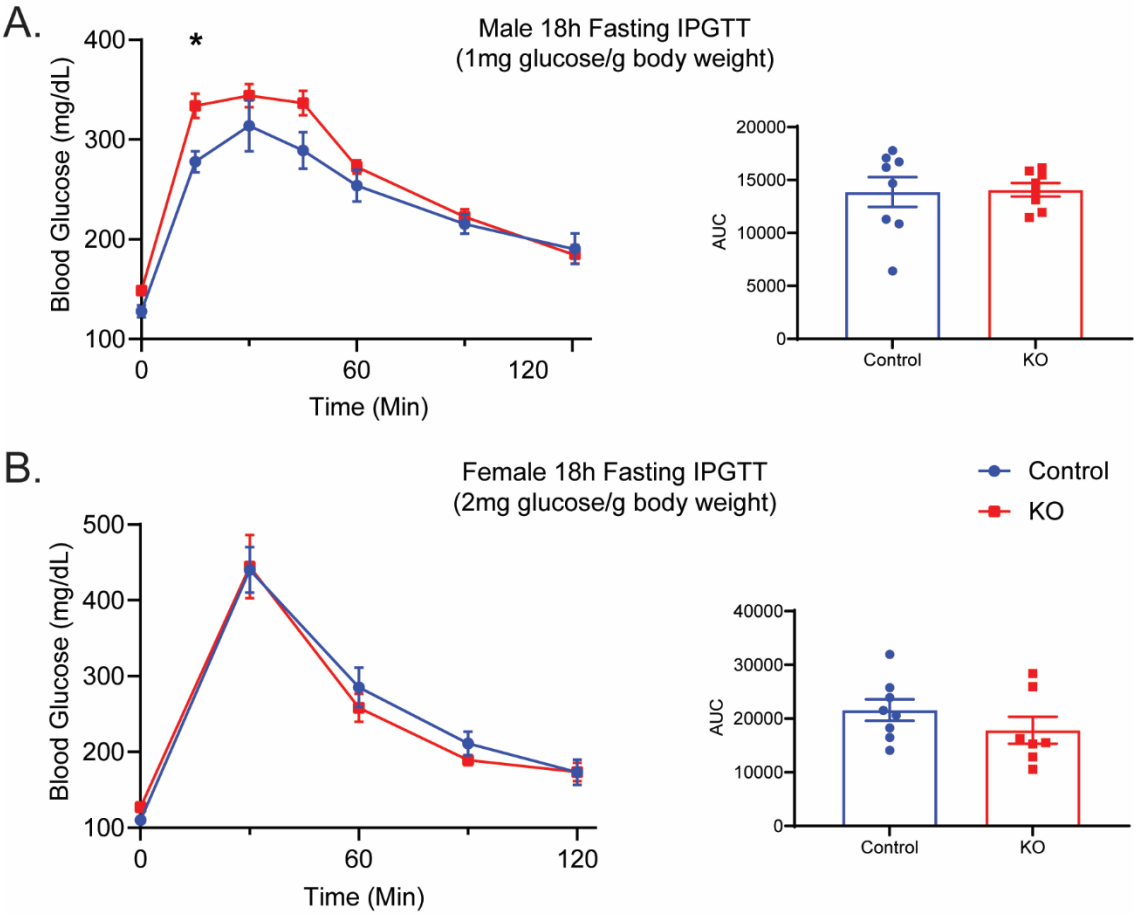

Supplemental Figure 2.9 (paired with Figure 2.7). Response to exogenous glucose in Hepatocyte-BDH1-KO mice. (A) 18h fasting IPGTT curve with calculated AUC graph in male (1 mg glucose/g body weight) and **(B)** female (2 mg glucose/g body weight) control and KO mice. (n = 8/group). Data presented as mean ± SEM. *P <0.05 by repeated measures ANOVA with Sidak's multiple comparisons.

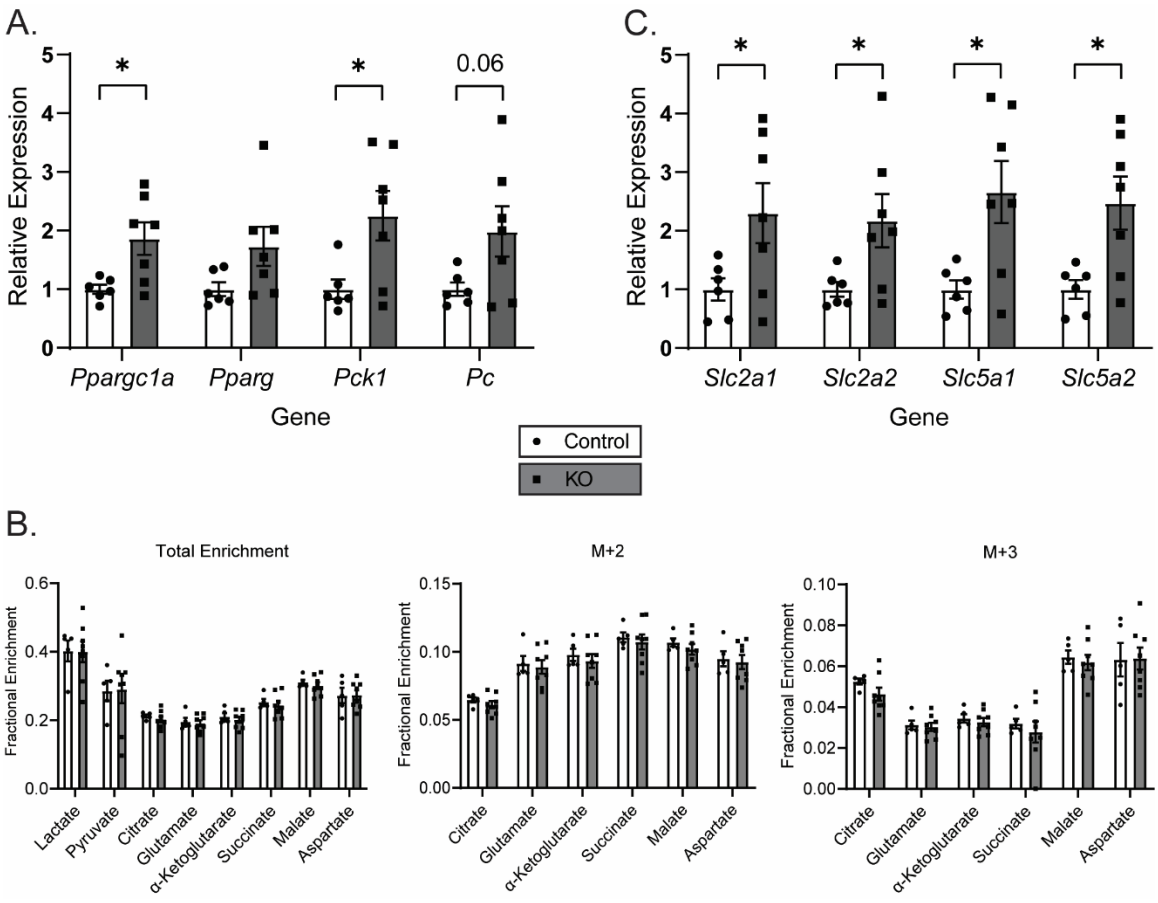

Supplemental Figure 2.10 (paired with Figure 2.7). Renal markers of glucose homeostasis. (A) Fasting (18h) kidney transcript abundances of *Ppargc1a*, *Pparg*, *Pck1*, and *Pc*, in control and KO mice. (*n* = 6-7/group). **(B)** Enrichment of fasting kidney TCA cycle intermediates 15 min post [U-$^{13}C_3$]lactate (5 µmol/g body weight) injection in control and KO mice (18h fasted) (*n* = 5-8/group). **(C)** Fasting (18h) kidney transcript abundances of *Slc2a1*, *Slc2a2*, *Slc5a1*, and *Slc5a2*, in control and KO mice. (*n* = 6-7/group). Data presented as mean ± SEM. **P* <0.05 by Student's *t* test.

Supplemental Table 2.1. Genotyping primer sequences

Primer	Sequence 5' to 3'	Product band size (base pairs)	
		WT	Mutant
Bdh1^{flox} Forward	TGCAGGAATCAGTGCTCTCTCCTAGCA	523	697
Bdh1^{flox} Reverse	GGTGTCAGGGCTGAAGGATG		
Alb-Cre Wild type Forward	TGCAAACATCACATGCACAC	350	
Alb-Cre Common Reverse	TTGGCCCCTTACCATAACTG		390
Alb-Cre Mutant Forward	GAAGCAGAAGCTTAGGAAGATGG		

Supplemental Table 2.2. MS parameters for energy metabolite quantification

Analyte	Retention Time (min)	Molecular ion	Precursor-product transition	Precursor-product transition of Internal Standards
ATP	7.7	$[ATP + DBAA + H]^+$	637.1548→136.0623	$[^{13}C_{10}, {}^{15}N_5]$ ATP 652.1735→ 146.0642
ADP	7.3	$[ADP + DBAA + H]^+$	557.1885→136.0623	
NAD^+	5.1	$[NAD^+ + H]^+$	664.1164→136.0623	
ADPR (NADH)	6.6	$[ADPR + DBAA + H]^+$	689.2307→136.0623	
AMP	6.6	$[AMP + DBAA + H]^+$	477.2222→136.0623	$[^{13}C_{10}, {}^{15}N_5]$ AMP 492.2408→ 146.0642
Acetyl-CoA	8.2	$[Acetyl\text{-}CoA + H]^+$	810.1333→303.1379	$[1,2\text{-}{}^{13}C_2]$ Acetyl-CoA 812.1400→ 305.1446
Malonyl-CoA	8.0	$[Malonyl\text{-}CoA + H]^+$	854.1229→303.1379	$[1,2,3,\text{-}{}^{13}C_3]$ Malonyl-CoA 857.1330→ 305.1446
Succinyl-CoA	8.1	$[Succinyl\text{-}CoA + H]^+$	868.1385→361.1434	
Propionyl-CoA	8.4	$[Propionyl\text{-}CoA + H]^+$	824.1487→317.1535	

Supplemental Table 2.3. Gene expression primer sequences

Gene	Forward Sequence 5' to 3'	Reverse Sequence 5' to 3'
Hmgcs2	TGGTTCAAGACAGGGACACAGAAC	AGAGGAATACCAGGGCCCAACAAT
Bdh1	TGCAACAGTGAAGAGGTGGAGAAG	CAAACGTTGAGATGCCTGCGTTGT
Ppargc1a	CGGAAATCATATCCAACCAG	TGAGGACCGCTAGCCAGTTTG
Pparg	AGACAAGATTTGAAAGAAGC	CTTCCATCACGGAGAGGTCC
Pck1	GGAAGGACAAAGATGGCAAGTTC	AGGCGTTTTCCTTAGGGATGTAG
Pc	ACAGCACACACACTACCTGCAATG	GCAGGCCCTTATTTGGCAAGAGAT
Acadm	TGTTAATCGGTGAAGGAGCAG	CTATCCAGGGCATACTTCGTG
Cpt1a	CATGTCAAGCCAGACGAAGA	TGGTAGGAGAGCAGCACCTT
Cpt2	GGCATTGCGTATGCTGTTCACGAT	AAGCACTTCTGGACACAGTGGAGA
Acaca	AAGTCCTTGGTCGGGAAGTATACA	ACTCCCTCAAAGTCATCACAAACA
Acacb	AACCCACTGTCTTCCAATGACA	GAAGGACAACCCATTAGCATCTG
Acsl1	AACTCGAAGGCCATTCGTAC	GATAGATGAACTGTACGCCACC
Acsl3	AGCGAGATGGAAAATGAGGTC	ACTTGAAGGCATCTGTCACC
Lipc	TGGGTTATGACATCCGCAAG	GTAAAAGTAGGCTCTACCGGC
Cd36	GATCCGAACACAGCGTAGATAG	GCGACATGATTAATGGCACAG
Slc2a1	TCGTTGGCATCCTTATTGC	ACGAAGACGACACTGAGCAG
Slc2a2	GTCACTATGCTCTGGTCTCTG	CAAGAGGGCTCCAGTCAATG
Slc5a1	CTTTGAATGGAACGCCTTGG	GGACAGAACGGAAAGGTAGATC
Slc5a2	TGGTTATCGCTGCCTATTTCC	ACTGTGCCTCTATTGGTTCTG
Rpl32	CCTCTGGTGAAGCCCAAGATC	TCTGGGTTTCCGCCAGTTT
Rna18s5	GTAACCCGTTGAACCCCATT	CCATCCAATCGGTAGTAGCG

Supplemental Table 2.4. MS parameters for glutamate dehydrogenase system metabolite quantification

Analyte	Retention Time (min)	Molecular ion	Precursor-product transition	Precursor-product transition of Internal Standard
α-ketoglutarate	5.1	[α-ketoglutarate - H]$^-$	145.0142→101.0243 N(CE) 30	[U-$^{13}C_5$]glutamine 150.0787→132.0679 N(CE) 30
glutamate	5.2	[glutamate - H]$^-$	146.0459→102.0560 N(CE) 40	

Supplemental Table 2.5. Distribution of genotypes in offspring of Albumin-Cre$^{+/-}$, *Bdh1*$^{flox/flox}$ X Cre$^{-/-}$, *Bdh1*$^{flox/flox}$ Crosses.

Male offspring at weaning				Female offspring at weaning			
Genotype	**Observations**	**Expected (%)**	**Actual (%)**	**Genotype**	**Observations**	**Expected (%)**	**Actual (%)**
Cre -/-	106	50	54	Cre -/-	90	50	51
Cre +/-	92	50	46	Cre +/-	85	50	49

p = 0.4569 expected vs. actual using chi-square analysis (n=373)

Chapter 3: Reduced hepatic TCA cycle flux, glucose production, and liver fibrosis in D-β-hydroxybutyrate dehydrogenase hepatocyte-deficient mice maintained on NAFLD-inducing diets

Abstract

Objective: The regulatory roles of ketogenesis and ketone metabolism on liver homeostasis and health remain incompletely understood, especially in the context of nonalcoholic fatty liver disease (NAFLD). As there is ever increasing interest in intermittent fasting, ketogenic diets, and exogenous ketone therapies as possible health-promoting agents, we sought to develop a better understanding of the metabolic consequences of hepatic ketone body metabolism by focusing on the mitochondrial enzyme D-β-hydroxybutyrate dehydrogenase (BDH1), which is required for NAD^+/NADH-dependent interconversion of ketone bodies.

Methods: Using targeted high-resolution liquid chromatography-mass spectrometry, dual stable isotope tracer nuclear magnetic resonance spectroscopy-based metabolic flux modeling, and complementary physiological approaches in hepatocyte-specific knockout mice, we quantified the roles of hepatocyte D-β-hydroxybutyrate dehydrogenase (BDH1), in multiple dietary-induced mouse models of NAFLD.

Results: Compared to littermate controls, hepatocyte specific BDH1 deficient mice maintained on western-style diet showed diminished liver tricarboxylic acid (TCA) cycle flux and impaired gluconeogenesis, but normal overall hepatic energy

charge. Insulin sensitivity after acute insulin challenge was enhanced in knockout mice, however, no alterations in hepatic or muscle insulin signaling were seen. Lastly, the livers of knockout mice maintained on a 60% high fat diet were less fibrotic than littermate controls.

Conclusions: Ketone bodies, and BDH1 activity, influence liver homeostasis and health in the context of NAFLD. Loss of the ability to interconvert ketone bodies in hepatocytes results in reduced TCA cycle flux and hepatic glucose production, with a beneficial effect on liver fibrosis. Therefore, augmentation of hepatic BDH1 activity could prove beneficial in the treatment of NAFLD.

3.1 Introduction

Nonalcoholic fatty liver disease (NAFLD), the most common cause of liver disease in Western countries, affecting twenty-five percent of Americans[1; 2], is a multi-organ condition that includes hepatic fat infiltration alone (simple steatosis) or steatosis plus inflammation, liver cell injury (ballooning) and death (nonalcoholic steatohepatitis [NASH]). Hepatic steatosis alone (storage of excess triacylglycerols in hepatocytes, >5% of liver weight) [3] can be a stable clinical condition existing as the hepatic manifestation of obesity-related insulin resistance. Cirrhosis due to NASH develops in 2% of all Americans, driven through failed attempts to regenerate healthy liver, promoting activated hepatic stellate cells' execution of fibrogenesis, and the risk of hepatocellular carcinoma in NASH patients is 2% per year [4]. With no durable pharmaceutical interventions and

lifestyle modification remaining the standard of care, a profound need exists for the identification of novel therapeutic targets in the treatment of NAFLD [14].

Mitochondrial dysfunction contributes to NAFLD pathogenesis, with multiple studies observing increased hepatic oxidative energy fluxes [i.e., tricarboxylic acid (TCA) cycle flux and gluconeogenesis] in obesity and/or NAFLD [16-20]. Oxidative flux provides a fate for a portion of excess delivered fat, but does not fully compensate for the hepatocyte load, contributing to ectopic fat accumulation. Acting as an overflow for the hepatocyte TCA cycle, particularly active when carbohydrates are in short supply, hepatic ketogenesis can provide an additional fate for excess fat.

Through a series of reactions requiring the fate-determining enzyme 3-hydroxymethylglutaryl-CoA synthase 2 (HMGCS2), ketogenesis synthesizes acetoacetate (AcAc) from β-oxidation-derived acetyl-CoA [22]. AcAc is then reduced to D-β-hydroxybutyrate (βOHB) by the mitochondrial matrix enzyme D-βOHB dehydrogenase (BDH1), which catalyzes a near-equilibrium reaction requiring reduced (NADH) and generating oxidized (NAD^+) forms of nicotinamide adenine dinucleotide [23; 24; 79]. AcAc and D-βOHB are then released into the circulation for extrahepatic terminal oxidation. In livers with simple steatosis, ketogenesis is preserved or increased [16-20; 36; 64], while NASH progression in humans and animal models correlates with decreased ketogenesis and decreased expression of enzymatic mediators of ketone metabolism, before TCA cycle flux becomes impaired [17; 20; 64-69]. Additionally, loss of hepatic ketone metabolism has been linked increased liver injury and fibrosis [35].

Previously, we observed that treatment with exogenous AcAc attenuates hepatic fibrosis in wild-type mice fed a fibrogenic diet for 4 weeks, while D-βOHB administration modestly exacerbates fibrosis [44]. As the interconversion of AcAc and D-βOHB involves an oxidation-reduction (redox) reaction catalyzed by BDH1, this result suggests that mitochondrial redox potential, which is predominantly set by the NAD^+/NADH ratio, may contribute to the fibrotic response. Additionally, we have shown that hepatocyte-specific BDH1 loss reduces TCA cycle flux and hepatic glucose production in mice maintained on a chow diet [102]. Together, these observations suggest that augmentation of hepatic BDH1 activity may be beneficial in the treatment of NAFLD. To test this hypothesis, using intersectional approaches in physiology and analytical biochemistry of static and dynamic metabolic signatures, we quantified the role of hepatic BDH1 on both liver and whole-body metabolism with multiple dietary-induced mouse models of NAFLD.

3.2 Materials and Methods

3.2.1 Animals and diet

The Institutional Animal Care and Use Committee at the University of Minnesota approved all animal experiments. Hepatocyte-specific BDH1 knockout mice (Albumin-Cre X *Bdh1*$^{flox/flox}$; KO) and Cre-negative (*Bdh1*$^{flox/flox}$; Control) littermate control mice on a C57BL/6NJ sub-strain hybrid background were generated and maintained as previously described [102]. Adult male mice over the age of 14 weeks were used for all experiments. Prior to experimental diets, mice were

maintained on a standard low-fat chow diet (Teklad Global; 2016; 12% kcal fat, 22% protein, and 66% carbohydrate). NAFLD-inducing diets included a western-style diet (WD; TD.88137 ; Envigo; 42% kcal fat, 15% protein, 43% carbohydrate; 0.2% cholesterol by weight), a high fat diet (HFD; D12492; Research Diets; 60% kcal fat, 20% protein, 20% carbohydrate), and a choline-deficient, methionine-limited, high fat diet (CDAHFD; Research Diets; A06071302; 62% kcal fat, 18% protein, 21% carbohydrate; 0.1% Methionine by weight with no added choline). Mice were placed on NAFLD-inducing diets at 8-10 weeks of age, guaranteeing complete hepatocyte deficiency of BDH1 before diet commencement [102]. Experiments were conducted after 16-20 weeks on diet. Mice received autoclaved water ad libitum and were housed on corncob bedding in groups of 4 with lights off between 2000 and 0600 in a room maintained at 22°C. 18h, overnight fasts commenced at 1600 with experiments conducted at 1000 the next day. 4h fasts commenced at 0900 with experiments conducted at 1300. If mice were used for multiple studies, at least 1 week lapsed between experiments.

3.2.2 Immunoblot

Whole tissue protein lysates were prepared from frozen tissues and homogenized in ten times volume (microliters) to mass protein lysis buffer containing 20 mM Tris, 150 mM NaCl, 1 mM EDTA, 1% Triton-X 100, protease inhibitors (Roche) and phosphatase inhibitors (Sigma) [45]. Protein targets of interest were probed with the following primary antibodies: HMGCS2 (Santa Cruz, Sc-33828), BDH1 (Atlas Antibodies, HPA030947), pAKT (Ser473), total AKT, pIRβ (Tyr1150/1151), and total IRβ (Cell Signaling, 9271, 9272, 3024, and 3020 respectively). Horseradish

peroxidase (HRP)-conjugated secondary antibodies included goat anti-rabbit IgG and goat anti-mouse IgG (Southern Biotech 4030-05 and 1015-05 respectively). Protein loading was assessed by BlotFastStain (G-Biosciences, 786-34). Blots were developed using SuperSignal West Pico Plus Chemiluminescent substrate (Thermo Fisher, 34577) and imaged using a Bio-Rad ChemiDoc MP imaging system.

3.2.3 Gene expression analysis

RNA was purified from liver lysates homogenized in RLT buffer (Qiagen) with 1% 2-Mercaptoethanol using the RNeasy Mini Kit (Qiagen, 74016) following the manufacturer's instructions. Reverse transcripts were generated using Iscript (Bio-Rad, 1708891) and real-time reverse-transcription polymerase chain reaction (RT-PCR) was performed using SsoAdvanced Universal SYBR Green Supermix (Bio-Rad, 172-5274) on a CFX384 Real-Time System (Bio-Rad). Transcripts were quantified using the $2^{-\Delta\Delta Ct}$ method. Transcripts were normalized to *Rpl32* gene expression. Primer sequences used for gene expression analyses are listed in **Supplemental Table 3.1**.

3.2.4 Ketone body quantification

Circulating ketones were quantified using a method recently described by our group [83]. For serum or perfusion effluent samples, 10 µL of diluted serum/perfusion effluent were extracted with 40 µL of cold 1:1 acetonitrile:methanol containing the internal standards [3,4,4,4-D_4]βOHB and [U-

$^{13}C_4$]AcAc both at 50 µM. Samples were vortexed, and centrifuged at 4°C, 15,000 x g for 10 min before analyzing the supernatant by UPLC-MS/MS.

3.3.5 Serum measurements

Blood was acquired via submandibular bleed for fasting serum measurements. Blood glucose measurements were performed in duplicate using two CVS Health Advanced glucometers per collection, and the mean was taken. Non-esterified fatty acids (NEFA; Fujifilm, HR Series NEFA-HR2), triacylglycerols (TAG; Thermo Scientific, TR22421), and cholesterol (Fujifilm, 999-02601 and 993-02501) serum measurements were made using colorimetric assays following the manufacturer's instructions. Serum insulin was measured by an ELISA (Millipore Sigma, EZRMI-13K). All colorimetric assays were quantified using a Biotek Synergy HTX plate reader. HOMA-IR values were calculated as (Blood glucose (mg/dL) X Insulin (µU/mL)] / 405) [85].

3.2.6 Histology

Following euthanasia by cervical dislocation, mouse liver sections were fixed in 10% neutral buffered formalin. Formalin tissue embedding, sectioning, and staining with hematoxylin and eosin (H&E) or picrosirius red was performed by the University of Minnesota Clinical and Translational Science Institute histology core. Bright field (for H&E) and polarized light (for picrosirius red) Images were obtained using a Leica DM5500 B microscope. Picrosirius red fibrosis staining was quantified using ImageJ software (version 1.53c), by obtaining the percent area of picrosirius red staining in randomly selected fields at 20X magnification. To

quantify only sinusoidal fibrosis, central veins and portal triads were excluded from the quantification, thereby excluding collagen juxtaposed to luminal openings of the central vasculature [44].

3.2.7 Metabolic flux studies

Portal vein perfusions were performed as previously described [36]. Briefly, mice were anesthetized with 50 µL of sodium pentobarbital (65 mg/mL, Vortech) administered i.p., and once fully unconscious and unresponsive to toe pinch (approximately 5 minutes following delivery), the portal vein was exposed and cannulated with a 24-gauge catheter needle, the abdominal aorta and inferior vena cava cut, and the catheter was firmly tied into the portal vein. The beating heart was then exposed, and right atrium cut to prevent recirculation of buffer to the liver and to terminate perfusion to the brain. Livers were perfused with an oxygenated, glucose-free Krebs-Henseleit buffer, containing 3% $^{2}H_2O$, 0.1 mM sodium [U-$^{13}C_3$]propionate, 1.5 mM sodium lactate, 0.15 mM sodium pyruvate, 0.25% glycerol, and a 0.2 mM mix of non-esterified free fatty acids (40% palmitic, 35% oleic, 15% linoleic, and 10% palmitoleic acids bound to fatty acid-free BSA) as an exogenous fat source. The buffer was prewarmed to 45°C (determined empirically to counter heat loss in tubing such that tissue delivery is maintained at physiological temperature) in a thermostat-controlled water bath. The buffer delivery was maintained at a rate of 8 mL/min using a peristaltic pump for a period of 1 hour. The perfusate effluent from the final 30 minutes of the procedure was collected and frozen for further processing. Hepatic oxidative fluxes were quantified using a ^{2}H-NMR and ^{13}C-NMR based approach as previously detailed

[35; 36] by profiling monoacetone [$^{13}C/^{2}H$] glucose derivatized from hepatic venous effluent $^{13}C/^{2}H$-labeled glucose. ^{1}H-NMR, as previously described, was used to quantify total hepatic glucose and acetate production, and the uniformity of the perfusion procedure from separate perfusate effluent aliquots collected every 10 minutes. Perfusion effluent ketone bodies were quantified by LC-MS/MS as described in **Section 3.2.4** to determine their rates of production.

3.2.8 Energy metabolite quantification

Frozen liver sections (weighed frozen) were homogenized in an 0.4 M perchloric acid, 0.5 mM EGTA extraction solution containing [$^{13}C_{10}$,$^{15}N_5$]ATP sodium salt (100 µM), [$^{13}C_{10}$,$^{15}N_5$]AMP sodium salt (100 µM), [1,2-$^{13}C_2$]acetyl-CoA lithium salt (5 µM), and [1,2,3-$^{13}C_3$]malonyl-CoA lithium salt (5 µM) purchased from Sigma. After incubation on ice for 10 min, samples were centrifuged at 15,000 x g for 15 min at 4°C. The resulting supernatants were neutralized with freshly prepared 0.5 M K_2CO_3, vortexed, and centrifuged at 15,000 x g for 30 min at 4°C. Final extracts were then analyzed by LC-MS/MS as previously described [102].

3.2.9 Glucose and insulin tolerance tests

Measurements of blood glucose were performed prior to, and at regular intervals following intraperitoneal glucose/insulin injection. For glucose tolerance tests (IPGTT), a bolus of a sterile-filtered glucose solution was delivered i.p. to mice at 1 mg glucose/g body weight for tests following an overnight fast (18h), or 0.8 mg glucose/g body weight for tests following a 4h fast. The dosage of glucose for 4h fasting experiments was lowered because the 1 mg glucose/g body weight dose

resulted in blood glucose readings outside the range of our glucometer. For intraperitoneal insulin tolerance tests (IPITT), mice were administered i.p. human insulin (Lilly, HI-213) at 2 U/Kg body weight following a 4h fast.

3.2.10 Quantification of 4-hydroxylalkenal species

Freeze-clamped liver samples were homogenized in ice-cold 0.1x PBS and protein concentrations were determined by bicinchoninic acid (BCA) assay. Per 1 mg of protein, 0.7 nmol of 4-hydroxynonenal-d_3 (Cayman) internal standard was added to the homogenates, which were then extracted using modified Bligh and Dyer method [103], dried, and diluted in chloroform/methanol (1/1, v/v). Approximately 20 µL of extract (equivalent to 400 µL/mg protein) was mixed with 22 µL of 125 mM carnosine and 250 µL of water, then incubated at 37ºC for 24h for derivatization [104]. Derivatization was ended by adding 1.5 mL of chloroform/methanol (1/1, v/v) and 0.5 mL water to the sample. Derivatized 4-hydroxynonenal species were extracted into the upper aqueous layer after centrifugation at 2700 rpm for 5 min. Collected aqueous phase was washed two times by addition of chloroform (0.75 mL) each time. Retained aqueous phase extracts were evaporated under the nitrogen stream. The residue was reconstituted in 100 µL of water/methanol (1:1, v/v). The resulting solution was further diluted 20X in methanol/water/formic acid (80/20/0.1, v/v/v) and infused in TSQ Quantis mass spectrometer (Thermo, San Jose, CA) equipped with automated nanospray device (Triversa Nanomate, Advion Bioscienc Ltd. Ithaca, NY). Ionization voltage was maintained at 1.0 kV, and gas pressure at 0.3 psi. A 2 min full scan period was allowed to obtain stable spray. Analysis was performed in

positive ion mode using neutral loss scans of 71.2 and 117.2 with collision energies 23 and 28 eV, respectively, and collision gas pressure at 1 mTorr. Quantitation of 4-hydroxynonenal species was obtained by averaging the results determined from neutral loss scans of 71.2 and 117.2 in comparison to internal standard using in-house software.

3.2.11 Statistical analyses

Analyses were performed with GraphPad version 9.0.0 software (Prism, San Diego, CA) using tests described in the figure legends. P values describe comparisons between (or among) group means for measured values, accounting for the variances. Confidence intervals (CI, 95%) or percent differences within the text define the range spanning fold- or percent differences between groups.

3.3 Results

3.3.1 Circulating ketones are diminished in hepatocyte-specific BDH1 KO mice maintained on a NAFLD-provoking western style diet

Previously, we showed that hepatic loss of BDH1 reduces total circulating ketones and hepatic ketogenesis in mice maintained on a chow diet [102]. To determine if these alterations are preserved in a model of NAFLD, male hepatocyte-specific BDH1 knockout mice (KO) were fed a western-style diet (WD) which has been shown to provoke NAFLD [105]. Hepatic BDH1 knockout on the WD was confirmed by hepatic protein (immunoblot) and mRNA abundance (**Figure 3.1A-B**). No significant differences in hepatic HMGCS2 protein (**Figure**

3.1A) or mRNA (**Figure 3.1C**) expression were seen between control and KO mice. Circulating ketones were quantified in the serum of mice following an 18h fast. Compared to littermate controls, serum AcAc levels were elevated, albeit not significantly, by 31.2 ± 16.4% (p = 0.108) in KO mice, while serum βOHB levels were diminished by 71.6 ± 13.9% (p < 0.001), yielding a net decrease of 53.4 ± 14.0% (p < 0.001) in circulating TKB in KO mice (**Figure 3.1D**).

To determine the distribution of ketones produced by the liver, we next performed ex-vivo portal vein perfusions in male KO and littermate control mice following an 18h fast. Sixty-minute perfusions were conducted using an oxygenated, glucose-free Krebs-Henseleit buffer, containing a 0.2 mM mix of non-esterified free fatty acids (40% palmitic, 35% oleic, 15% linoleic, and 10% palmitoleic acids bound to fatty acid-free BSA) as an exogenous fat source. The hepatic venous effluent was collected and used for LC-MS/MS ketone quantification. Livers of KO mice produced AcAc at a rate 3.9-fold (95% CI 2.8 - 5.6, p < 0.01) greater than livers from littermate controls, while βOHB production was approaching zero at a rate of 0.010-fold (95% CI 0.007 – 0.014, p < 0.0001) that of littermate controls (**Figure 3.1E**). However, the TKB production rate in livers of KO mice was comparable to littermate controls at a rate of 0.8-fold (95% CI 0.6 – 1.1, p = 0.2433).

Mirroring what we previously saw in chow fed mice [102], the [AcAc]/[βOHB] ratio in hepatic venous effluent [112.8 (± 17.3)-to-1] from livers of perfused KO mice (**Figure 3.1E**) was discordant from that of the circulating ketone pool [1.01 (± 0.05)-to-1] in these mice (**Figure 3.1D**), whereas hepatic venous effluents from

perfused livers of littermate control mice showed [AcAc]/[βOHB] ratios [0.25 (± 0.04)-to-1] that were much more concordant with circulating ratios [0.21 (± 0.01)-to-1]. The recovery of [AcAc]/[βOHB] ratios in the circulation of Hepatocyte-BDH1-KO mice maintained on western diet suggests the continued presence of extrahepatic ketone equilibration [102].

Fasting body weights (34-week-old mice), weight gained (tracked for first 18 weeks of diet), and fasting liver weights were similar between control and KO mice maintained on WD (**Figure 3.2A-C**), with no significant differences in fasting serum levels of triacylglycerols (TAG), non-esterified fatty acids (NEFA), or cholesterol (**Figure 3.2D-F**). Additionally, no hepatic morphological differences were observed in hematoxylin and eosin-stained liver sections obtained from control and KO mice that were fasted for 18h prior to tissue harvest (**Figure 3.2G**). In cohorts of mice maintained on either a 60% high fat diet (HFD; **Supplemental Figure 3.1A-G**) or choline deficient, methionine-limited high fat diet (CDAHFD; **Supplemental Figure 3.2A-F**), KO mice were also phenotypically similar to littermate controls with a few noted exceptions. KO mice maintained on HFD showed a trending increase of 21.8 ± 9.1% ($p = 0.061$) and a significant increase of 52.1 ± 17.1% ($p < 0.05$) in 18h fasting circulating TAG and NEFA respectively (**Supplemental Figure 3.1D-E**). Although their weight trajectories were similar over the course of the diet, following an 18h fast, KO mice maintained on CDAHFD weighed significantly more than littermate controls (24.7 ± 0.2 vs. 23.2 ± 0.6 respectively, $p < 0.05$; **Supplemental Figure 3.2A**), with increases in 18h fasting circulating TAG (36.4 ± 10.0%, $p < 0.01$) and both ester (58.8 ± 19.5%, $p < 0.05$)

and total cholesterol (28.9 ± 11.9%, $p < 0.05$) species (**Supplemental Figure 3.2C & E**).

3.3.2 Loss of hepatic BDH1 diminishes total hepatic glucose production without altering liver energy charge in mice maintained on a NAFLD-provoking western-style diet.

Our previous work using ex-vivo 60-minute portal vein perfusions, utilizing the medium chain fatty acid octanoate as an exogenous fat source, revealed that hepatic loss of BDH1 reduces both TCA cycle flux, and phospho*enol*pyruvate sourced gluconeogenesis in 18h overnight-fasted mice. We therefore hypothesized that loss of hepatic BDH1 could beneficially reduce the increased hepatic glucose production (HGP) that is associated with NAFLD [106; 107]. To test this hypothesis, ex-vivo 60-minute portal vein perfusions were performed on littermate control and Hepatocyte-BDH1-KO mice maintained on WD following an overnight fast. Perfusions were performed using oxygenated Krebs-Henseleit buffer lacking glucose, but containing unlabeled 0.2 mM mix of non-esterified free fatty acids (40% palmitic, 35% oleic, 15% linoleic, and 10% palmitoleic acids bound to fatty acid-free bovine serum albumin) as an exogenous fat source, and flux tracers 3% $^{2}H_2O$ and 0.1 mM sodium [U-$^{13}C_3$]propionate, then collecting the hepatic venous effluent. After quantification of total HGP using ^{1}H-NMR, the hepatic ^{13}C/^{2}H–labeled glucose pool was extracted and converted to monoacetone glucose, from which ^{2}H- and ^{13}C-NMR spectra were collected, allowing hepatic oxidative fluxes and glucose sourcing to be determined.

TCA cycle flux in livers of KO mice was diminished to 0.7-fold (95% CI 0.5 - 0.9, $p < 0.05$) that of littermate controls (**Figure 3.3A**) with corresponding decreases in the rates of anaplerosis, (0.6-fold, 95% CI 0.4 - 0.7, $p < 0.001$, **Figure 3.3B**), and pyruvate cycling (0.6-fold, 95% CI 0.4 - 0.9, $p < 0.01$, **Figure 3.3C**). Total HGP was decreased to 0.7-fold (95% CI 0.6 - 0.9, $p < 0.01$, **Figure 3.3D**) that of controls in KO mice, with significant decreases in the both the contribution of phospho*enol*pyruvate (PEP, *i.e.,* TCA cycle-sourced, 0.5-fold, 95% CI 0.4 - 0.7, $p < 0.0001$, **Figure 3.3E**), and glycogenolysis (0.7-fold, 95% CI 0.6 - 0.9, $p < 0.05$, **Figure 3.3F**) to HGP. Additionally a trending decrease in glycerol flux (0.7-fold, 95% CI 0.5 – 1.0, $p = 0.0546$, **Figure 3.3G**) to HGP was also observed. Strikingly, given that the experiments were performed following an 18h fast, glycogen remained the major contributor to total HGP for both KO (53.9 ±2.2%) and control (51.6 ± 2.8%) mice (**Figure 3.3H**). Glycerol contributed 36.5 ± 2.1% and 35.8 ± 2.7% of total HGP for KO and control mice respectively. Neither of these contributes, as percentages of total HGP, varied between KO and control mice. However, the percentage contribution of PEP sourced glucose to total HGP was significantly smaller KO mice (9.6 ± 0.9% versus 12.7 ± 0.7% in controls, $p < 0.05$).

Given the reductions in oxidative fluxes in KO mice, we next assessed if KO mice maintained on WD would maintain liver energy charge. Echoing our previous assessments using a chow diet [102], static whole, liver tissue concentrations of AMP, ADP, ATP, NAD^+, and NADH, measured by LC-MS/MS using authentic internal standards [84] from unperfused livers of fasting mice, showed no differences between genotypes (**Figure 3.4A-B**), resulting in comparable

NAD^+/NADH and EC ratios (**Figure 3.4C**). Additionally, no differences in whole liver tissue Acyl CoA species were observed between KO and control mice (**Figure 3.4D**). Lastly no differences in gene expression on a panel of metabolism genes, including *Ppargc1a*, *Pparg*, *Pck1*, *Pc*, *Cpt1a*, *Cpt2, Acaca*, *Acacb*, *Acadm*, *Acadl*, *Acsl1*, *Acsl3*, *Lipc*, and *Cd36* were seen between KO and control mice (**Figure 3.4E**).

3.3.3 Alternated whole body glucose homeostasis in Hepatocyte-BDH1-KO mice maintained on a western-style diet.

Given the impairment of hepatic gluconeogenesis in KO mice (**Figure 3.3D**), we next wanted to determine whether loss of hepatocyte BDH1 also affects whole-body glucose homeostasis in mice maintained on a western-style diet. While 4h fasting blood glucose levels were significantly higher in KO mice, (212.2 ± 9.0 mg/dL versus 183.4 ± 7.3 mg/dL in controls, $p < 0.05$, **Figure 3.5A**),18h fasting blood glucose levels in male KO mice were only modestly, and not significantly, elevated over controls (**Figure 3.5B**). 18h fasting serum insulin showed a trending decrease in KO mice (4.1 ± 0.7ng/mL versus 6.8 ± 1.2 ng/mL in controls, $p = 0.0751$, **Figure 3.5C**), and calculated HOMA-IR (**Figure 3.5D**) was similar between control and KO mice. To assess glycemic excursion after an exogenous glucose load, we performed a fasting (18h) i.p. glucose tolerance test (IPGTT). Area of the curve (AOC) analysis showed a trending improvement in glucose tolerance (increasing AOC corresponding to less glucose tolerance), with the AOC of KO mice 0.8 fold (95% CI 0.6 – 1.0, $p = 0.073$, **Figure 3.5E**) that of controls. To determine the ability of these mice to defend glycemia after an insulin challenge,

we performed a fasting (4h) i.p. insulin tolerance tests (IPITT). The acute response to insulin in KO mice was more pronounced (compare the initial curve slopes in **Figure 3.5F**) resulting in a significantly higher AOC (increasing AOC corresponding to increased insulin sensitivity) in KO mice of 2.0 fold (95% CI 1.4 – 2.8, $p < 0.001$) that of controls. Taken that serum levels of insulin were comparable following the IPITT (**Figure 3.5G**), this increase in AOC suggests improved whole body insulin sensitivity in KO mice when compared with controls.

With this result, suggesting improved systemic insulin sensitivity in KO mice, we next looked for molecular evidence of alterations in insulin signaling in both liver and muscle (gastrocnemius) tissue of KO mice. Following a 4h fast, mice were injected with either insulin (2 U/Kg body weight) or vehicle (saline) and tissues were harvested (post cervical dislocation euthanasia) 10 minutes post injection. Following insulin treatment, levels of AKT phosphorylation were similar between KO and control mice in both liver and gastrocnemius tissues (**Figure 3.6A-B**). Additionally, no differences in insulin receptor beta (IRβ) phosphorylation were seen between KO and control mice in both liver and gastrocnemius tissues (**Figure 3.6C-D**). Together, these results suggest that alterations in insulin signaling, either in liver or gastrocnemius tissue, are not responsible for the improvement in whole body insulin sensitivity seen in KO mice.

3.3.4 Loss of hepatic BDH1 reduces markers of fibrosis and oxidative stress in mice in models of NAFLD

As alterations in ketone body metabolism have been shown to worsen fibrosis in mouse models of NAFLD [35; 44], we next determined the impact of hepatic BDH1

loss on liver fibrosis in mice maintained on either a WD or HFD. Assessment of liver fibrosis using picrosirius red staining revealed similar levels of fibrosis in KO and control animals maintained on WD (**Supplemental Figure 3.3A**). However, in mice maintained on a HFD, KO animals qualitatively appeared to have less fibrotic livers (**Figure 3.7A**). In comparing 20X fields, quantitative assessment of picrosirius red-positive area revealed significantly decreased fibrosis (56.1 ± 0.1% reduction, $p < 0.0001$) in fields obtained from KO mice when compared with controls (**left graph, Figure 3.7B**). When taking the average field per mouse, levels of fibrosis remained reduced (56.1 ± 0.3% reduction, $p = 0.0630$) in KO mice, however this result was not quite statistically significant (**right graph, Figure 3.7B**).

Complementing these results, transcript abundances of the fibrotic gene markers *Col1a1* (0.25-fold, 95% CI 0.04 – 0.65, $p < 0.01$) and *Col3a1* (0.4-fold, 95% CI 0.02 – 0.7, $p < 0.05$) were both significantly reduced, in addition to nonsignificant reductions in *Col4a1* and *Acta2*, in the livers of KO mice maintained on a HFD (**Figure 3.7C**). However, none of these markers of liver fibrosis varied between KO and control mice maintained on a WD (**Supplemental Figure 3.3B**).

With reductions in fibrosis seen on the HFD, we next assessed markers of oxidative stress, and found a significant reduction (0.5-fold, 95% CI 0.3 – 0.9, $p < 0.01$) in *Nox2* gene expression in the livers of KO mice on HFD (**Figure 3.7D**). Additionally, although no differences in *Nox2* gene expression were seen between KO and control mice on WD (**Supplemental figure 3.3C**), a shotgun lipidomics-based quantification of 4-hydroxyalkenal species, a class of peroxidative products

of polyunsaturated acids [104], revealed a significant reduction (23.9 ± 16.8%, $p < 0.05$) in 4-hydroxy-2E-nonenal (HNE) in KO mice when comparted with controls (**Supplemental Figure 3.3D**).

Lastly, qualitative assessment of liver fibrosis using picrosirius red staining suggested less liver fibrosis in KO mice maintained on CDAHFD when compared with controls (**Supplemental Figure 3.4**). Furthermore, out of the 8 control animals assessed, 2 (25%) had liver tumors (presumably hepatocellular carcinoma) at time of harvest, whereas no tumors were seen in KO livers (0 out of 8), suggesting a protective effect of hepatic BDH1 loss on the fibrosis-to-tumor-formation progression. Although not definitive, these results, using multiple dietary models of NAFLD, suggest that hepatic specific loss of BDH1 may be beneficial in reducing fibrosis, oxidative stress, and the progression to tumor formation in NAFLD.

3.4 Discussion

Using high-resolution LC-MS/MS, dual isotope tracer NMR spectroscopy, and integrated physiological approaches in hepatocyte-specific BDH1 knockout mice, our results reveal new insights into the role hepatic BDH1 in NAFLD. In mice maintained on a NAFLD-inducing WD, hepatocyte-specific loss of BDH1 diminished total circulating ketone concentrations. While circulating AcAc levels were similar to controls, KO mice showed large decreases in both circulating βOHB and TKB levels in the 18h fasting state. Long chain fatty acid perfusion studies showed similar rates of liver TKB production, however KO mice almost exclusively

exported AcAc, whereas the majority of the AcAc produced by livers of control mice is reduced to D-βOHB before its export from the liver.

Together, the decrease in circulating ketone concentrations in Hepatocyte-BDH1-KO mice, in the context of near normal liver TKB production, suggests increased ketone clearance by extrahepatic tissues [80; 102], which could possibly be explained by increased substrate availability. Normally, the liver releases substantially less AcAc than βOHB than into the circulation ([AcAc]/[βOHB] ratio of [0.25 (± 0.04)-to-1] for control mice in this study). Whereas all extrahepatic tissues are capable of utilizing AcAc, only a subset express BDH1, such as heart, muscle, and kidney, meaning βOHB utilization is more restricted. By increasing the availability of circulating AcAc, hepatocyte-specific BDH1 loss, shifts the balance of circulating ketones, allowing for increased usage by the extrahepatic tissues that cannot utilize βOHB.

We previously showed that hepatocyte-specific BDH1 loss reduced TCA cycle flux, and TCA cycle-soured gluconeogenesis in chow fed mice. Here, our perfusion studies, utilizing long-chain fatty acids as an exogenous fat source, showed that these reductions remain in Hepatocyte-BDH1-KO mice maintained on a WD. Additionally, a significant reduction in total HGP was seen, suggesting that the reductions in HGP conferred by hepatocyte-specific BDH1 loss are more pronounced with WD feeding. Without BDH1, liver mitochondria have lost a conduit to re-generate NAD^+ from NADH. Impairment in TCA cycle flux, and the corresponding decreases in gluconeogenesis, both observed in livers of KO mice, most likely results primarily a consequence of this redox perturbation. It is also

possible that without BDH1, liver mitochondria could retain more NADH, decreasing the demand for oxidative metabolism in the liver.

As BDH1 is one of several mitochondrial dehydrogenases [24; 87], loss of BDH1 in hepatocytes may provoke compensations that protect against more pronounced abnormalities of redox homeostasis. Indeed, while hepatic TCA cycle flux was diminished in livers lacking BDH1, overall energy balance fell within normal limits, and energy charge and whole liver tissue redox were normal. To determine these compensations and therefore fully understand the redox effects of BDH1 loss on hepatocyte mitochondria, dynamic measurements of specific mitochondrial dehydrogenase activities against incrementally controlled variations of energy charge will be required.

The perfused liver model employed herein, utilizing a mix of long-chain fatty acids, better reflects the physiological fatty acid supply sampled by hepatocytes in vivo, than our previous studies, which utilized the carnitine palmitoyltransferase–independent medium chain fatty acid, octanoate. This difference in experimental design, precludes a perfect comparison with our previous study utilizing Hepatocyte-BDH1 KO mice maintained on a chow diet, and any oxidative flux comparisons between these datasets must consider fuel source as a potential variable. Nonetheless, reductions in TCA cycle flux and HGP in Hepatocyte-BDH1 KO mice have now been shown not only in two dietary states, but also with two different exogenous fuel sources, further supporting the validity of these alterations.

Comparable to our previous study using chow-fed mice, hepatocyte-specific loss of BDH1 alters systemic glucose homeostasis in WD-fed mice. Although 18h fasting HGP is reduced in KO mice maintained on WD, 18h fasting glucose is maintained with a trending decrease in 18h fasting insulin. Additionally systemic insulin sensitivity, as assessed by IPITT is increased in KO mice, although this increase could not be linked to differences in either hepatic or muscle insulin signaling. The insulin-stimulated drop in glycemia, in the IPITT, could therefore be due to greater glucose uptake in other tissues, such as heart, brain. With the complexity of whole body Insulin sensitivity, experiments in isolated tissues might not be able to fully explain the systemic effects.

In addition to the elevations in 4h fasting blood glucose in KO mice maintained on WD, multiple models of insufficient hepatic ketogenesis have shown mild elevations in fasting blood glucose. A recent report of whole body BDH1 knockout mice showed higher blood glucose after a 48h starvation [34]. HMGCS2 knockdown results in mild hyperglycemia, and increased HGP from pyruvate [35; 36]. With extended periods of fasting, hepatic fat oxidation by the liver normally increases ketone production, which can then be utilized by tissues, such as the brain, which oxidizes fat much less avidly compared to the liver, heart, or skeletal muscle. With programmed deficits in hepatic ketone production, the brain loses a primary fuel source during fasting [27]. Perhaps due to high energy requirements in human brains (relative to mouse), ketogenic insufficiency is not as well tolerated by fasting humans and yields severe hypoglycemia [108]. However, based on prior studies of HMGCS2 deficiency in mice [35], and the studies performed herein,

ketogenic insufficiency likely provokes compensatory mechanisms that preserve glycemia in mice. Nonetheless, further study is needed to fully understand the link between ketogenic insufficiency and glucose homeostasis at both liver and whole-body levels.

By far the most exciting results from this study were the evidence suggestive that hepatocyte-specific loss of BDH1 might slow disease progression in NAFLD. In the HFD model, reduced hepatic fibrosis with hepatocyte-specific BDH1 loss was evident in picrosirus red-stained liver sections. There was evidence of less oxidative stress with hepatocyte-specific BDH1 in both the HFD model (*Nox2* expression) and WD model (HNE quantification). Furthermore, whereas hepatic tumors were seen in 25% of littermate controls maintained on CDAHFD, none were seen in KO mice. Further study will be required to determine the mechanisms behind these beneficial effects of hepatocyte-specific loss of BDH1. It is possible that the decrease in fibrosis and oxidative stress could be due to the redox implications of hepatic BDH1 loss. However, as Hepatocyte-BDH1 KO mice maintain whole liver energy charge and NAD^+/NADH ratio, a global change in redox explaining the fibrosis phenotype is less likely. Nevertheless, compensation mechanism to maintain total energy charge and redox state might contribute to the fibrosis phenotype, and dynamic mitochondrial redox measurements will be needed to determine this.

Another possible explanation for the improved fibrosis in KO mice could be from the altered ketone concentrations in the liver sinusoid. We previously observed that treatment with exogenous AcAc attenuates hepatic fibrosis in wild-

type mice fed a fibrogenic diet for 4 weeks, while D-βOHB administration modestly exacerbates fibrosis [44]. Without BDH1, the liver sinusoidal environment has increased AcAc availability, affording non-hepatocyte sinusoidal cells, for instance stellate cells and macrophages, with an additional fuel source. Conversely decreased BOHB availability could be beneficial. Furthermore, AcAc and βOHB each confer distinct signaling effects through unique G protein coupled receptor targets, components of the immune and inflammatory signaling systems, cytoplasmic signal transduction cascades, as well as post-translational histone modification [54; 109; 110]. Therefore, the improvement in fibrosis seen with hepatocyte-specific BDH1 loss could be the result of a distinct signaling outcome attributable to the preservation/enhancement of AcAc signaling and loss of βOHB signaling.

The study herein utilized three different NAFLD-including diets, each with differing degrees of fibrotic progression. The WD had the lowest fat content (42% Kcal fat), with a much higher proportion of kcals from carbohydrates (43%), possibly explaining why glycogen remains the primary source of gluconeogenesis in these mice. With its higher fat content (60% kcal fat), the HFD was likely more ketogenic, possibly explaining why a clearer effect on fibrosis was seen in this diet, but not as evident with the WD. Mice maintained on CDAHFD, which had comparable macronutrients to the HFD but with no choline and limited methionine, gained little to no weight over the course of the diet, contrasting with what has been shown previously [111]. Although it did confer a progressive NAFLD/NASH liver phenotype, the CDAHFD was not obesogenic, and this distinction must be

considered when interpreting the present results. The subtle, and sometimes pronounced, differences between these diets highlight the variability that can exist between studies using different diet-induced mouse models of NAFLD [112]. Therefore, without one perfect model system, hypotheses should be investigated utilizing multiple models before definitive conclusions are made.

In conclusion, ketone bodies, and BDH1 activity, influence liver homeostasis and health in the context of NAFLD. Loss of the ability to interconvert ketone bodies in hepatocytes results in reduced TCA cycle flux and glucose production, increased systemic insulin sensitivity, and a beneficial effect on liver fibrosis, all with minimal overall effect on liver energy charge. Therefore, augmentation of hepatic BDH1 activity could prove beneficial in the treatment of NAFLD. Future studies that quantify the impact of hepatocyte BDH1 in additional metabolic contexts, such as response to exogenous ketone body supplements, exercise, or intermittent fasting, may provide further insight into the roles of ketone body-governed mitochondrial redox homeostasis in metabolic physiology.

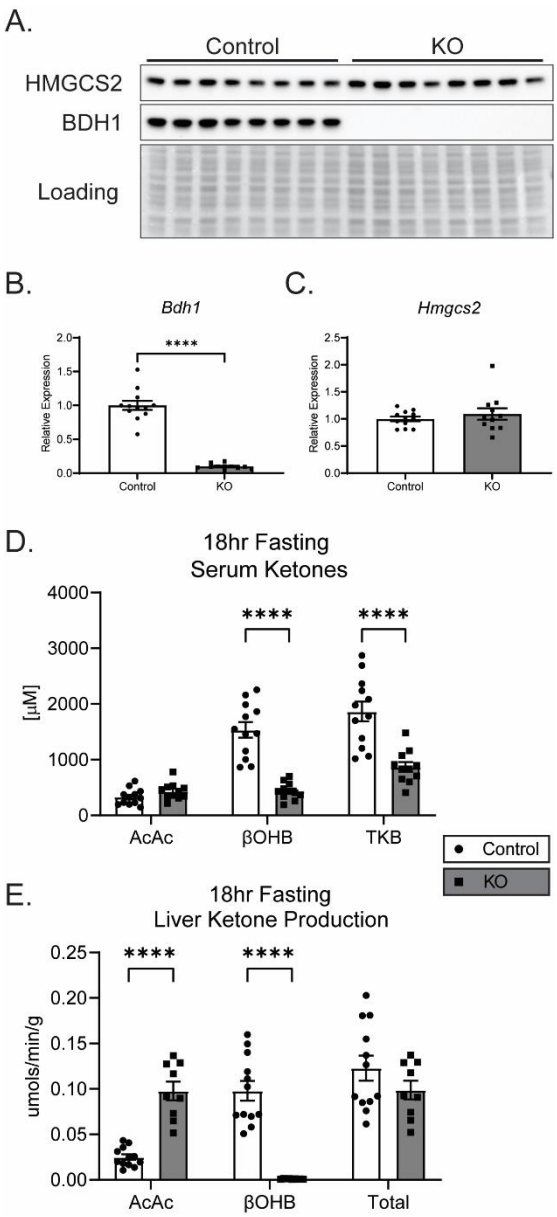

Figure 3.1. Diminished circulating ketones and impaired hepatic ketogenesis in hepatocyte-specific BDH1 KO mice maintained on a NAFLD-provoking western style diet. (A) Immunoblots of HMGCS2, BDH1, and protein loading obtained from liver protein lysates of fasting (18hr) littermate control (*Bdh1*$^{flox/flox}$) and Hepatocyte-BDH1-KO (Albumin-Cre X *Bdh1*$^{flox/flox}$) mice maintained on a western-style diet (*n* = 8/group). **(B)** Fasting liver transcript abundances of *Bdh1* and **(C)** *Hmgcs2* in control and KO mice (*n* = 11-12/group). **(D)** Fasting serum ketones (µM; *n* = 11-12/group). **(E)** Liver ketone production, quantified by LC-MS of hepatic venous effluent from 60-min portal vein perfusion using an oxygenated buffer containing 0.2 mM unlabeled mix of non-esterified free fatty acids as exogenous fat from 18h fasted mice (µmol/min/g liver; *n* = 9-12/group). Data presented as mean ± SEM. ****P <0.0001 by Student's *t* test or by two-way ANOVA with Sidak's multiple comparisons.

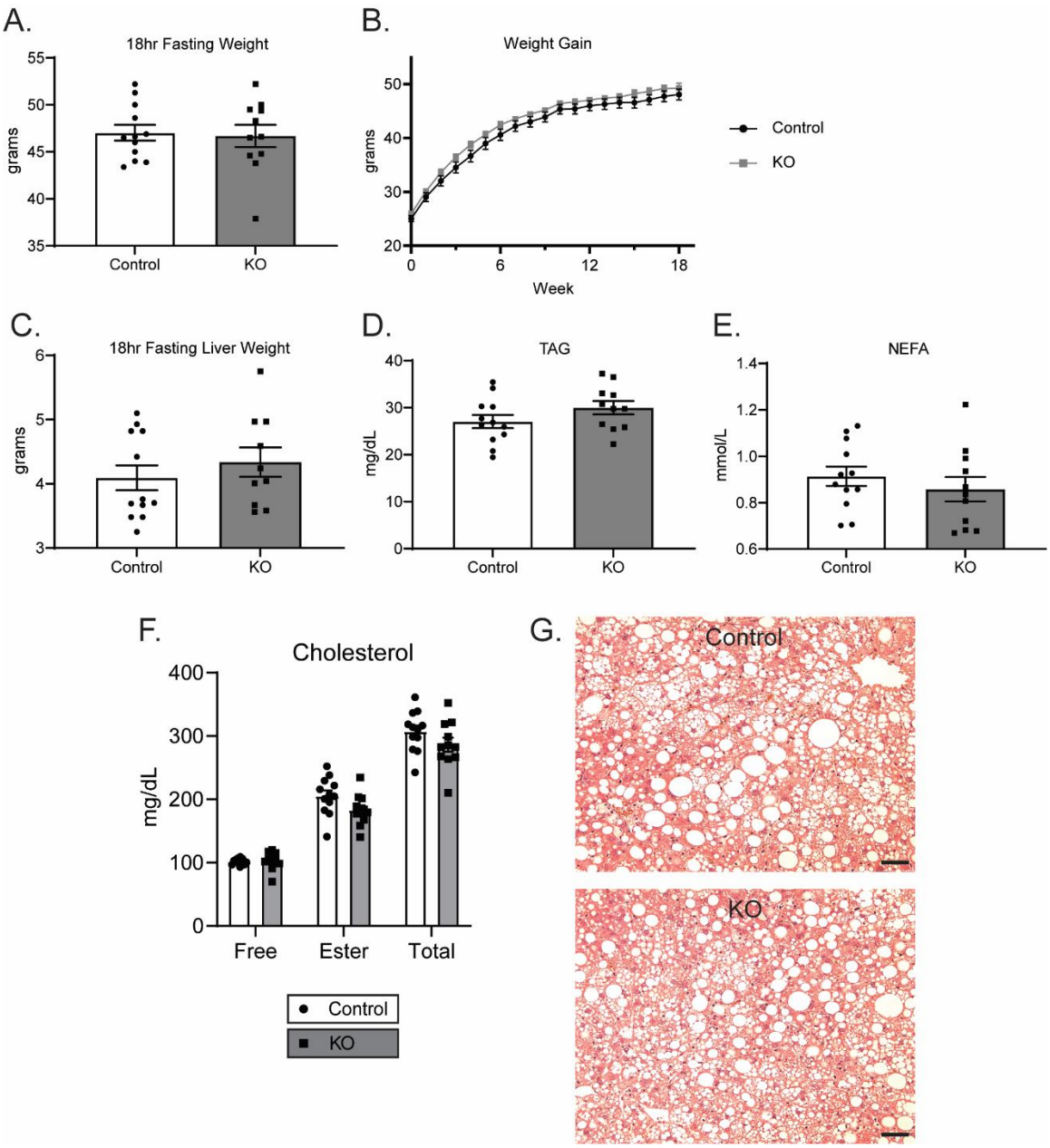

Figure 3.2. In mice maintained on a western-style diet, fasting body weights and circulating lipids do not differ with hepatic BDH1 loss. (A) Fasting (18h) body weight (g), **(B)** weight gain (g), **(C)** liver weight (g), **(D)** serum triacylglycerols (TAG; mg/dL), **(E)** non-esterified fatty acids (NEFA, mmol/L) and **(F)** free, ester-bound, and total circulating cholesterol (mg/dL) in fasting male control and KO mice (*n* = 10-12/group). **(G)** Representative H&E staining of liver sections from fasting control and KO mice. Data presented as mean ± SEM. Scale bars = 50 μm.

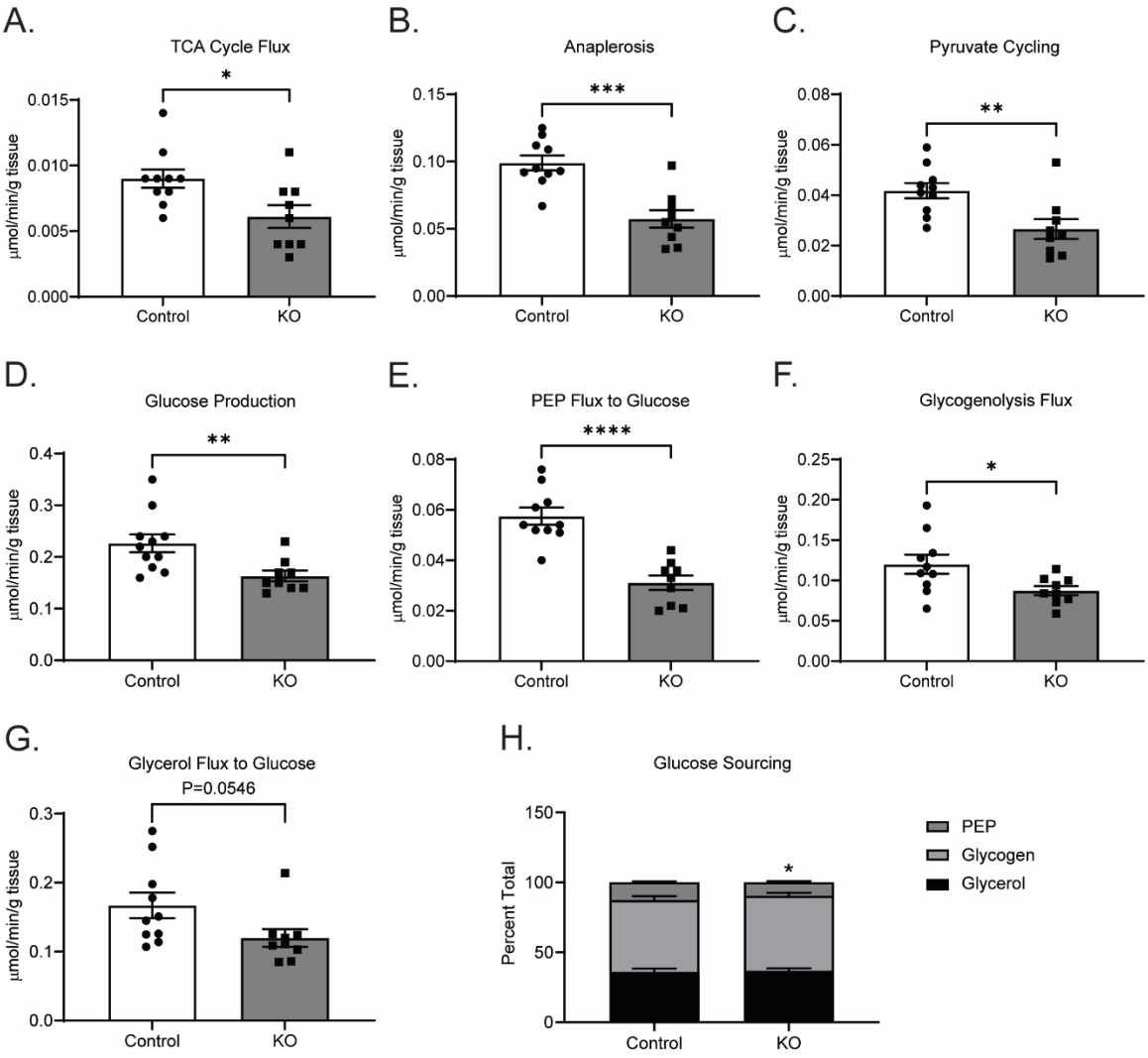

Figure 3.3. Loss of hepatic BDH1 diminishes hepatic oxidative fluxes in mice maintained on a western-style diet. (A) TCA cycle flux, **(B)** anaplerosis flux, **(C)** pyruvate cycling, **(D)** hepatic glucose production, **(E)** phospho*enol*pyruvate (PEP)-supported (TCA cycle-sourced) flux to gluconeogenesis, **(F)** glycogenolysis flux to hepatic glucose production, and **(G)** glycerol flux to hepatic glucose production quantified by ^{13}C-, ^{2}H-, and ^{1}H-NMR, from perfusions using an oxygenated buffer containing 0.2 mM unlabeled mix of non-esterified free fatty acids, 3% $^{2}H_2O$, and 0.1 mM sodium [U-$^{13}C_3$]propionate in fasting (18hr) control and KO mice (µmol/min/g liver; *n* = 9-11/group). **(H)** Relative contributions of PEP, glycogen, and glycerol to hepatic glucose production, imputed from data presented in panels **D-G**. Data presented as mean ± SEM. **P* <0.05; ***P* <0.01; ****P* <0.001 *****P* <0.0001 by Student's *t* test.

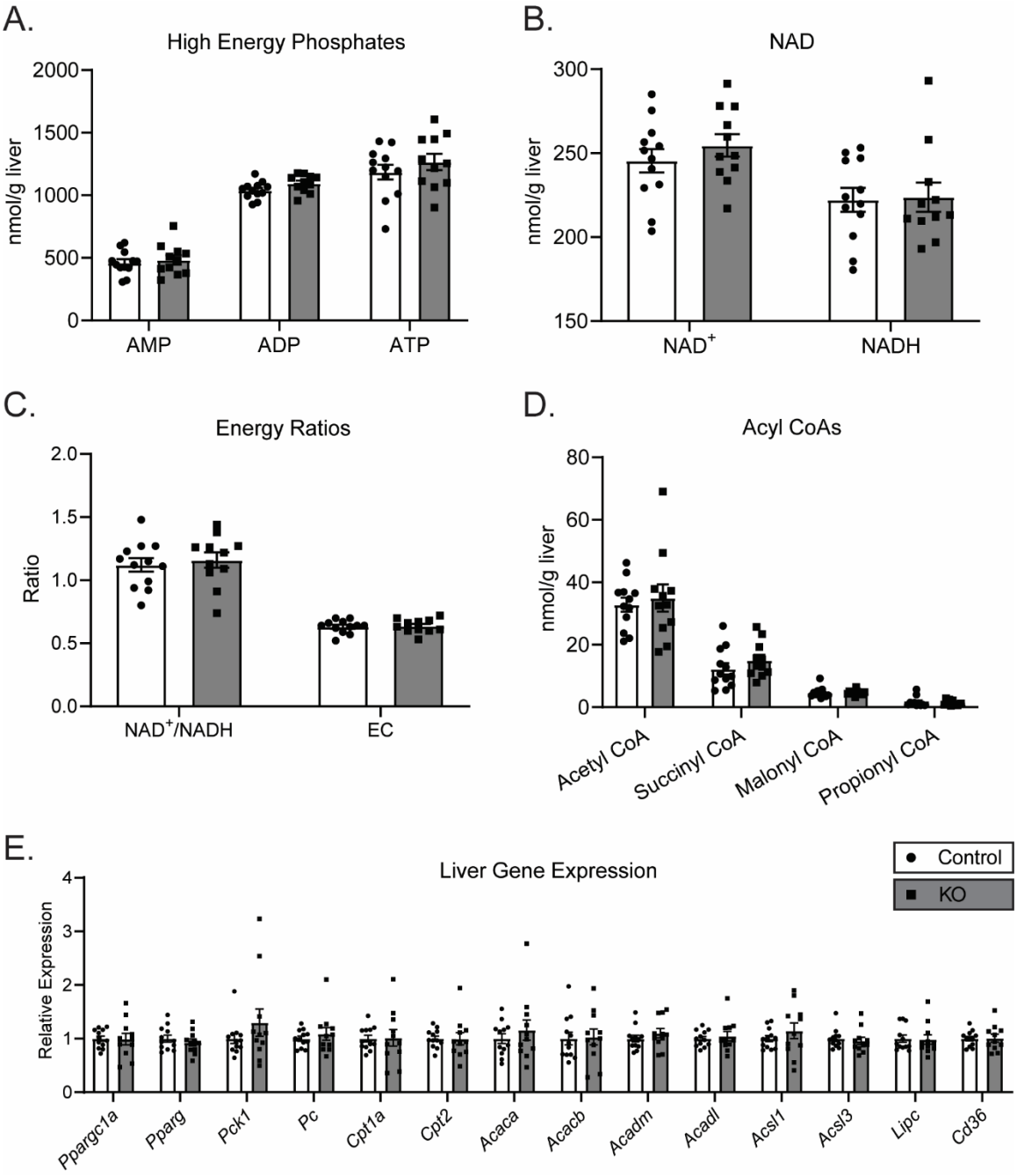

Figure 3.4. Preserved liver energy charge in Hepatocyte-BDH1-KO mice maintained on a western-style diet. (A) LC-MS-determined static quantities of liver AMP, ADP, ATP and **(B)** NAD^+ and NADH in fasting (18hr) control and KO mice (nmol/g liver; *n* = 11-12/group). **(C)** Whole liver NAD^+/NADH and energy charge (EC) ratios calculated from data presented in **A-B**. **(D)** Measured static quantities of whole liver (nmol/g liver) total acetyl-CoA, succinyl-CoA, malonyl-CoA, and propionyl-CoA in fasting control and KO mice (*n* = 11-12/group). **(E)** Transcript abundances of *Ppargc1a*, *Pparg*, *Pck1*, *Pc*, *Cpt1a*, *Cpt2, Acaca*, *Acacb*, *Acadm*, *Acadl*, *Acsl1*, *Acsl3*, *Lipc*, and *Cd36* from livers of fasting control and KO mice. (*n* = 11-12/group). Data presented as mean ± SEM.

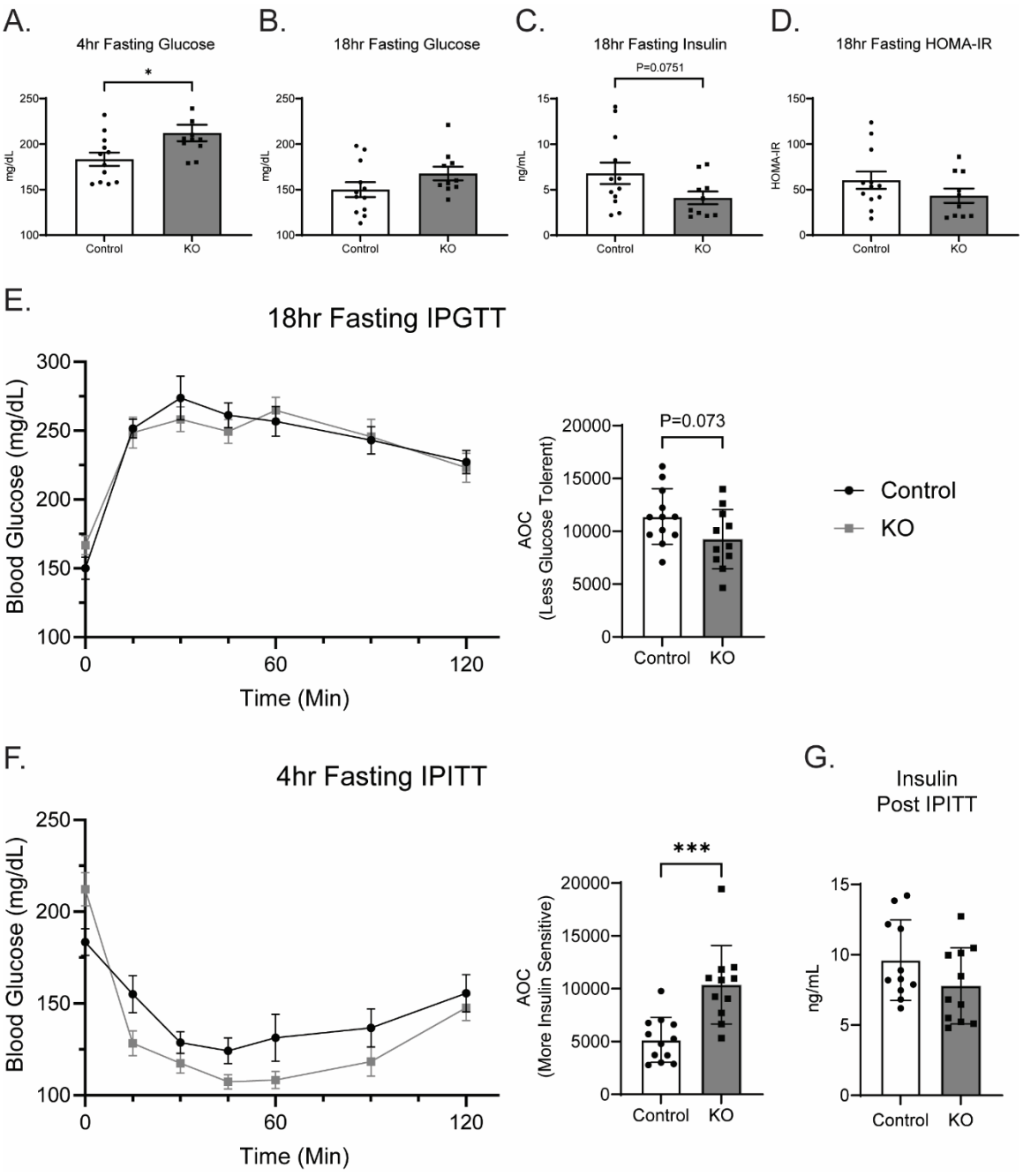

Figure 3.5. Altered glucose homeostasis in Hepatocyte-BDH1-KO mice maintained on a western-style diet. (A) 4hr fasting blood glucose (mg/dL) in control and KO mice (*n* = 10-12/group). **(B)** 18hr fasting serum measures of glucose (mg/dL), **(C)** insulin (ng/mL), and **(D)** HOMA-IR in control and KO mice (*n* = 10-12/group). **(E)** 18h fasting IPGTT (1 mg glucose/g body weight) and **(F)** 4hr fasting IPITT (2 U/Kg body weight) curves with calculated AOC graphs in control and KO mice. (*n* = 11-12/group). **(G)** Post IPITT serum insulin (ng/mL) in control and KO mice. (*n* = 11-12/group). Data presented as mean ± SEM. **P* <0.05; ****P* <0.001 by Student's *t* test.

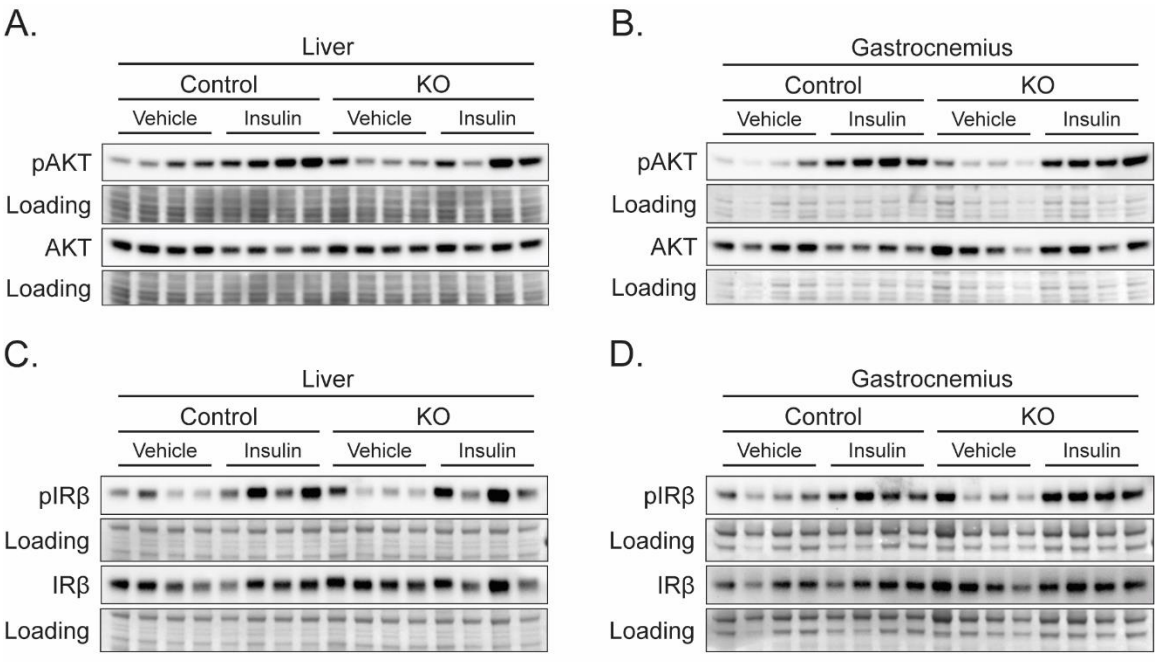

Figure 3.6. Insulin signaling in Hepatocyte-BDH1-KO mice maintained on a western-style diet remains comparable to controls. (**A**) Immunoblots of phosphorylated AKT (pAKT), total AKT, and protein loading obtained from 4hr fasting liver and **(B)** gastrocnemius protein lysates of control and KO mice 10 min post insulin (2 U/Kg body weight) or saline vehicle injection (*n* = 4/group). (**C**) Immunoblots of phosphorylated IRβ (pIRβ), total IRβ, and protein loading obtained from 4hr fasting liver and **(D)** gastrocnemius protein lysates of control and KO mice 10 min post insulin (2 U/Kg body weight) or saline vehicle injection (*n* = 4/group).

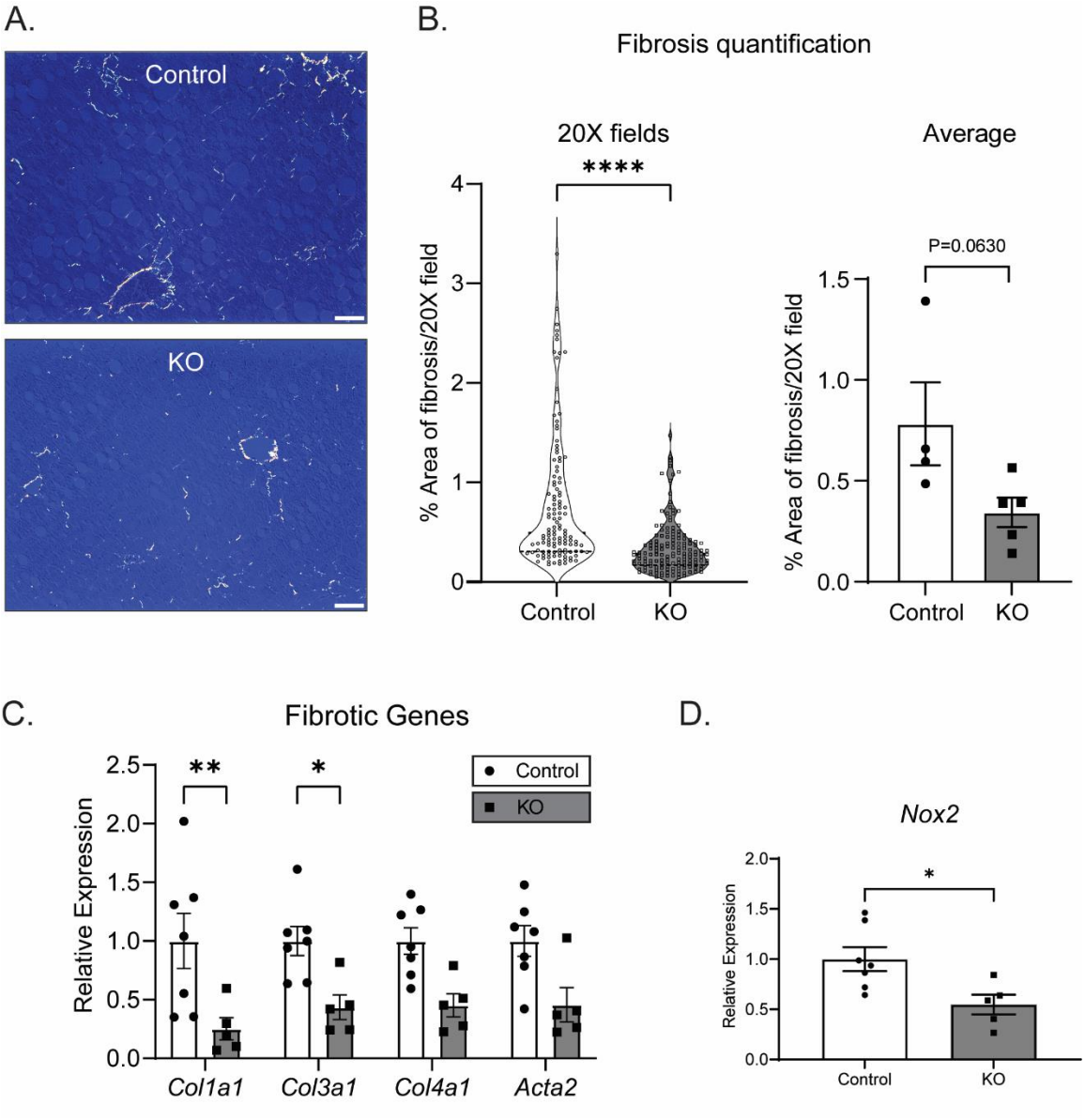

Figure 3.7. Loss of hepatic BDH1 reduces markers of fibrosis in mice maintained on a 60% high fat diet. (A) Representative picrosirius red staining of liver sections from control and KO mice maintained on a 60% HFD. **(B)** Quantification of picrosirius red-positive area (%area/20X field) for all fields obtained (left, *n* = 120-150/group) and mouse averages (right *n* = 4-5/group) in control and KO mice. **(C)** Transcript abundances of fibrotic markers *Col1a1*, *Col3a1*, *Col4a1*, and *Acta2*, and **(D)** oxidative stress marker *Nox2* from livers of control and KO mice. (*n* = 5-7/group). Scale bars = 50 μm. Data presented as mean ± SEM. **P* <0.05; ***P* <0.01; *****P* <0.0001 by Student's *t* test or by two-way ANOVA with Sidak's multiple comparisons.

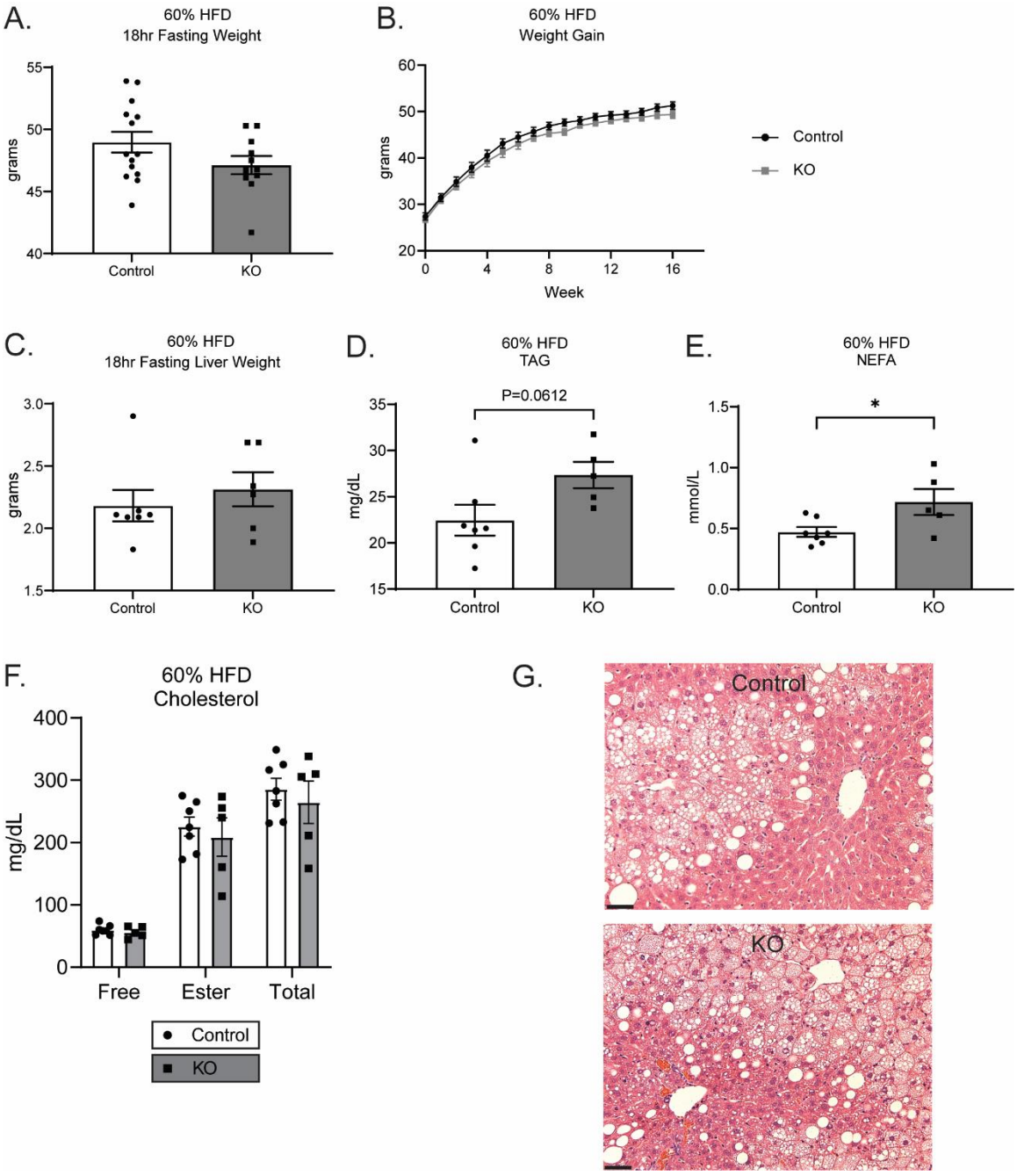

Supplemental Figure 3.1 (paired with Figure 3.2). Body weight and circulating lipid assessment in Hepatocyte-BDH1-KO mice maintained on a 60% high fat diet. (A) Fasting (18hr) body weight (g) and **(B)** weight gain (g), in control and KO mice maintained on a 60% HFD (*n* = 11-14/group). **(C)** Liver weight (g), **(D)** serum triacylglycerols (TAG; mg/dL), **(E)** non-esterified fatty acids (NEFA, mmol/L) and **(F)** free, ester-bound, and total circulating cholesterol (mg/dL) in fasting control and KO mice (*n* = 5-7/group). **(G)** Representative H&E staining of liver sections from fasting control and KO mice. Scale bars = 50 μm. Data presented as mean ± SEM. **P* <0.05 by Student's *t* test.

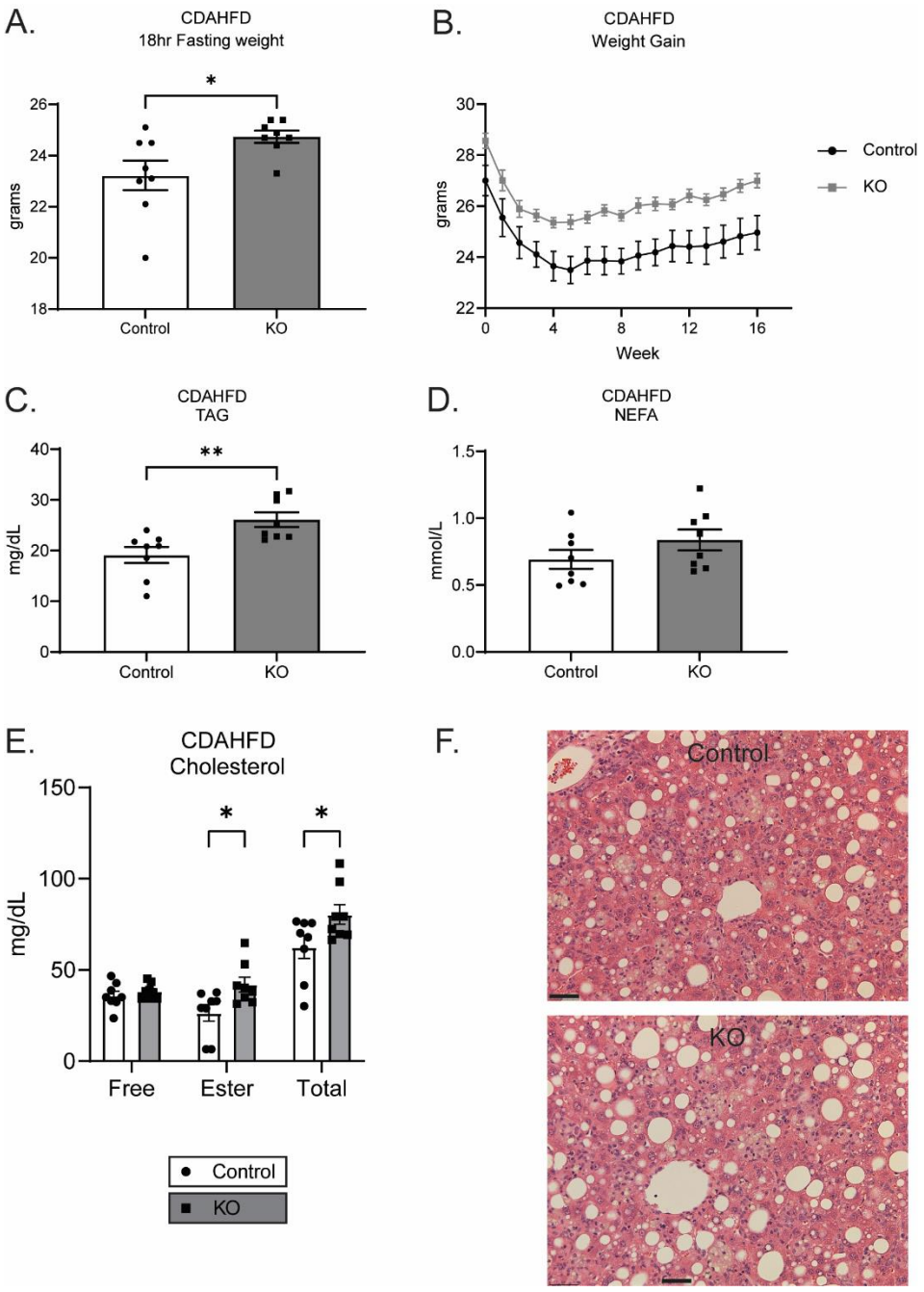

Supplemental Figure 3.2 (paired with Figure 3.2). Body weight and circulating lipid assessment in Hepatocyte-BDH1-KO mice maintained on a choline-deficient, methionine-limited high fat diet. (A) Fasting (18h) body weight (g), **(B)** weight gain (g), **(C)** serum triacylglycerols (TAG; mg/dL), **(D)** non-esterified fatty acids (NEFA, mmol/L) and **(E)** free, ester-bound, and total circulating cholesterol (mg/dL) in fasting control and KO mice maintained on CDAHFD (*n* = 8/group). **(F)** Representative H&E staining of liver sections from fasting control and KO mice. Data presented as mean ± SEM. Scale bars = 50 μm. **P* <0.05; ***P* <0.01 by Student's *t* test.

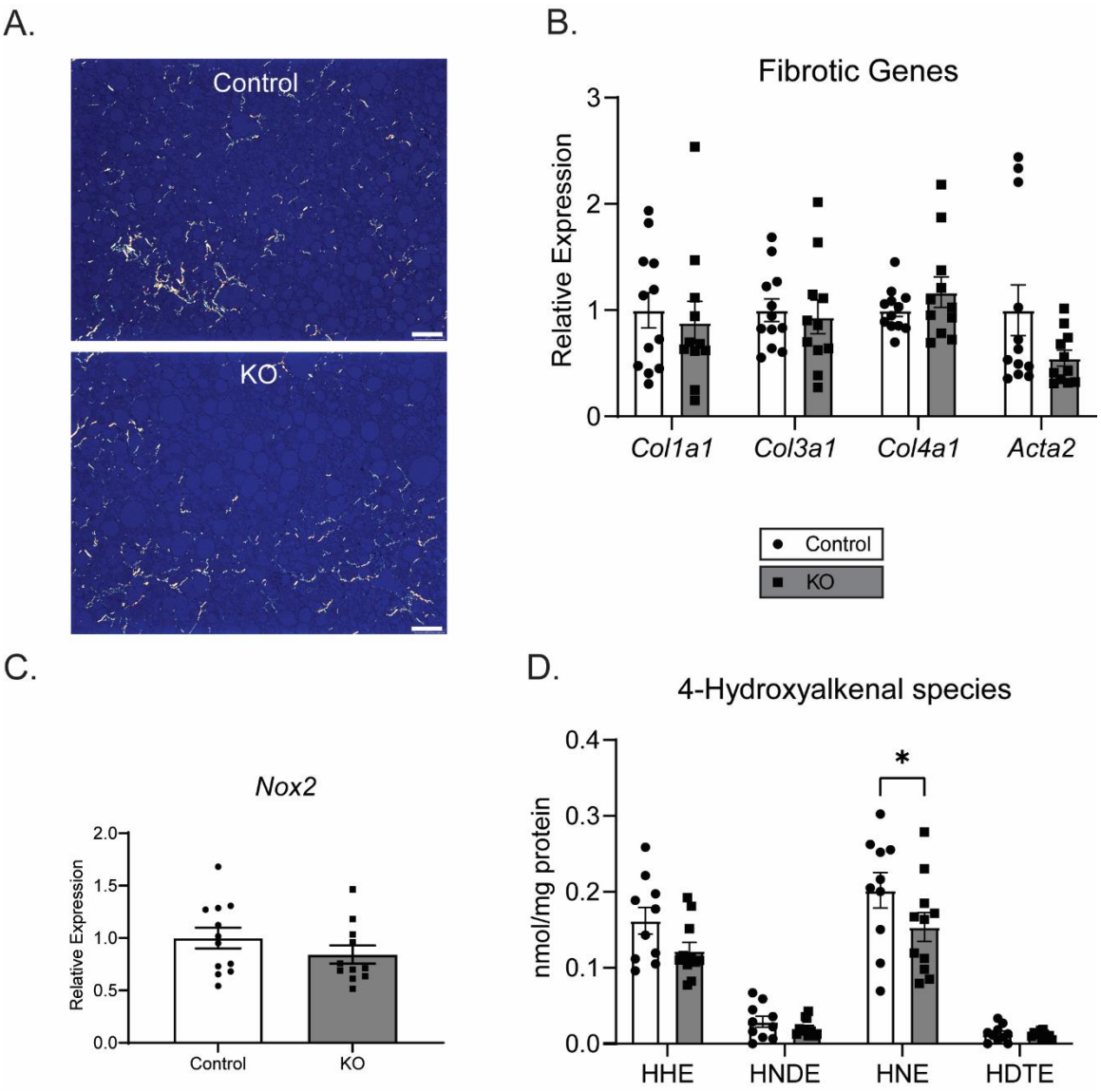

Supplemental Figure 3.3 (paired with Figure 3.7). Markers of fibrosis and oxidative stress in Hepatocyte-BDH1-KO mice maintained on a western-style diet. (A) Representative picrosirius red staining of liver sections from control and KO mice maintained on WD. **(B)** Transcript abundances of fibrotic markers *Col1a1*, *Col3a1*, *Col4a1*, and *Acta2*, and **(C)** oxidative stress marker *Nox2* from livers of control and KO mice. (*n* = 11-12/group). **(D)** Shotgun lipidomics-based quantification of the 4-hydroxyalkenal species 4-hydroxy-nondienal (HNDE), 4-hydroxy-2E-hexenal (HHE), 4-hydroxy-2E-nonenal (HNE), and 4-hydroxy-dodecatrienal (HDTE) in the livers of control and KO mice. Scale bars = 50 μm. Data presented as mean ± SEM. **P* <0.05 by two-way ANOVA with Sidak's multiple comparisons

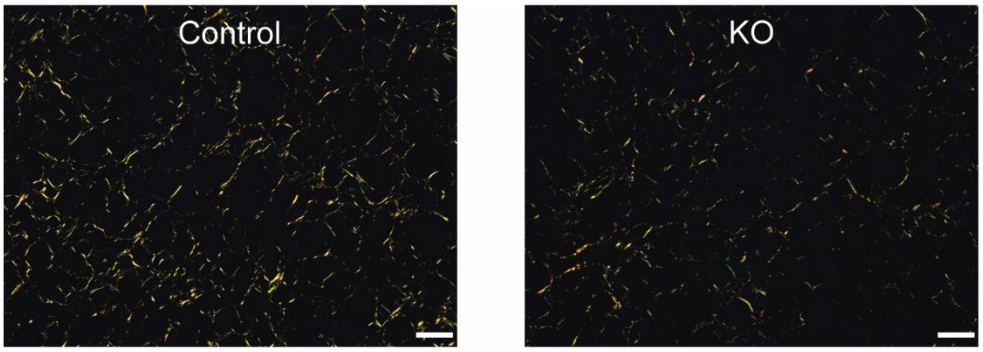

Supplemental Figure 3.4 (Paired with Figure 3.7). Assessment of fibrosis in Hepatocyte-BDH1-KO mice maintained on a choline-deficient, methionine-limited high fat diet. Representative picrosirius red staining of liver sections from control and KO mice maintained on CDAHFD. Scale bars = 50 μm.

Supplemental Table 3.1. Gene expression primer sequences

Gene	Forward Sequence 5’ to 3’	Reverse Sequence 5’ to 3’
Hmgcs2	TGGTTCAAGACAGGGACACAGAAC	AGAGGAATACCAGGGCCCAACAAT
Bdh1	TGCAACAGTGAAGAGGTGGAGAAG	CAAACGTTGAGATGCCTGCGTTGT
Ppargc1a	CGGAAATCATATCCAACCAG	TGAGGACCGCTAGCCAGTTTG
Pparg	AGACAAGATTTGAAAGAAGC	CTTCCATCACGGAGAGGTCC
Pck1	GGAAGGACAAAGATGGCAAGTTC	AGGCGTTTTCCTTAGGGATGTAG
Pc	ACAGCACACACACTACCTGCAATG	GCAGGCCCTTATTTGGCAAGAGAT
Cpt1a	CATGTCAAGCCAGACGAAGA	TGGTAGGAGAGCAGCACCTT
Cpt2	GGCATTGCGTATGCTGTTCACGAT	AAGCACTTCTGGACACAGTGGAGA
Acaca	AAGTCCTTGGTCGGGAAGTATACA	ACTCCCTCAAAGTCATCACAAACA
Acacb	AACCCACTGTCTTCCAATGACA	GAAGGACAACCCATTAGCATCTG
Acadm	TGTTAATCGGTGAAGGAGCAG	CTATCCAGGGCATACTTCGTG
Acadl	CAGTTGCATGAAACCAAACG	GAGTTGCACACATTCATAAGC
Acsl1	AACTCGAAGGCCATTCGTAC	GATAGATGAACTGTACGCCACC
Acsl3	AGCGAGATGGAAAATGAGGTC	ACTTGAAGGCATCTGTCACC
Lipc	TGGGTTATGACATCCGCAAG	GTAAAAGTAGGCTCTACCGGC
Cd36	GATCCGAACACAGCGTAGATAG	GCGACATGATTAATGGCACAG
Col1a1	TGCTTCGTGTAAACTCCCTC	TTGTTCGTCTGTTTCCAGGG
Col3a1	GAAGTCTCTGAAGCTGATGGG	TTGCCTTGCGTGTTTGATATT
Col4a1	AGACCATTCAGATTCCGCAG	CGCTTCTAAACTCTTCCAGACAG
Acta2	CCGCAAATGCTTCTAAGTCC	TTTGGGCAGGAATGATTTGG
Nox2	AGAGCATCTCCAACTCAGAATCCG	ACACTGGTTTCCTGGTGAAAGAGC
Rpl32	CCTCTGGTGAAGCCCAAGATC	TCTGGGTTTCCGCCAGTTT

Chapter 4: Conclusions and future directions

With the use of high-resolution LC-MS/MS, dual isotope tracer NMR spectroscopy, and integrated physiological approaches in novel hepatocyte specific BDH1 knockout mice, this thesis has revealed new insights into the role of hepatic BDH1 in ketone body metabolism and liver health. Likewise, a host of new questions have emerged. Here, the main conclusions from this work are summarized and future directions are discussed.

4.1 Distinct effects of exogenous AcAc versus D-βOHB on circulating ketones and liver redox

Rather than remaining in circulation until terminal ketolysis, exogenously administered AcAc is first reduced to D-βOHB in a BDH1-dependent manner by the liver and other BDH1-expressing tissues. Furthermore, exogenously administered AcAc can transiently increase static liver NAD^+/NADH ratios. Conversely, bolus-delivered D-βOHB does not as readily equilibrate in the circulation to the same extent as AcAc.

The mechanisms and utility behind these differences remain unknown, and can only be speculated upon. Perhaps this is a homeostatic response to maintain the normal circulating ratio of AcAc to D-βOHB. However, if this were the case, a larger portion of exogenously delivered D-βOHB would be expected to be converted to AcAc. Alternatively, the conversion of circulating AcAc to D-βOHB may target circulating AcAc to BDH1-expressing tissues, such as the brain, heart, and skeletal muscle. This could be physiologically significant, because while all

extrahepatic cells express SCOT, BDH1 is not ubiquitously expressed [44]. Regardless, the growing interest in exogenous ketone therapies, which vary in their deliveries of D-βOHB or AcAc [77; 100; 101], merits broader study into these kinetic differences.

Additionally, the liver redox implications of exogenous ketones will need to be further assessed. For instance, as exogenous AcAc treatment transiently increases liver NAD^+/NADH in wild-type mice, this likely perturbs oxidative fluxes, like TCA cycle flux. Future studies looking at the acute effects of exogenous ketones on hepatic oxidative fluxes in both wild-type and hepatocyte-specific BDH1 KO mice will be beneficial.

4.2 Hepatic BDH1 loss reduces circulating ketones, but hepatic BDH1 is not required for systemic ketone equilibration

While our studies showed similar to slightly increased circulating AcAc levels over controls, KO mice showed large decreases in both circulating βOHB and TKB levels in the 18h fasting state. Additionally, our perfusion studies showed similar to modestly reduced rates of liver TKB production in KO mice, with KO mice almost exclusively exporting AcAc, whereas the majority of the AcAc produced by livers of control mice was reduced to D-βOHB before its export from the liver.

Together, the decrease in circulating ketone concentrations in Hepatocyte-BDH1-KO mice, in the context of near normal liver TKB production, suggests increased ketone clearance by extrahepatic tissues [80; 102], with only a marginal effect on liver ketogenesis. Additional assessments will be needed to determine if

this increase in ketone clearance is systemic or due to enhanced ketolysis in only a subset of tissues. For instance, ketone perfusions on mouse hearts or kidneys, followed by quantification of ketones in the resulting perfusate, would allow for a direct determination of extrahepatic ketone clearances in BDH1 mice. Regardless of the mechanism, hepatic loss of BDH1 greatly reduces circulating ketone levels, and targeting hepatic BDH1 could prove useful in pathological ketotic states such as diabetic ketoacidosis.

Additionally, the studies herein indicate that although the liver is a primary site of ketone body equilibration, extrahepatic organs can contribute to ketone equilibration, thus adding nuance to a fifty-year-old mechanism [80]. This illustrates the utility of revisiting and expanding upon older studies, especially with the vast improvements in technology and techniques over the past decades.

In all the experiments presented in this work, the assessments occurred in the context of chronic BDH1 loss, and therefore compensatory mechanisms are invariably playing a role. Studies assessing the acute effects of BDH1 loss will undoubtedly reveal even further insights. Currently, no inhibitors of BDH1, including hepatic specific inhibitors, are available, meaning an inducible Cre-lox genetic system will be needed to assess acute BDH1 loss.

4.3 Loss of hepatic BDH1 diminishes liver oxidative fluxes without altering whole liver energy charge

Using two different diet models and two different exogenous fuel sources, this work has shown that hepatic loss of BDH1 reduces both TCA cycle flux and hepatic

glucose production. Without BDH1, liver mitochondria have lost a conduit to re-generate NAD^+ from NADH. Conversely, liver mitochondria may retain more NADH, decreasing the demand for oxidative metabolism in the liver. As overall energy balance fell within normal limits, and as whole liver tissue redox remained normal, additional experiments will be needed to mechanistically link the oxidative flux impairments with a perturbation in liver redox.

As BDH1 is one of several mitochondrial dehydrogenases [24; 87], loss of BDH1 in hepatocytes likely provokes compensations that protect against more pronounced abnormalities of redox homeostasis. Future dynamic measurements of specific mitochondrial dehydrogenase activities will prove insightful. Another potential way to assess the TCA flux impairment in KO mice would be to perform additional perfusion studies with nicotinamide supplementation, thereby augmenting the available NAD^+ pool. If nicotinamide supplementation normalizes TCA flux in KO mice to control levels, this would strongly suggest a liver redox mechanism.

4.4 Hepatic BDH1 loss alters systemic glucose homeostasis

Hepatocyte-specific loss of BDH1 alters systemic glucose homeostasis, with reductions in hepatic glucose production in the setting of normal to elevated circulating blood glucose. Additionally, alterations in systemic insulin sensitivity, as assessed by IPITTs are apparent in KO mice, although these differences could not be linked to differences in either hepatic or muscle insulin signaling. The ability of KO mice with impaired HGP to maintain normal, or even elevated, levels of systemic glycemia suggests either enhanced extrahepatic gluconeogenesis or

reduced whole body glucose utilization. While some gene expression evidence supports increased kidney gluconeogenesis in KO mice, we were unable to confirm this finding. Without increases in extrahepatic gluconeogenesis, compensations in systemic glucose utilization are more likely, justifying an assessment of muscle, heart, and brain glucose utilization in KO mice. Additionally, with gene expression evidence suggestive of increased glucose reuptake in the kidney, an experiment measuring urine glucose in KO mice could prove useful. Furthermore, if KO mice have increased kidney glucose reuptake, experiments with sodium/glucose cotransporter inhibitors would be informative as well.

Although our assessments with hepatic BDH1 loss have focused on the liver, assessment of the systemic effects, beyond glucose homeostasis, could prove interesting. What happens to the heart or brain when other tissues are able to use a greater portion of the circulating ketone pool? Would hepatic BDH1 loss be a benefit or detriment in heart failure? How are immune cells, like macrophages, affected by the increased availability of AcAc? Could this alter systemic fibrotic responses? What about the redox implications in extrahepatic BDH1 expressing tissues that are now converting AcAc to BOHB. With so many possibilities, further investigation into the systemic consequences of hepatic BDH1 loss is necessary.

4.5 Loss of hepatic BDH1 reduces markers of fibrosis and oxidative stress in mice in models of NAFLD

Given the lack of durable treatments currently available, the evidence suggestive that hepatocyte-specific loss of BDH1 might slow NAFLD progression is enticing. The results herein suggested improvements in hepatic fibrosis, oxidative stress,

and even disease progression (tumor formation) with loss of hepatocyte-specific BDH1. However, further study will be required to determine the mechanisms behind these beneficial effects.

Experiments utilizing exogenous ketones could help determine if the improvements in fibrosis are the result of a redox phenomenon or changes in AcAc and D-βOHB concentrations. We previously observed that treatment with exogenous AcAc attenuates hepatic fibrosis in wild-type mice fed a fibrogenic diet for 4 weeks, while D-βOHB administration modestly exacerbates fibrosis [44]. If these results are also seen in AcAc/D-βOHB treated hepatocyte BDH1 KO mice, this would suggest that the fibrotic changes are dependent on AcAc and D-βOHB concentration changes. In contrast, if neither of these results are seen in AcAc/D-βOHB treated KO mice (comparable levels of fibrosis in vehicle, AcAc, and D-βOHB treated KO mice), this would suggest that the improvements in fibrosis are redox dependent.

Given the distinct kinetics of exogenous AcAc and D-βOHB [102], the former hypothesis, that fibrosis improvement is dependent on AcAc and D-βOHB concentration, is slightly favored over the latter, redox dependent hypothesis. In both AcAc treated wild-type mice and hepatocyte BDH1 KO mice, the liver sinusoidal environment will have increased AcAc concentration, albeit only transiently in the case of AcAc treated wild-type mice, meaning increased AcAc could explain improvements in fibrosis in both models. On the other hand, with exogenous AcAc treatment, the liver readily reduces exogenous AcAc to D-βOHB, representing an increase in the redox reaction catalyzed by BDH1, while in

hepatocyte BDH1 KO mice, this reaction does not occur. Therefore, two distinct redox mechanisms would be needed to adequately describe the improvements in fibrosis. Future studies will hopefully better define the fibrosis improving mechanisms with both exogenous AcAc treatment and hepatic BDH1 loss. Furthermore, the mechanisms might extend to other forms of liver fibrosis, and experiments determining the effects of AcAc treatment or hepatic BDH1 loss in models of alcoholic and hepatitis induced liver disease would be of interest.

Collectively, this thesis illustrates how ketone bodies and BDH1 activity, influence liver homeostasis and health. While liver BDH1 is not required for whole body equilibration of AcAc and D-βOHB, loss of the ability to interconvert these ketone bodies in hepatocytes results in impaired TCA cycle flux and glucose production, with a beneficial effect on liver fibrosis. Therefore, BDH1 is a significant contributor to hepatic mitochondrial redox, liver physiology, and organism-wide ketone body homeostasis, and augmentation of hepatic BDH1 activity could prove beneficial in the treatment of NAFLD.

References

[1] Younossi, Z., Anstee, Q.M., Marietti, M., Hardy, T., Henry, L., Eslam, M., et al., 2017. Global burden of NAFLD and NASH: trends, predictions, risk factors and prevention. Nature Reviews Gastroenterology &Amp; Hepatology 15:11.

[2] Ferguson, D., Finck, B.N., 2021. Emerging therapeutic approaches for the treatment of NAFLD and type 2 diabetes mellitus. Nature Reviews Endocrinology.

[3] Chalasani, N., Younossi, Z., Lavine, J.E., Charlton, M., Cusi, K., Rinella, M., et al., 2018. The diagnosis and management of nonalcoholic fatty liver disease: Practice guidance from the American Association for the Study of Liver Diseases. Hepatology 67(1):328-357.

[4] Diehl, A.M., Day, C., 2017. Cause, Pathogenesis, and Treatment of Nonalcoholic Steatohepatitis. N Engl J Med 377(21):2063-2072.

[5] Kang, J.H., Cho, K.I., Kim, S.M., Lee, J.Y., Kim, J.J., Goo, J.J., et al., 2012. Relationship between Nonalcoholic Fatty Liver Disease and Carotid Artery Atherosclerosis Beyond Metabolic Disorders in Non-Diabetic Patients. J Cardiovasc Ultrasound 20(3):126-133.

[6] Kim, D., Choi, S.-Y., Park, E.H., Lee, W., Kang, J.H., Kim, W., et al., 2012. Nonalcoholic fatty liver disease is associated with coronary artery calcification. Hepatology 56(2):605-613.

[7] Park, H.E., Kwak, M.-S., Kim, D., Kim, M.-K., Cha, M.-j., Choi, S.-Y., 2016. Nonalcoholic Fatty Liver Disease Is Associated With Coronary Artery Calcification Development: A Longitudinal Study. The Journal of Clinical Endocrinology & Metabolism 101(8):3134-3143.

[8] Hallsworth, K., Hollingsworth, K.G., Thoma, C., Jakovljevic, D., MacGowan, G.A., Anstee, Q.M., et al., 2013. Cardiac structure and function are altered in adults with non-alcoholic fatty liver disease. Journal of Hepatology 58(4):757-762.

[9] VanWagner, L.B., Wilcox, J.E., Colangelo, L.A., Lloyd-Jones, D.M., Carr, J.J., Lima, J.A., et al., 2015. Association of nonalcoholic fatty liver disease with subclinical myocardial remodeling and dysfunction: A population-based study. Hepatology 62(3):773-783.

[10] Mantovani, A., 2017. Nonalcoholic Fatty Liver Disease (NAFLD) and Risk of Cardiac Arrhythmias: A New Aspect of the Liver-heart Axis. Journal of clinical and translational hepatology 5(2):134-141.

[11] Targher, G., Mantovani, A., Pichiri, I., Rigolon, R., Dauriz, M., Zoppini, G., et al., 2013. Non-alcoholic fatty liver disease is associated with an increased prevalence of atrial fibrillation in hospitalized patients with type 2 diabetes. Clin Sci (Lond) 125(6):301-309.

[12] Hung, C.-S., Tseng, P.-H., Tu, C.-H., Chen, C.-C., Liao, W.-C., Lee, Y.-C., et al., 2015. Nonalcoholic Fatty Liver Disease Is Associated With QT Prolongation in the General Population. J Am Heart Assoc 4(7):e001820.

[13] Stahl, E.P., Dhindsa, D.S., Lee, S.K., Sandesara, P.B., Chalasani, N.P., Sperling, L.S., 2019. Nonalcoholic Fatty Liver Disease and the Heart: JACC State-of-the-Art Review. J Am Coll Cardiol 73(8):948-963.

[14] Friedman, S.L., Neuschwander-Tetri, B.A., Rinella, M., Sanyal, A.J., 2018. Mechanisms of NAFLD development and therapeutic strategies. Nature medicine 24(7):908-922.
[15] Petersen, K.F., Befroy, D.E., Dufour, S., Rothman, D.L., Shulman, G.I., 2016. Assessment of Hepatic Mitochondrial Oxidation and Pyruvate Cycling in NAFLD by (13)C Magnetic Resonance Spectroscopy. Cell Metab 24(1):167-171.
[16] Felig, P., Wahren, J., Hendler, R., Brundin, T., 1974. Splanchnic glucose and amino acid metabolism in obesity. J Clin Invest 53(2):582-590.
[17] Koliaki, C., Szendroedi, J., Kaul, K., Jelenik, T., Nowotny, P., Jankowiak, F., et al., 2015. Adaptation of hepatic mitochondrial function in humans with non-alcoholic fatty liver is lost in steatohepatitis. Cell Metab 21(5):739-746.
[18] Iozzo, P., Bucci, M., Roivainen, A., Nagren, K., Jarvisalo, M.J., Kiss, J., et al., 2010. Fatty acid metabolism in the liver, measured by positron emission tomography, is increased in obese individuals. Gastroenterology 139(3):846-856, 856.e841-846.
[19] Satapati, S., Kucejova, B., Duarte, J.A., Fletcher, J.A., Reynolds, L., Sunny, N.E., et al., 2015. Mitochondrial metabolism mediates oxidative stress and inflammation in fatty liver. J Clin Invest 125(12):4447-4462.
[20] Sunny, N.E., Parks, E.J., Browning, J.D., Burgess, S.C., 2011. Excessive hepatic mitochondrial TCA cycle and gluconeogenesis in humans with nonalcoholic fatty liver disease. Cell Metab 14(6):804-810.
[21] Balasse, E.O., Féry, F., 1989. Ketone body production and disposal: effects of fasting, diabetes, and exercise. Diabetes Metab Rev 5(3):247-270.
[22] Puchalska, P., Crawford, P.A., 2017. Multi-dimensional Roles of Ketone Bodies in Fuel Metabolism, Signaling, and Therapeutics. Cell Metab 25(2):262-284.
[23] Lehninger, A.L., Sudduth, H.C., Wise, J.B., 1960. D-Beta Hydroxybutyric Dehydrogenase of Mitochondria. Journal of Biological Chemistry 235(8):2450-2455.
[24] Williamson, D., Lund, P., Krebs, H., 1967. The redox state of free nicotinamide-adenine dinucleotide in the cytoplasm and mitochondria of rat liver. Biochemical Journal 103(2):514-527.
[25] Cotter, D.G., d'Avignon, D.A., Wentz, A.E., Weber, M.L., Crawford, P.A., 2011. Obligate role for ketone body oxidation in neonatal metabolic homeostasis. J Biol Chem 286(9):6902-6910.
[26] Halestrap, A.P., 2012. The monocarboxylate transporter family--Structure and functional characterization. IUBMB Life 64(1):1-9.
[27] Cahill, G.F., Jr., 2006. Fuel metabolism in starvation. Annu Rev Nutr 26:1-22.
[28] Cox, P.J., Kirk, T., Ashmore, T., Willerton, K., Evans, R., Smith, A., et al., 2016. Nutritional Ketosis Alters Fuel Preference and Thereby Endurance Performance in Athletes. Cell Metab 24(2):256-268.
[29] Robinson, A.M., Williamson, D.H., 1980. Physiological roles of ketone bodies as substrates and signals in mammalian tissues. Physiol Rev 60(1):143-187.

[30] Hegardt, F.G., 1999. Mitochondrial 3-hydroxy-3-methylglutaryl-CoA synthase: a control enzyme in ketogenesis. Biochem J 338 (Pt 3)(Pt 3):569-582.
[31] Williamson, J.R., Scholz, R., Browning, E.T., 1969. Control Mechanisms of Gluconeogenesis and Ketogenesis: II. Interactions between fatty acid oxidation and the citric acid cycle in perfused rat liver. Journal of Biological Chemistry 244(17):4617-4627.
[32] McGarry, J.D., Foster, D.W., 1980. Regulation of Hepatic Fatty Acid Oxidation and Ketone Body Production. Annual Review of Biochemistry 49(1):395-420.
[33] Quant, P.A., Robin, D., Robin, P., Girard, J., Brand, M.D., 1989. Control of acetoacetate production from exogenous palmitoyl-CoA in isolated rat liver mitochondria. Biochem Soc Trans 17(6):1089-1090.
[34] Otsuka, H., Kimura, T., Ago, Y., Nakama, M., Aoyama, Y., Abdelkreem, E., et al., 2020. Deficiency of 3-hydroxybutyrate dehydrogenase (BDH1) in mice causes low ketone body levels and fatty liver during fasting. Journal of Inherited Metabolic Disease 43(5):960-968.
[35] Cotter, D.G., Ercal, B., Huang, X., Leid, J.M., d'Avignon, D.A., Graham, M.J., et al., 2014. Ketogenesis prevents diet-induced fatty liver injury and hyperglycemia. J Clin Invest 124(12):5175-5190.
[36] d'Avignon, D.A., Puchalska, P., Ercal, B., Chang, Y., Martin, S.E., Graham, M.J., et al., 2018. Hepatic ketogenic insufficiency reprograms hepatic glycogen metabolism and the lipidome. JCI Insight 3(12).
[37] Wolfrum, C., Asilmaz, E., Luca, E., Friedman, J.M., Stoffel, M., 2004. Foxa2 regulates lipid metabolism and ketogenesis in the liver during fasting and in diabetes. Nature 432(7020):1027-1032.
[38] von Meyenn, F., Porstmann, T., Gasser, E., Selevsek, N., Schmidt, A., Aebersold, R., et al., 2013. Glucagon-induced acetylation of Foxa2 regulates hepatic lipid metabolism. Cell Metab 17(3):436-447.
[39] Badman, M.K., Pissios, P., Kennedy, A.R., Koukos, G., Flier, J.S., Maratos-Flier, E., 2007. Hepatic fibroblast growth factor 21 is regulated by PPARalpha and is a key mediator of hepatic lipid metabolism in ketotic states. Cell Metab 5(6):426-437.
[40] Fukao, T., Lopaschuk, G.D., Mitchell, G.A., 2004. Pathways and control of ketone body metabolism: on the fringe of lipid biochemistry. Prostaglandins Leukot Essent Fatty Acids 70(3):243-251.
[41] Al Batran, R., Gopal, K., Capozzi, M.E., Chahade, J.J., Saleme, B., Tabatabaei-Dakhili, S.A., et al., 2020. Pimozide Alleviates Hyperglycemia in Diet-Induced Obesity by Inhibiting Skeletal Muscle Ketone Oxidation. Cell Metab 31(5):909-919.e908.
[42] Cotter, D.G., Schugar, R.C., Wentz, A.E., d'Avignon, D.A., Crawford, P.A., 2013. Successful adaptation to ketosis by mice with tissue-specific deficiency of ketone body oxidation. Am J Physiol Endocrinol Metab 304(4):E363-374.
[43] García-Caballero, M., Zecchin, A., Souffreau, J., Truong, A.-C.K., Teuwen, L.-A., Vermaelen, W., et al., 2019. Role and therapeutic potential of dietary ketone bodies in lymph vessel growth. Nature Metabolism 1(7):666-675.

[44] Puchalska, P., Martin, S.E., Huang, X., Lengfeld, J.E., Daniel, B., Graham, M.J., et al., 2019. Hepatocyte-Macrophage Acetoacetate Shuttle Protects against Tissue Fibrosis. Cell Metab 29(2):383-398 e387.
[45] Schugar, R.C., Moll, A.R., Andre d'Avignon, D., Weinheimer, C.J., Kovacs, A., Crawford, P.A., 2014. Cardiomyocyte-specific deficiency of ketone body metabolism promotes accelerated pathological remodeling. Mol Metab 3(7):754-769.
[46] Orii, K.E., Fukao, T., Song, X.Q., Mitchell, G.A., Kondo, N., 2008. Liver-specific silencing of the human gene encoding succinyl-CoA: 3-ketoacid CoA transferase. Tohoku J Exp Med 215(3):227-236.
[47] Thorrez, L., Laudadio, I., Van Deun, K., Quintens, R., Hendrickx, N., Granvik, M., et al., 2011. Tissue-specific disallowance of housekeeping genes: the other face of cell differentiation. Genome Res 21(1):95-105.
[48] Williamson, D.H., Bates, M.W., Page, M.A., Krebs, H.A., 1971. Activities of enzymes involved in acetoacetate utilization in adult mammalian tissues. Biochemical Journal 121(1):41-47.
[49] Horton, J.L., Davidson, M.T., Kurishima, C., Vega, R.B., Powers, J.C., Matsuura, T.R., et al., 2019. The failing heart utilizes 3-hydroxybutyrate as a metabolic stress defense. JCI Insight 4(4).
[50] Grinblat, L., Pacheco Bolaños, L.F., Stoppani, A.O., 1986. Decreased rate of ketone-body oxidation and decreased activity of D-3-hydroxybutyrate dehydrogenase and succinyl-CoA:3-oxo-acid CoA-transferase in heart mitochondria of diabetic rats. Biochem J 240(1):49-56.
[51] Grimsrud, P.A., Carson, J.J., Hebert, A.S., Hubler, S.L., Niemi, N.M., Bailey, D.J., et al., 2012. A quantitative map of the liver mitochondrial phosphoproteome reveals posttranslational control of ketogenesis. Cell Metab 16(5):672-683.
[52] Dittenhafer-Reed, K.E., Richards, A.L., Fan, J., Smallegan, M.J., Fotuhi Siahpirani, A., Kemmerer, Z.A., et al., 2015. SIRT3 mediates multi-tissue coupling for metabolic fuel switching. Cell Metab 21(4):637-646.
[53] Rardin, M.J., He, W., Nishida, Y., Newman, J.C., Carrico, C., Danielson, S.R., et al., 2013. SIRT5 regulates the mitochondrial lysine succinylome and metabolic networks. Cell Metab 18(6):920-933.
[54] Shimazu, T., Hirschey, M.D., Hua, L., Dittenhafer-Reed, K.E., Schwer, B., Lombard, D.B., et al., 2010. SIRT3 deacetylates mitochondrial 3-hydroxy-3-methylglutaryl CoA synthase 2 and regulates ketone body production. Cell Metab 12(6):654-661.
[55] Wagner, G.R., Bhatt, D.P., O'Connell, T.M., Thompson, J.W., Dubois, L.G., Backos, D.S., et al., 2017. A Class of Reactive Acyl-CoA Species Reveals the Non-enzymatic Origins of Protein Acylation. Cell Metab 25(4):823-837.e828.
[56] Goedeke, L., Peng, L., Montalvo-Romeral, V., Butrico, G.M., Dufour, S., Zhang, X.-M., et al., 2019. Controlled-release mitochondrial protonophore (CRMP) reverses dyslipidemia and hepatic steatosis in dysmetabolic nonhuman primates. Science translational medicine 11(512):eaay0284.
[57] Kim, C.W., Addy, C., Kusunoki, J., Anderson, N.N., Deja, S., Fu, X., et al., 2017. Acetyl CoA Carboxylase Inhibition Reduces Hepatic Steatosis but Elevates

Plasma Triglycerides in Mice and Humans: A Bedside to Bench Investigation. Cell Metab 26(2):394-406.e396.
[58] Samuel, V.T., Shulman, G.I., 2018. Nonalcoholic Fatty Liver Disease as a Nexus of Metabolic and Hepatic Diseases. Cell Metab 27(1):22-41.
[59] Sanyal, A., Charles, E.D., Neuschwander-Tetri, B.A., Loomba, R., Harrison, S.A., Abdelmalek, M.F., et al., 2019. Pegbelfermin (BMS-986036), a PEGylated fibroblast growth factor 21 analogue, in patients with non-alcoholic steatohepatitis: a randomised, double-blind, placebo-controlled, phase 2a trial. Lancet 392(10165):2705-2717.
[60] Neufer, P.D., 2019. Cutting fuel offers new clues in diabetic mystery. The Journal of Biological Chemistry 294(33):12328-12329.
[61] Lee, J., Choi, J., Selen Alpergin, E.S., Zhao, L., Hartung, T., Scafidi, S., et al., 2017. Loss of Hepatic Mitochondrial Long-Chain Fatty Acid Oxidation Confers Resistance to Diet-Induced Obesity and Glucose Intolerance. Cell Rep 20(3):655-667.
[62] Fletcher, J.A., Deja, S., Satapati, S., Fu, X., Burgess, S.C., Browning, J.D., 2019. Impaired ketogenesis and increased acetyl-CoA oxidation promote hyperglycemia in human fatty liver. JCI Insight.
[63] Kakehashi, A., Stefanov, V.E., Ishii, N., Okuno, T., Fujii, H., Kawai, K., et al., 2017. Proteome Characteristics of Non-Alcoholic Steatohepatitis Liver Tissue and Associated Hepatocellular Carcinomas. Int J Mol Sci 18(2).
[64] Satapati, S., Sunny, N.E., Kucejova, B., Fu, X., He, T.T., Mendez-Lucas, A., et al., 2012. Elevated TCA cycle function in the pathology of diet-induced hepatic insulin resistance and fatty liver. J Lipid Res 53(6):1080-1092.
[65] Soeters, M.R., Sauerwein, H.P., Faas, L., Smeenge, M., Duran, M., Wanders, R.J., et al., 2009. Effects of insulin on ketogenesis following fasting in lean and obese men. Obesity (Silver Spring) 17(7):1326-1331.
[66] Mannisto, V.T., Simonen, M., Hyysalo, J., Soininen, P., Kangas, A.J., Kaminska, D., et al., 2015. Ketone body production is differentially altered in steatosis and non-alcoholic steatohepatitis in obese humans. Liver Int 35(7):1853-1861.
[67] Ballestri, S., Nascimbeni, F., Baldelli, E., Marrazzo, A., Romagnoli, D., Lonardo, A., 2017. NAFLD as a Sexual Dimorphic Disease: Role of Gender and Reproductive Status in the Development and Progression of Nonalcoholic Fatty Liver Disease and Inherent Cardiovascular Risk. Adv Ther 34(6):1291-1326.
[68] Safaei, A., Arefi Oskouie, A., Mohebbi, S.R., Rezaei-Tavirani, M., Mahboubi, M., Peyvandi, M., et al., 2016. Metabolomic analysis of human cirrhosis, hepatocellular carcinoma, non-alcoholic fatty liver disease and non-alcoholic steatohepatitis diseases. Gastroenterology and hepatology from bed to bench 9(3):158-173.
[69] Bragoszewski, P., Habior, A., Walewska-Zielecka, B., Ostrowski, J., 2007. Expression of genes encoding mitochondrial proteins can distinguish nonalcoholic steatosis from steatohepatitis. Acta Biochim Pol 54(2):341-348.
[70] Veech, R.L., Bradshaw, P.C., Clarke, K., Curtis, W., Pawlosky, R., King, M.T., 2017. Ketone bodies mimic the life span extending properties of caloric restriction. IUBMB Life 69(5):305-314.

[71] Nielsen, R., Møller, N., Gormsen Lars, C., Tolbod Lars, P., Hansson Nils, H., Sorensen, J., et al., 2019. Cardiovascular Effects of Treatment With the Ketone Body 3-Hydroxybutyrate in Chronic Heart Failure Patients. Circulation 139(18):2129-2141.
[72] Vilar-Gomez, E., Athinarayanan, S.J., Adams, R.N., Hallberg, S.J., Bhanpuri, N.H., McKenzie, A.L., et al., 2019. Post hoc analyses of surrogate markers of non-alcoholic fatty liver disease (NAFLD) and liver fibrosis in patients with type 2 diabetes in a digitally supported continuous care intervention: an open-label, non-randomised controlled study. BMJ Open 9(2):e023597.
[73] Caffa, I., Spagnolo, V., Vernieri, C., Valdemarin, F., Becherini, P., Wei, M., et al., 2020. Fasting-mimicking diet and hormone therapy induce breast cancer regression. Nature 583(7817):620-624.
[74] de Cabo, R., Mattson, M.P., 2019. Effects of Intermittent Fasting on Health, Aging, and Disease. New England Journal of Medicine 381(26):2541-2551.
[75] Hopkins, B.D., Pauli, C., Du, X., Wang, D.G., Li, X., Wu, D., et al., 2018. Suppression of insulin feedback enhances the efficacy of PI3K inhibitors. Nature 560(7719):499-503.
[76] Brenner, D.A., 2018. Of Mice and Men and Nonalcoholic Steatohepatitis. Hepatology 68(6):2059-2061.
[77] Stubbs, B.J., Cox, P.J., Evans, R.D., Santer, P., Miller, J.J., Faull, O.K., et al., 2017. On the Metabolism of Exogenous Ketones in Humans. Frontiers in Physiology 8(848).
[78] Yurista, S.R., Chong, C.R., Badimon, J.J., Kelly, D.P., de Boer, R.A., Westenbrink, B.D., 2021. Therapeutic Potential of Ketone Bodies for Patients With Cardiovascular Disease: JACC Focus Seminar. J Am Coll Cardiol:00194-00197.
[79] Krebs, H., Mellanby, J., Williamson, D., 1962. The equilibrium constant of the β-hydroxybutyric-dehydrogenase system. Biochemical Journal 82(1):96-98.
[80] McGarry, J.D., Guest, M.J., Foster, D.W., 1970. Ketone body metabolism in the ketosis of starvation and alloxan diabetes. J Biol Chem 245(17):4382-4390.
[81] Krebs, H.A., Wallace, P.G., Hems, R., Freedland, R.A., 1969. Rates of ketone-body formation in the perfused rat liver. Biochem J 112(5):595-600.
[82] Postic, C., Shiota, M., Niswender, K.D., Jetton, T.L., Chen, Y., Moates, J.M., et al., 1999. Dual roles for glucokinase in glucose homeostasis as determined by liver and pancreatic beta cell-specific gene knock-outs using Cre recombinase. J Biol Chem 274(1):305-315.
[83] Puchalska, P., Nelson, A.B., Stagg, D.B., Crawford, P.A., 2021. Determination of ketone bodies in biological samples via rapid UPLC-MS/MS. Talanta 225:122048.
[84] Fu, X., Deja, S., Kucejova, B., Duarte, J.A.G., McDonald, J.G., Burgess, S.C., 2019. Targeted Determination of Tissue Energy Status by LC-MS/MS. Anal Chem 91(9):5881-5887.

[85] Parks, B.W., Sallam, T., Mehrabian, M., Psychogios, N., Hui, S.T., Norheim, F., et al., 2015. Genetic architecture of insulin resistance in the mouse. Cell Metab 21(2):334-347.
[86] Spalding, J.L., Naser, F.J., Mahieu, N.G., Johnson, S.L., Patti, G.J., 2018. Trace Phosphate Improves ZIC-pHILIC Peak Shape, Sensitivity, and Coverage for Untargeted Metabolomics. Journal of Proteome Research 17(10):3537-3546.
[87] Krebs, H.A., Veech, R.L., 1969. Equilibrium relations between pyridine nucleotides and adenine nucleotides and their roles in the regulation of metabolic processes. Advances in enzyme regulation 7:397-413.
[88] Heinrich, P., Kohler, C., Ellmann, L., Kuerner, P., Spang, R., Oefner, P.J., et al., 2018. Correcting for natural isotope abundance and tracer impurity in MS-, MS/MS- and high-resolution-multiple-tracer-data from stable isotope labeling experiments with IsoCorrectoR. Sci Rep 8(1):17910.
[89] Raje, V., Ahern, K.W., Martinez, B.A., Howell, N.L., Oenarto, V., Granade, M.E., et al., 2020. Adipocyte lipolysis drives acute stress-induced insulin resistance. Sci Rep 10(1).
[90] Guo, K., Lukacik, P., Papagrigoriou, E., Meier, M., Lee, W.H., Adamski, J., et al., 2006. Characterization of human DHRS6, an orphan short chain dehydrogenase/reductase enzyme: a novel, cytosolic type 2 R-beta-hydroxybutyrate dehydrogenase. J Biol Chem 281(15):10291-10297.
[91] Veech, R.L., Todd King, M., Pawlosky, R., Kashiwaya, Y., Bradshaw, P.C., Curtis, W., 2019. The “great” controlling nucleotide coenzymes. IUBMB Life 71(5):565-579.
[92] Deja, S., Fu, X., Fletcher, J.A., Kucejova, B., Browning, J.D., Young, J.D., et al., 2020. Simultaneous tracers and a unified model of positional and mass isotopomers for quantification of metabolic flux in liver. Metab Eng 59:1-14.
[93] Violante, S., Achetib, N., Roermund, C.W.T., Hagen, J., Dodatko, T., Vaz, F.M., et al., 2019. Peroxisomes can oxidize medium- and long-chain fatty acids through a pathway involving ABCD3 and HSD17B4. The FASEB Journal 33(3):4355-4364.
[94] Bian, F., Kasumov, T., Thomas, K.R., Jobbins, K.A., David, F., Minkler, P.E., et al., 2005. Peroxisomal and mitochondrial oxidation of fatty acids in the heart, assessed from the 13C labeling of malonyl-CoA and the acetyl moiety of citrate. J Biol Chem 280(10):9265-9271.
[95] Krebs, H.A., Speake, R.N., Hems, R., 1965. ACCELERATION OF RENAL GLUCONEOGENESIS BY KETONE BODIES AND FATTY ACIDS. Biochem J 94(3):712-720.
[96] Cappel, D.A., Deja, S., Duarte, J.A.G., Kucejova, B., Inigo, M., Fletcher, J.A., et al., 2019. Pyruvate-Carboxylase-Mediated Anaplerosis Promotes Antioxidant Capacity by Sustaining TCA Cycle and Redox Metabolism in Liver. Cell Metab 29(6):1291-1305.e1298.
[97] Cotter, D.G., Ercal, B., d'Avignon, D.A., Dietzen, D.J., Crawford, P.A., 2013. Impact of peripheral ketolytic deficiency on hepatic ketogenesis and gluconeogenesis during the transition to birth. J Biol Chem 288(27):19739-19749.

[98] Deja, S., Kucejova, B., Fu, X., Browning, J.D., Young, J.D., Burgess, S., 2021. In Vivo Estimation of Ketogenesis Using Metabolic Flux Analysis—Technical Aspects and Model Interpretation. Metabolites 11(5).
[99] Miles, J.M., Schwenk, W.F., McClean, K.L., Haymond, M.W., 1986. A dual-isotope technique for determination of in vivo ketone body kinetics. Am J Physiol 251(2 Pt 1):E185-191.
[100] Mujica-Parodi, L.R., Amgalan, A., Sultan, S.F., Antal, B., Sun, X., Skiena, S., et al., 2020. Diet modulates brain network stability, a biomarker for brain aging, in young adults. Proceedings of the National Academy of Sciences 117(11):6170-6177.
[101] D'Agostino, D.P., Pilla, R., Held, H.E., Landon, C.S., Puchowicz, M., Brunengraber, H., et al., 2013. Therapeutic ketosis with ketone ester delays central nervous system oxygen toxicity seizures in rats. American Journal of Physiology-Regulatory, Integrative and Comparative Physiology 304(10):R829-R836.
[102] Stagg, D.B., Gillingham, J.R., Nelson, A.B., Lengfeld, J.E., d'Avignon, D.A., Puchalska, P., et al., 2021. Diminished ketone interconversion, hepatic TCA cycle flux, and glucose production in D-β-hydroxybutyrate dehydrogenase hepatocyte-deficient mice. Molecular Metabolism 53:101269-101269.
[103] Wang, C., Wang, M., Zhou, Y., Dupree, J.L., Han, X., 2014. Alterations in mouse brain lipidome after disruption of CST gene: a lipidomics study. Mol Neurobiol 50(1):88-96.
[104] Wang, M., Fang, H., Han, X., 2012. Shotgun lipidomics analysis of 4-hydroxyalkenal species directly from lipid extracts after one-step in situ derivatization. Analytical Chemistry 84(10):4580-4586.
[105] Piacentini, M., Baiocchini, A., Del Nonno, F., Melino, G., Barlev, N.A., Rossin, F., et al., 2018. Non-alcoholic fatty liver disease severity is modulated by transglutaminase type 2. Cell Death & Disease 9(3):257.
[106] Petersen, M.C., Shulman, G.I., 2018. Mechanisms of Insulin Action and Insulin Resistance. Physiol Rev 98(4):2133-2223.
[107] Petersen, M.C., Vatner, D.F., Shulman, G.I., 2017. Regulation of hepatic glucose metabolism in health and disease. Nature reviews. Endocrinology 13(10):572-587.
[108] Thompson, G.N., Hsu, B.Y.L., Pitt, J.J., Treacy, E., Stanley, C.A., 1997. Fasting Hypoketotic Coma in a Child with Deficiency of Mitochondrial 3-Hydroxy-3-Methylglutaryl-CoA Synthase. New England Journal of Medicine 337(17):1203-1207.
[109] Huang, H., Zhang, D., Weng, Y., Delaney, K., Tang, Z., Yan, C., et al., 2021. The regulatory enzymes and protein substrates for the lysine β-hydroxybutyrylation pathway. Sci Adv 7(9).
[110] Kang, H.B., Fan, J., Lin, R., Elf, S., Ji, Q., Zhao, L., et al., 2015. Metabolic Rewiring by Oncogenic BRAF V600E Links Ketogenesis Pathway to BRAF-MEK1 Signaling. Mol Cell 59(3):345-358.
[111] Matsumoto, M., Hada, N., Sakamaki, Y., Uno, A., Shiga, T., Tanaka, C., et al., 2013. An improved mouse model that rapidly develops fibrosis in non-alcoholic steatohepatitis. Int J Exp Pathol 94(2):93-103.

[112] Im, Y.R., Hunter, H., de Gracia Hahn, D., Duret, A., Cheah, Q., Dong, J., et al., 2021. A Systematic Review of Animal Models of NAFLD Finds High-Fat, High-Fructose Diets Most Closely Resemble Human NAFLD. Hepatology n/a(n/a).